THE EFFECTS OF TRAILING EDGE COOLANT ON TRAILING EDGE LOSSES

by

S. J. Edwards, B. Eng.

"Thesis submitted in accordance with the requirements of the University of Liverpool for the degree of Master of Engineering."

Department of Mechanical Engineering,
University of Liverpool

[1980?]

ACKNOWLEDGEMENTS

I would like to express my gratitude to the people who have been involved with this thesis:

Professor J. F. Norbury for his guidance and supervision of the project.

Dr. J. C. Gibbings (The University of Liverpool), Dr. I. Halliwell (Rolls-Royce Limited) and Mr. R. Jaspel (Rolls-Royce Limited), with whom I have had many helpful discussions.

Mr. J. F. Patterson, the Laboratory Technician.

The University of Liverpool workshop personnel for their high standard of workmanship.

Finally my thanks are due to Rolls-Royce Limited for financing the project.

SUMMARY

This thesis reports on an experimental investigation into the trailing edge pressure and losses of a symmetrical isolated aerodynamic body under transonic flow conditions. Tests were made in the 4" x 4" transonic wind tunnel at the University of Liverpool.

The test programme included bleed through three different base configurations and the effect on base pressure and losses. Experimental measurements included base pressures, static pressure variation over the model surface and wake total pressure traverses. Schlieren photographs were taken and samples of these are presented to indicate the nature of the flow in the wake region.

CONTENTS

NOTATION

C	chord length
℄	centre line
Cpb	base pressure coefficient
Cq	$\dot{m}/\rho_\infty \cdot U_\infty$ 2hs
Cv	viscous loss coefficient
h	semi-thickness of base
L	length of splitter plate
$\dot{m}$	base bleed mass flow
M	Mach number based on settling chamber total pressure
$\overline{Me_1}$	Mach number at the edge of the boundary layer at a distance of 0.03" upstream of the trailing edge
Me_1	Mach number at the edge of the boundary layer at a distance of 0.4" upstream of the trailing edge
Mi	Mach number of a layer in the boundary layer (Fig.4)
M_∞	Mach number based on settling chamber total pressure and plenum chamber static pressure
Mp	Mach number calculated from pitot-static tube
n	Vortex shedding frequency
Þb	base pressure
Þo	pitot total pressure (corrected for shock)
$Þo_\infty$	settling chamber total pressure
$Þ_\infty$	plenum chamber static pressure
s	span
U	local velocity
Ue	velocity at edge of boundary layer
U_∞	free stream velocity
Wd	transition wire diameter
x,y	cartesian co-ordinates
α	angle of incidence
ρ_∞	free stream density
δ	boundary layer thickness
θ	boundary layer momentum thickness
δ^*	boundary layer displacement thickness
γ	ratio of specific heats

1. INTRODUCTION

Interest in the practical use of aerofoil sections with trailing edges of fairly large thickness has been aroused during recent years in the aircraft gas turbine industry. The demand for increased efficiency and especially the development of the high bypass ratio engine has pushed the temperature of the gas upwards so that blade cooling is increasingly necessary to reduce metal temperatures. One of the proposed systems for the cooling of the blade involves ejection of the coolant gas through the trailing edge. To facilitate this the trailing edge of the blade has to be increased in thickness and as a consequence this creates a blunt base.

It has long been recognised that an essential feature of the flow past a blunt trailing edge is the flow separation at the trailing edge and the existence of a low pressure region behind the separation point as compared with the pressure in the undisturbed stream. There is a high value of total pressure loss as a consequence of the separated region behind the trailing edge and the low value of base pressure. This loss is particularly high in the transonic flow regime.

While analytical approaches have not been able to keep pace with the need for reliable design data a great number of experimental investigations have helped establish the significant parameters influencing the base pressure.

The object of this investigation is to compare the base pressure and losses in the wake of three base configurations with and without the ejection of air through the base. The

base geometries investigated are that of a rectangular slot; a series of circular holes and finally a series of flared holes. For the latter base geometry the hole diameters at inlet are the same as those for the circular holes but they merge together at their outlets. The flared holes were manufactured at Rolls-Royce as an insert to the model: this was done by electrochemical means using a nimonic material. It is anticipated that this geometry will represent the most relevant form for a possible production blade. All the base cross-sectional areas are the same. For details of the base geometry see fig. (12).

The work has been carried out on a simple isolated aerodynamic body since the objective was to investigate the nature of the flow round the base.

Finally, the author must direct attention to the work of Kadir (Ref. 24) from which this thesis follows on. Numerous references will be made to his work, and where applicable his results will be reproduced for the purpose of comparison.

2. REVIEW OF PREVIOUS WORK

This chapter presents a review of recent experimental and theoretical research on two-dimensional base flows. The main object is to illustrate the extent to which the basic nature of the flow is understood in each of the flow regimes: subsonic, transonic and supersonic.

2.1 Subsonic flow

One essential feature of subsonic base flows is the periodic shedding of vortices. This was first demonstrated by Hoerner (Ref. 1,2) when investigating base flows on aerofoils. He found that for both aerofoil and backward facing step the base drag depended on the ratio of the base height to that of the boundary layer thickness ahead of the base. However, the two sets of results remained distinct from one another, the base pressure on a blunt-trailing-edged aerofoil being rather less than that on a backward facing step for the same ratio of base height to boundary layer thickness. Hoerner attributed the discrepancy to the existence of a Karman vortex street in the wake of the aerofoil, whereas in the case of a backward facing step the presence of a down stream wall inhibited the formation of any such vortex system.

In support of this was the work conducted by Roshko (Ref. 3, 4) on cylinders. He was able to show that as a splitter plate was moved downstream out of the body the base pressure rose and the shedding frequency of the periodic vortices decreased. Thomann (Ref. 5) conducted some tests on a single-wedge at M = 0.556 to show that as the length of the splitter plate was increased the point at which the vortices formed was pushed further downstream and their strength reduced.

Thomann suggested that the likelihood of the wake breaking down into strong vortices was greatest when the shear layers springing from the body surface were thin compared with the distance between them. Thus the action of the splitter

plate was to allow the shear layers to diffuse to some extent before they were free to engage, thereby reducing the severity of any possible instability. The concept that wake instability is attenuated by the reduction or cancellation of the large transverse velocity gradients is in accordance with the conclusions of Hoerner who pointed out that the base pressure on wings with only a small trailing-edge thickness, where the velocity gradients are quickly cancelled by the merging of the shear layers, tended towards the values for the backward facing steps. It has since been shown, however, that the periodicity is still present on sections with a very small base height. Presumably the strength of the vortices is then greatly reduced.

2.2 Transonic flow

Apart from a very few measurements of base pressure through this speed range (Ref. 6, 7, 8, 9) little advance in understanding of transonic base flow has been made.

The breakdown of the wake into periodic vortices which dominated the flow picture at low subsonic speeds extends through the transonic range also and values of the base pressure on models with a severe degree of trailing-edge bluntness are found to be considerably lower than could be estimated from tentative steady-flow calculations.

With an increase of Mach number from subsonic speeds, shock waves develop on the body surface and the movement of these towards the trailing-edge appears to be associated in some cases with small rises and falls in base pressure.

Further increase in Mach number causes the shocks to trail behind the section at the end of short well-defined shear layers extending almost parallel to each other downstream of the trailing edge. In this condition there is a complicated interplay between movements of the trailing shock system and the formation of the vortices. Measurements (Ref. 10) have shown that the Strouhal number (non-dimensional vortex shedding frequency $^{nh}/_{U_\infty}$) increases through this short Mach number range. The wake downstream of the trailing shock waves spreads out, accompanied by the fall of the base pressure coefficient to a minimum value.

A small increase of Mach number from this condition causes an abrupt change in flow pattern. The shear layers from the body surface now turn sharply at the trailing edge and converge to a narrow waist approximately two base-heights downstream. There is a short Mach number range in which the trailing shocks are bifurcated but very shortly the more familiar supersonic type base flow with a simple trailing shock system is established and further increase of Mach number does not produce any significant change in the flow picture. Between Mach numbers of 1.0 to 1.4 the intensity of the vortices does not appear to be very great but there is no evidence that the periodicity entirely dies out at higher Mach numbers. Indeed certain Schlieren photographs (Ref. 11) suggest that discrete eddies may persist in the wake behind the blunt trailing edge sections even up to M = 4. Above a Mach numer of 1.4, however, it can be safely concluded that any instability which persists will no longer have a significant effect on the base flow.

2.3 Supersonic flow

In supersonic base-flow, the shear flows originating in the boundary layers on the body surface are deflected by centred expansions at the trailing edge to converge to a narrow waist a short distance down-stream of the base. The base pressure depends on the ability of the shear layers to negotiate the sharp pressure rise through the region of confluence: the low velocity fluid in the shear layers is reversed to form a slowly circulating vortical flow in the cavity while the higher velocity fluid is able to overcome the pressure rise and escape into the downstream wake.

When the flow in the early part of the wake is entirely laminar or entirely turbulent the problem is simplified and the dependence on other parameters can be examined in more detail. Tests have shown that the base pressure is a function of the thickness of the boundary layer on the body surface just upstream of the trailing edge. At a given Mach number the base pressure increases with the ratio (θ/h) of the boundary-layer momentum thickness to the base height (Ref. 12, 13, 14). As yet there is insufficient data to predict accurately the base pressure given the conditions of the boundary layer on the surface of the body.

Geometrical parameters such as body shape appear to influence the base pressure on two-dimensional sections mainly in the way they control the effect of the boundary layers on the base flow. Numbers of experiments have been made to measure the base pressure on wing models over a range of incidence (Ref. 16) but any effect was very slight so long as

the flow remained attached to both surfaces and in different cases an increase or a decrease in base pressure was observed. Section boat-tailing appears to have a larger effect than angle of attack (Ref. 15, 16). Slight positive boat-tailing, i.e. with section thickness decreasing towards the trailing edge, gives a small increase in base pressure until the boundary layer separates from the afterbody.

2.4 The reduction of base drag

Base drag constitutes an appreciable part of the total drag. MacMartin and Norbury (Ref. 17) found that in a particular supersonic turbine cascade a very large proportion, perhaps 80 to 90 per cent, of the high value of total pressure loss was a consequence of the thickness of the trailing edge and the value of the base pressure coefficient.

Experiments concerned with the reduction base drag can usually be divided into two groups: the first is concerned with the use of mechanical devices; the second with the ejection of air through the base (base bleed).

The most common mechanical device is the splitter plate. This is a thin, two-dimensional flat plate extending into the wake from the centre of the base. This device works on the principle that it interferes with and suppresses the formation of a vortex street. Such methods have resulted in a 50% reduction of base drag.

Bearman (Ref. 18) investigated the effect of varying the length of a splitter plate on the subsonic base drag. He found that the base pressure rose rapidly as the length of the splitter

plate was increased. When the ratio of the length of the splitter plate to the height of the base was unity the base pressure was a maximum. Thereafter the base pressure decreased until ($^{L}/_{2h}$) was approximately equal to 1.5 and then the base pressure began to rise again.

The effect of the splitter plate on base drag reduction decreases as the Mach number is increased.

Another device which has been found to reduce the base drag is a trailing edge cavity. Little is known about the effects of cavity geometry in the simple case of no base bleed. The test reported in Ref.(10) showed a reduction in base drag of about 20 per cent for a square cavity of stream wise depth equal to the trailing edge thickness.

A most extensive study of the effect of trailing edge configuration on base drag was conducted by Jaspel (Ref. 19). Such configurations as square cut, half rounded, rounded bevel and flat bevel shapes were compared. He found that the drag for rounded bevel and flat bevel shaped trailing edges was less than that for the more conventional square cut or rounded trailing-edge models for the same ratio of trailing edge thickness to chord. The effect of cavity or base bleed on drag was not investigated.

The other group of experiments concerned with the reduction of base drag is that involving base bleed, i.e. the continuous ejection of air through holes in the base. Some early exploratory work on base bleed was done by Holder and this was followed up by some tests on the same model by Moulden (Ref. 20). This work established that significant reductions in drag could be achieved over a range of bleed quantities. From the work of

Bearmen (Ref. 21, 22) and Woods (Ref. 23) it is clear that base bleed affects the vortex formation in a similar manner to that of the splitter plate, but the general question of the mechanism behind the effect of bleed on the base flow has not yet been elucidated.

2.5 The flow in the base region

The steady flow in the wake behind the base of a symmetrical aerofoil at zero incidence is assumed to be symmetrical about the centre line.

Fig. 1 shows sketches of the base flow at subsonic and supersonic speeds. The flow separates at S and reattaches at R. Thus a dead-air region (SRA) is formed in which the velocity is low and the pressure is assumed to be constant everywhere and equal to the base pressure. The streamline SR is called the dividing stream line.

Because of the viscous interaction between the external stream and the fluid inside the dead-air region, a mixing layer which is called the free shear layer is developed after separation and entrains fluid from the dead-air region. Since the mass in this region must be conserved, a recompression is needed at the reattachment zone to slow down and eventually reverse part of the free shear layer back to the dead-air region.

The recompression process was investigated by Kadir. Fig. 3 shows some of his results. It is seen from these results that the pressure remains almost constant and equal to the base pressure for a distance of about $x/2h = 2/3$. Thereafter, the pressure starts to rise rapidly and the flow reattaches in a

region where the pressure is still rising. There is an appreciable pressure to be recovered by the flow between the reattachment point and far down stream. Eventually, the rate of the pressure rise becomes smaller and the flow presumably will recover to the free stream conditions far downstream. The adverse pressure gradient facilitates flow reversal and hence returns mass that has been entrained by the shear layers.

The features which distinguish boundary layer separation at a corner from the usual boundary layer separation are the sign and magnitude of the pressure gradient. In the classical separation the shear stress is zero at the point of separation and the pressure gradient is adverse causing the boundary layer to thicken, whilst at a corner the shear stress is high but finite and the pressure gradient is favourable causing the boundary layer thickness to decrease. Fig. 2 shows the flow approaching a corner with a boundary layer thickness δ_1, and expanding at the base to form a new boundary layer of thickness δ_2 just after separation.

The shape of the boundary layer velocity profile just after separation will play an important role in governing the rate of fluid entrainment by the free shear layer and hence the base pressure values.

The relationship between base pressure and Mach number for s particular case can be seen in Fig. 4 which is reproduced from Kadir's work.

In that part of the curve marked AB the flow up to the trailing edge is subsonic. As $\overline{M}e_1$ is increased towards unity, boundary layer thinning occurs. Together with increased flow speed, entrainment is increased, and increased flow reversal

produces a reduction in the base pressure.

At B the value of $\overline{Me}_1$ becomes unity. From this point a Prandlt-Meyer expansion centred near the corner causes the flow to turn towards the centre line. As $\overline{Me}_1$ increases beyond unity, that part of the curve marked BC, the angle of turn increases rapidly causing increased entrainment and rapid reduction in base pressure.

In Fig. 4 is shown Kadir's plot of the Prandlt Glauert solution:

$$\frac{Pb}{P_\infty} = 1 + \frac{\gamma M_\infty^2 \; Cpi}{2(1-M_\infty^2)^{\frac{1}{2}}}$$

where Cpi is the equivalent pressure coefficient for incompressible flow. For Cpi Kadir used experimentally measured values recorded by Gibbings and Sproston (Ref. 26). There is seen to be excellent agreement when the flow in the mainstream is subsonic.

At the point marked C, Pb/P_∞ is at a minimum value.

It is interesting to note that the minimum value of Pb/P_∞ occurswhen the Mach number just ahead of the trailing edge ($\overline{Me}_1$) is approximately 1.42. According to Weinbaum's analysis (Ref. 25), if the supersonic portion of the boundary layer is assumed to consist of an infinite number of layers with slightly different Mach numbers, then there will be waves reflecting from the slip lines that separate these layers, see Fig. 5. If $Mi < \sqrt{2}$ or $Mi > \sqrt{2}$ then the reflected waves are compression and expansion waves respectively. These waves will reflect at the sonic lines as waves of different signs. Therefore, compression waves are reflected as expansion waves at the sonic line as

shown in Fig. 6a. Both these sets of waves are such as to increase the angle through which the flow turns. The increase in the degree of expansion will increase the thinning of the boundary layer at separation, leading to a more vigorous entrainment effect, and consequently p_b/p_∞ will decrease.

When $Mi > \sqrt{2}$, then the reflected expansion waves will reflect as compression waves at the sonic line as shown in Fig. 6b. Now both sets of waves are such as to decrease the deflection of the flow. The reduction in the degree of expansion, will reduce the thinning of the boundary layer at separation and consequently p_b/p_∞ will increase.

3. APPARATUS

3.1 The transonic wind tunnel

The tests were carried out in a transonic wind tunnel with slotted walls (Fig. 7).

The test section is nominally 4" by 4" with slotted upper and lower surfaces. In each wall there are slots having a total open to closed area ratio of 1/14.

Schlieren glass windows are provided on the two solid side walls of the test section to enable flow visualisation.

The general layout of the closed air circuit for the transonic wind tunnel is shown in Fig. 8. The air is passed through a filter on an intake valve which is controlled by a remote control pressure regulator in the wind tunnel room. The air is compressed by a 4 stage turbo air compressor up to three atmospheres absolute.

The compressed air is then passed through an after cooler

and a settling chamber before entering the slotted wind tunnel, an after cooler by-pass being provided for fine temperature adjustment. After leaving the tunnel, air is cycled back to the intake valve. The humidity of the closed circuit air can be controlled by passing some of the air through a dryer.

A pitot-tube is provided in the settling chamber for measuring the total pressure. The settling chamber temperature is measured using a thermocouple.

To measure the boundary layer velocity profile and to investigate the wake, pressure probes can be inserted inside the working section through the solid side wall. A traverse gear is designed for this purpose. Movement along the length of the tunnel was facilitated by a crank and pinion mechanism, with the crank shaft extending through the tunnel wall. A rotation of 1.0° of the crank (measured with the use of a protractor as a dial) produced 0.001" movement of the probe along the length of the tunnel. Vertical movement was measured by the use of a dial-gauge graduated in intervals of 0.001".

3.2 The base bleed air supply system

Fig. 9 shows the bleed air supply system. Air from the reciprocating compressor passes through throttle valves, a pressure control valve and an orifice plate. The orifice plate is made according to B.S. specifications with inside and outside diameters of 27/32" and $1\frac{3}{8}$" respectively. A thermometer is used to measure the air total temperature downstream of the orifice.

3.3 The test models

Fig. 10 shows the model dimensions. The models are symmetrical about the centre-line with pressure tappings on both upper and lower surfaces and at the base (Fig. 11). For the circular hole base and the flared hole base the base pressure tapping was situated above the centre-line of one of the holes near the centre of the base. The three models used are identical in form and dimensions and only differ in the nature of their base geometries (Fig. 12).

To provide for the base bleed, the models are hollow with an air inlet port through each side.

The aft part of the model is designed with a contour similar to that of a supersonic nozzle, in which the contour must first curve outward and then backward until it is parallel to the flow direction.

The model can be set at different angles of incidence with respect to the tunnel. In this way different Mach number distributions can be created on the upper and lower surfaces of the model. In particular, differences of Mach number and boundary layer thickness across the trailing edge can be obtained to simulate conditions at the trailing edge of a turbine blade.

3.4 The pressure probe

The measurement of static pressures in the transonic flow regime presents some difficulty. In this flow regime the static pressure tapping does not give an easily interpretable measurement. However, experimental results (Ref. 27) have

shown that by using a conical probe, a correction of 0.002 to 0.004 is needed for the Mach number correction over the range of 0.98 to 1.2.

The probe (Fig. 13) was calibrated in the uniform flow in the otherwise empty test section; the static pressure tapping being at the same streamwise position as that of the plenum chamber tappings. It was assumed that there was no difference between the static pressure recorded by the plenum chamber tappings and the true static pressure of the undisturbed flow. Fig. 14 shows the calibration curve for the pilot-static probe.

4. EXPERIMENTAL PROCEDURE

Two identical circular wires were fixed along the span on the upper and lower surfaces of the model at a chord-wise distance of 0.475" from the leading edge. The purpose of the wires was to fix transition at the wire position and to afford a variety of boundary layer thicknesses. Kadir in his investigation on the slotted model used two wire diameters: 0.007" and 0.024". For comparison with Kadir's results and invesitigation of the effect of boundary layer thickening, a pair of 0.092" diameter wires was attached to the model with a slot base and a pair of 0.007" diameter wires was attached to each of the other two models.

The model was aligned at zero angle of incidence by balancing the pressure recorded by the tappings on the upper and lower surfaces.

The base pressure was investigated for a free stream Mach number range of 0.6 to 1.3.

5. EXPERIMENTAL RESULTS AND DISCUSSION

5.1 Surface pressure distributions

These are shown as a variation of Mach number corresponding to local static pressure on the upper surface of the model.

Figs. 15 (a, b, c, d) show surface Mach number variation for the slotted base with zero base bleed flow and a transition wire diameter of 0.092".

For 0^{o} incidence there are two principal features, the first being the penetration of the low base pressure upstream of the trailing edge giving expansion towards the corner. The distance to which the low base pressure penetrates upstream diminishes with increasing Mach number. The second principal feature is that for Mach numbers greater than 0.85 a surface shock wave develops.

At 2^{o} incidence the surface pressure distribution is very much the same as for 0^{o} incidence.

When the angle of incidence is 4^{o} the shock wave causes separation of the boundary layer from the model surface for Mach numbers of 0.9 and 1.01. At a Mach number of 1.15 the flow has reattached to the model surface.

For an angle of 6^{o} the shocks have increased in strength. The flow is separated at the trailing edge for Mach numbers of 0.93 to 1.07, and reattaches at a Mach number of 1.16. It is apparent that as the Mach number is increased the position of the shock wave moves towards the trailing edge.

Figs. 16 (a, b, c, d) show surface Mach number variation for the circular hole base with zero base bleed flow and a

transition wire diameter of 0.007".

For 0^{o} incidence the penetration of the low base pressure upstream is again evident.

At 2^{o} incidence the surface pressure distribution is very much the same as for 0^{o} incidence.

At 4^{o} incidence, separation of the flow from the model surface occurs at Mach numbers of 0.8 and 0.9. The flow reattaches at a Mach number of 1.0.

For 6^{o} incidence the flow is separated for Mach numbers of 0.9 and 1.0.

Generally, the same features occur for the circular hole base as for the slot but the general level of Mach number over the downstream part of the blade is lower than in Figs. 15 and therefore lower than in Kadir's case. This implies higher values of static pressure, less diffusion and therefore thicker boundary layers (for wd = 0.007") than in Kadir's at the trailing edge.

Fig. 17 shows the surface Mach number variation for the flared hole base with zero base bleed flow and a transition wire diameter of 0.007".

The results are similar to Fig. 16a for the circular hole base.

5.2 Boundary layer traverses upstream of the trailing edge

Boundary layer measurements were taken at 0^{o} incidence and at a point 0.4" upstream of the trailing edge. At this point the pressure gradient in the stream-wise direction was small. Therefore, the static pressure across the boundary layer was

assumed constant and equal to the pressure recorded by the surface tapping at that point.

Figs. 18 (a, b, c) are non-dimensional and show the same general form of velocity distribution. A near-correspondence with the 1/7 power law confirms that the boundary layers are turbulent.

Table 1 gives the boundary layer momentum and displacement thicknesses for M_∞ = 0.6, 1.0 and 1.3 for the three models and their respective transition wire diameters. Table 2 shows the boundary layer characteristics as measured by Kadir on the slotted model for transition wire diameters of 0.007" and 0.024".

Comparing the results for the slotted model shows that as the transition wire diameter is increased so is the boundary layer thickness (and as a consequence so is the base pressure). This is discussed further in section 5.3.

The effect of increasing the Mach number is to reduce the boundary layer thickness.

The boundary layer characteristics for the circular hole and flared hole base are virtually identical. Comparison of these results with those measured by Kadir on the slotted base with a 0.007" diameter transition wire shows that in all cases the boundary layer thickness on the slotted base is larger.

5.3 Base pressure - slotted base, Wd = 0.092"

Figs. 19 (a, b, c, d) show the variation of p_b/p_∞ with Mach number for the slotted base with a transitionwire diameter of 0.092". Kadir's results for thinner transition wires are also shown.

For 0^{o} incidence the results for wd = 0.092" lie everywhere above those for wd = 0.024" and wd = 0.007". Thus a thicker boundary layer gives a higher value of $^{Pb}/P_{\infty}$.

As the Mach number (M_{∞}) is increased $^{Pb}/P_{\infty}$ decreases to a minimum value at which M_{∞} is approximately 1.1. Thereafter $^{Pb}/P_{\infty}$ increases as the Mach number is increased. When $^{Pb}/P_{\infty}$ is a minimum, Me_1 (the Mach number at the edge of the boundary layer 0.4" upstream of the trailing edge) is approximately 1.27 and $\overline{Me}_1$ (the Mach number immediately before the trailing edge) is approximately 1.41. This evidence supports the hypothesis given in section 2.5.

For M_{∞} approximately equal to 0.8 ($\overline{Me}_1 \simeq 1.0$), $^{Pb}/P_{\infty}$ begins to fall more rapidly than for lower Mach numbers. This is in accordance with the idea that as the Mach number at the point of separation becomes unity a Prandlt-Meyer expansion develops, causing the flow to turn more severely, which results in greater entrainment in the shear layers and as a consequence the base pressure decreases.

For 2^{o} incidence and a Mach number of 0.6 there is very little difference in $^{Pb}/P_{\infty}$ to that at 0^{o}. For $0.7 \leqslant M_{\infty} \leqslant 0.85$ the greater diffusion on the blade surface gives a thicker boundary layer and therefore less entrainment. This leads to a higher $^{Pb}/P_{\infty}$ value. At $M_{\infty} = 0.85$ ($\overline{Me}_1 \simeq 1.0$) $^{Pb}/P_{\infty}$ begins to fall more rapidly (as for $\alpha = 0^{o}$) but diffusion is greater and therefore $^{Pb}/P_{\infty}$ remains higher. At $M_{\infty} = 1.1$ ($\overline{Me}_1 \simeq 1.4$) a minimum is reached and for $M_{\infty} > 1.1$ the results are similar to those for zero angle of incidence.

At 4^{o} incidence, the point at which $^{Pb}/P_{\infty}$ begins to fall rapidly occurs between $M_{\infty} = 0.85$ and 0.9 ($\overline{Me}_1 \simeq 1.02$).

Diffusion on the blade surface is greater still and therefore p_b/p_∞ is higher for all Mach numbers up to 1.1 ($\overline{Me}_1 \simeq 1.4$ to 1.5) at which the minimum value of p_b/p_∞ is equal to 0.4. For a Mach number greater than 1.1, the effect of incidence is small.

At 6° incidence and for Mach numbers up to 1.0, the results are similar to those for 4° incidence. Above $M_\infty = 1.0$ the surface shock wave approaches the trailing edge giving flow separation for $M \leq 1.07$. At $M_\infty = 1.16$ ($\overline{Me}_1 \simeq 1.6$) the flow is attached. At this Mach number p_b/p_∞ is a minimum and is approximately 0.46, i.e. higher than for $0^\circ < \alpha < 4^\circ$.

In general the effect of the thicker transition wire (and consequently a thicker boundary layer) is to increase the value of p_b/p_∞ including the minimum value.

The Weinbaum-based hypothesis given in section 2.5 appears quite good up to six degrees incidence - but at this incidence and for M_∞ greater than 1.0 the trailing edge boundary layer is greatly influenced by the shock wave on the model surface upstream of the trailing edge.

Also, from Kadir's results it is seen that the increase in wire size from 0.007" to 0.24" has little effect on p_b/p_∞ for a given angle of incidence. However, the further increase to 0.092" does have an appreciable effect.

5.4 Base pressure - circular hole base

Figs. 19 (a, b, c, d) show the variation of p_b/p_∞ with Mach number for the circular hole base with a transition wire diameter of 0.007".

For 0° incidence and $0.6 < M_{\infty} < 1.25$ the values of p_b/p_{∞} are everywhere higher than those for the slotted base with the same transition wire diameter. For $M_{\infty} > 0.8$, Fig. 16 shows lower values (than those recorded by Kadir) of surface Mach number near the trailing edge, so that the boundary layer will be thicker, giving higher values of p_b/p_{∞}.

At 2° incidence there is a close correspondence between the results for the slot and the circular hole base up to $M_{\infty} = 1.0$. Thereafter the curve for the circular hole base follows that for the slot base with a transition wire diameter of 0.092".

At 4° incidence there is a complete correspondence with Kadir's results up to $M_{\infty} = 1.1$, including the minimum value of p_b/p_{∞}.

For 6° incidence the correspondence with Kadir's results is good except for one point at $M_{\infty} = 1.1$.

A comparison of the general character of the curves for the slotted base and the circular hole base with the same transition wire diameter for zero incidence and in the Mach number range $0.6 < M_{\infty} < 1.0$ shows a close similarity even though the base pressure for the circular hole base are higher. It is for $1.0 < M_{\infty} < 1.25$ that differences in the character of the curves develop. In this Mach number range the curve for the circular hole base is similar in nature to that for the slotted base with a transition wire diameter of 0.092". As indicated in section 2.2 it is in this Mach number range that the transition from unstdady periodic base flow to steady base flow probably occurs.

5.5 Base pressure - flared hole base

Fig. 20 shows the variation of P_b/P_∞ with Mach number for the flared hole base and the circular hole base with a transition wire diameter of 0.007".

It is seen that the results are identical. The difference in the nature of the base geometries has no effect on the base pressure for the case of no base bleed.

5.6 Effect of base bleed - slotted base, wd = 0.092"

Figs. 21 (a, b, c, d) show the variation of P_b/P_∞ with Cq for various Mach numbers and angles of incidence.

The general trend of these results is that as the rate of base bleed is increased the base pressure is increased until the base pressure reaches a maximum value. Thereafter, the base pressure decreases with a further increase of base bleed rate. The bleed rate at which P_b/P_∞ is a maximum will be referred to as the optimum bleed rate.

The effect of the bleed air on the base pressure is explained as follows (refer to Fig. 22). As Cq increases from zero the bleed air occupies an increasing part of the separation region. The bubble of recirculating air is moved away from the slot and reduces in size. As the amount of recirculation diminishes the pressure gradient to reattachment diminishes and P_b/P_∞ increases to a maximum value. As Cq increases further the recirculation becomes confined to the lee of the two lips on either side of the slot. The bleed air now acts to increase entrainment from these regions and P_b/P_∞ is reduced.

The effect of base bleed on base pressure for the slotted base with a transition wire diameter of 0.024" was investigated by Kadir (these results are not presented here). Comparing his results with those for the slotted base with a transition wire diameter of 0.092" at zero angle of incidence reveals that for subsonic flow the effect of the thicker boundary layer is to produce higher values of p_b/p_∞ throughout the range of bleed rates. However, at $M_\infty = 1.0$ there is not much difference and for $M_\infty > 1$ the value of (p_b/p_∞) max., for the case with a thicker transition wire, is marginally lower.

Therefore for the thicker boundary layer, blowing is less effective in increasing the value of base pressure up to (p_b/p_∞) max. At higher values of Cq the differences due to boundary layer thickness are quite small, indicating that the entrainment due to the bleed air is the determining factor.

For angles of incidence greater than 0° the effect of incidence is to increase the values of p_b/p_∞ everywhere (as in the case for zero blowing). The effect of the thicker boundary layer is quite small over the whole range of bleed rates.

5.7 Effect of base bleed - circular hole base, wd = 0.007"

Refer to Figs. 23 (a, b, c, d). A comparison with Kadir's results for the slotted base with a transition wire diameter of 0.024" will be made where relevant.

At 0° incidence and for Mach numbers up to 1.3 there is little difference between the curves for the slotted base and the circular hole base for small values of Cq. However, the value of (p_b/p_∞) max. occurs at lower values of Cq for the

circular hole base. For higher values of Cq, i.e. greater blowing rates, the values of p_b/p_∞ for the circular hole base are substantially smaller than for the slot. It appears that the greater peripheral area of a circular jet when compared with that of the sheet-like nature of the ejected air from the slot, promotes greater entrainment of air from the base region.

At $M_\infty = 1.3$ there is little difference between the results for the circular hole base and the slot.

For angles of incidence greater than 0° and $M_\infty = 0.6$ (Fig. 23b) the incidence angle has less effect for the circular holes than in the case of the slot - values of p_b/p_∞ are generally lower for higher values of Cq.

For $M_\infty = 1.0$ (Fig. 23c) there is virtually no effect of incidence for $\alpha \leqslant 4^\circ$. The values of p_b/p_∞ are much lower than for the slot and the curves have a sharper maximum. At 6° incidence, values of base pressure are much increased over the whole range of bleed rates - but still lower than for the slot.

It appears that there is a substantial change in flow regime between $\alpha = 4^\circ$ and $\alpha = 6^\circ$. The bleed air maintains lower values of p_b/p_∞ until the effect of the blade surface shock becomes assertive at 6° incidence.

For a Mach number of 1.3 (Fig. 23d) the curves are identical for $\alpha = 0^\circ$ and $\alpha = 2^\circ$ and for $\alpha = 4^\circ$ and $\alpha = 6^\circ$. Once again there is evidence of a change of flow regime. For $2^\circ \leqslant \alpha \leqslant 6^\circ$, values of p_b/p_∞ are everywhere lower than for the slotted base, reflecting the greater entrainment effect.

5.8 Effect of base bleed - flared holes, wd = 0.007"

Refer to Fig. 24. Results are only available for 0^{o} incidence.

The effect of base bleed is much the same as for the circular hole base (compare Fig. 24 with Fig. 22a). The only difference is that for $M_{\infty} > 1$ the values of (P_b/P_{∞}) max. are smaller and occur at higher values of Cq. The effect of flaring is to diffuse the jets of bleed air and it appears that at sonic and supersonic speeds they become less effective in opposing the recirculation and moving the recirculation zone downstream. However, at higher values of Cq they are equally effective in producing entrainment and reducing the value of base pressure.

5.9 Wake total pressure profile - circular hole base, wd = 0.007"

A viscous loss coefficient, Cv_L, is defined as:

$$C_{v_L} = \int_{-\delta/h}^{+\delta/h} \frac{P_{o\infty} - P_o}{P_{o\infty} - P_{\infty}} \, d(y/h)$$

where $\pm \delta$ marks the edges of the viscous shear flow in the wake.

Values of Cv_L are given in Tables 3 and 4 along with a pressure coefficient, Cpb, defined as:

$$C_{p_b} = \frac{P_{\infty} - P_b}{P_{o\infty} - P_{\infty}}$$

All the wake traverses were taken at a distance of $x/2h = 8.33$ downstream of the trailing edge.

Figs. 25 (a, b, c, d) show the wake profiles for the circular hole base at 0° incidence.

Fig. 25a gives the results for $M_{\infty} = 0.6$. As the base bleed rate increases from zero to the optimum value (i.e. for (P_b/P_{∞}) max.) there is an increase in base pressure even though the total pressure on the wake centre line is lower than for the case of no base bleed. This is probably because the initial effect of the base bleed is to move the recirculation zone away from the trailing edge and therefore nearer to the traverse plane.

The value of Cv_L is reduced from 1.7 for the case of no bleed to 1.41 for optimum blowing. This is in spite of the reduced total pressure on the centre line.

Fig. 25b shows the results for $M_{\infty} = 1.0$. The value of Cq optimum, i.e. for (P_b/P_{∞}) max., is smaller than for $M_{\infty} = 0.6$ and correspondingly the bleed mass flow rate is smaller. P_b/P_{∞} is also lower corresponding to more acute turning of the shear layer. Presumably the recirculation zone remains nearer to the trailing edge so that the total pressure distribution at the traverse plane is more orthodox - as blowing increases the base pressure the total pressure on the wake centre line also increases. It is at this Mach number that the maximum value of viscous wake loss occurs. However, the effect of blowing for (P_b/P_{∞}) max. gives a large reduction in Cv_L.

At the edge of the viscous wake the total pressure is reduced as a result of losses through shock waves.

The results for $M_{\infty} = 1.135$ are given in Fig. 26c and are

qualitatively similar to those for $M_\infty = 1.0$.

Fig. 25d shows the results for $M_\infty = 1.3$.

The effect of optimum blowing is to reduce the total pressure on the centre line of the wake (as for $M_\infty = 0.6$). For this case Cq opt. is lower than for $M_\infty \leqslant 1.0$ and therefore M opt. is lower. The recirculation zone will be near to the trailing edge but the flow immediately adjacent will be the low-momentum bleed air and this presumably causes the low centre-line total pressure. However, the effect of blowing on Cv_L is very small.

For the effect of angle of incidence on Cv_L refer to Figs. 26 (a, b), 27 (a, b) and 28 (a, b).

The general character of the results is similar to that for 0° incidence but with the wake centre line offset. At 6° incidence and $M_\infty = 0.6$ the value of Cv_L is increased by blowing which causes a marked asymetry of the total pressure distribution in the wake, possibly by a displacement of the recirculation zone. For a Mach number of 1.0 and an angle of incidence of 2° and 4° the values of Cv_L are lower than for 0°, but the effect of blowing changes little. At $M_\infty = 1.3$ the effect of blowing in reducing Cv_L is somewhat enhanced for 2° and 4° as compared with 0°. In this case by contrast with $M_\infty = 0.6$ the effect of blowing is to improve the symmetry of the flow in the wake.

5.10 Wake total pressure profile - flared hole base, wd = 0.007"

Refer to Figs. 29 (a, b, c, d). Results are only available for 0^{o} incidence.

The general form of the wake profiles is similar to that for the circular hole base and values of Cpb are virtually identical. For $M_{\infty} \leqslant 1.0$, however, the values of Cv_L are smaller than for the circular hole base. Presumably, the difference in Cv_L is occurring as a result of the effect of the base geometry on the base flow. The difference becomes smaller at $M_{\infty} = 1.135$ and practically disappears at $M_{\infty} = 1.3$.

The effect of blowing virtually eliminates any differences as can be seen from the values of Cv_L^*. It may be that the differences for the different base geometries arise from the effect of the base shape on shed vortices and that the effect of base bleed is to reduce the strength of the vortices in a similar manner to that of a splitter plate (refer to section 2.4).

5.11 Results of Schlieren Photography

Schlieren photographs were taken of the base region with the models set at 0^{o} incidence and for Mach numbers of 1.0, 1.1 and 1.3. For each Mach number the case of no base bleed and optimum base bleed were photographed.

Plates 1 (a, b), 2 (a, b) and 3 (a, b) show the base flow for the circular hole base for Mach numbers of 1.0, 1.1 and 1.3 respectively.

Plate 1a shows the base flow with zero bleed rate and Plate 1b shows the base flow with optimum bleed rate. In Plate 1a the dark region set at an angle and extending downstream from the corner of the base, marks the region in which a Prandlt-Meyer expansion occurs. Also visible are the thin shear layers and further downstream a trailing-edge shock.

A comparison of Plate 1a with 1b shows that the effect of base bleed is to reduce the angle through which the flow turns at the separation point.

In Plate 2a the increased Mach number results in an increased angle of turn and a more prominent trailing edge shock. Once again the effect of base bleed (Plate 2b) is to reduce the angle through which the flow turns at the separation point.

Plates 3a and 3b were taken with a longer exposure time for the purpose of showing the reflected pressure waves from the tunnel wall. This set of photographs shows a typical supersonic base flow pattern. The effect of base bleed on the flow pattern is small, although the change in direction of the shear layers is again reduced.

Plates 4 (a, b), 5 (a, b) and 6 (a, b) show the base flow for the flared hole base for Mach numbers of 1.0, 1.1 and 1.3 respectively.

The features of the base flow for the flared hole base appear to be much the same as for the circular hole base. However, the greater diffusion of the base bleed jets affects the base flow to a greater degree. The shear layers are less evident than for the circular hole base.

6. PROPOSALS FOR FUTURE WORK

It appears that a full understanding of the fluid mechanics of the base region requires an understanding of the role of periodic shed vorticity. It would be valuable to undertake an indepth investigation of the nature of shed vortex motions and the effect on them of base geometry and base bleed.

If data from the isolated aerofoil is to be used for turbine blade loss prediction it will be necessary to develop a means of calculating flows through turbine cascades taking account of base pressure effects and then to carry out cascade experiments to correlate the cascade results with those from the isolated aerodynamic body.

7. CONCLUSIONS

1. For the slotted base, as the transition wire diameter is increased and hence the boundary layer thickness, the base pressure is increased as a consequence.

2. The base pressure for the circular hole base and the flared hole base was found to be the same throughout the Mach number range for zero incidence.

3. For the same diameter transition wire of 0.007" and zero angle of incidence, the base pressure on the circular hole base was greater than that for the slotted base. However, at positive angles of incidence the base pressures were very similar.

4. As the bleed flow rate is increased from zero the base pressure rises to a maximum. With further increase in bleed flow rate the base pressure begins to fall. The rise to and including the maximum base pressure for the slot and circular hole base are much the same. At greater bleed rates the rate of fall of base pressure for the circular hole base is greater. This reflects the greater entrainment occurring as a result of the larger peripheral area of the circular jets.

5. The viscous wake losses for the flared hole base are smaller than for the circular hole base with zero bleed; however, with base bleed the losses are approximately the same. The effect of base bleed on

the total pressure losses in the wake is most effective at Mach numbers of 1.0 and 1.135. At these Mach numbers the total pressure loss in the wake flow was reduced by approximately 40% as a result of base bleed.

REFERENCES

Reference Number	Author	Title
1.	S. F. Hoerner	Base Drag and Thick Trailing-Edges. J. Aero. Sci. Vol.17, p.622. (1950)
2.	S. F. Hoerner	Fluid Dynamic Drag Published by the author
3.	A. Roshko	On the drag and shedding frequency of two-dimensional bluff bodies. N.A.C.A. TN - 3169 (1954)
4.	A. Roshko	On the wake and drag of bluff bodies. J. Aero. Sci., Vol.22, p.124. (1955)
5.	H. Thomann	Measurement of the recovery temperature in the wake of a cylinder and of a wedge at Mach numbers between 0.5 and 3.0. F.F.A. Report 84, Sweden (1959)
6.	R. H. Sawyer F. L. Daum	Measurements through the speed of sound of static pressures on the rear of unswept and sweptback circular cylinders and on the rear and sides of a wedge by N.A.C.A. wing-flow method. N.A.C.A. Research Memo L8B13 (1948)
7.	J. W. Cleary G. L. Stevens	The effects at transonic speeds of thickening the trailing-edge of a wing with a 4 per cent thick circular-arc aerofoil. N.A.C.A. Research Memo A51511 (1951)

Reference Number	Author	Title
8.	D. W. Dugan	Effects of three types of blunt trailing-edges on the aero-dynamic characteristics of a plane tapered wing of aspect ratio 3:1, with a 3 per cent thick biconvex section. N.A.C.A. Research Memo A52E01 (1952)
9.	J. D. Morrow E. Katz	Flight investigation at Mach numbers from 0.6 to 1.7 to determine the drag and base pressure on a blunt trailing-edge aerofoil and drag of a diamond and circular-arc airfoil at zero lift. N.A.C.A. Tech. Note 3548. (1955)
10.	J. F. Nash V. G. Quincey J. Callinan	Experiments on two-dimensional base flow at subsonic and transonic speeds. A.R.C. Reports and Memoranda No. 3427
11.	G. E. Gadd D. W. Holder J. D. Regan	Base pressures in supersonic flow. A.R.C. C.P. 271. (1955)
12.	D. R. Chapman	An analysis of base pressure at supersonic velocities and comparison with experiment. N.A.C.A. Tech. Note 2137 (1950)
13.	D. R. Chapman W. R. Wimbrow R. H. Kester	Experimental investigation of base pressure on blunt trailing-edge wings at supersonic velocities. N.A.C.A. Tech. Note 2611 (1952)
14.	A. F. Charwat J. K. Yakura	An investigation of two-dimensional base pressures. J. Aero. Sci., Vol. 25, p.122. (1958)
15.	L. Fuller J. Reid	Experiments on two-dimensional base flow at M = 2.4. A.R.C.R. 3064 (1956)

Reference Number	Author	Title
16.	E. S. Love	Base pressures at supersonic speeds on two-dimensional airfoils and on bodies of revolution with and without fins having turbulent boundary layers. N.A.C.A. Tech. Note 3819 (1957)
17.	I. MacMartin J. F. Norbury	The Aerodynamics of a Turbine Cascade with Supersonic Discharge and Trailing Edge Blowing. A.S.M.E. publication.
18.	D. W. Bearman	Investigation of the flow behind a two-dimensional model with a blunt trailing edge. J.F.M. Vol.21, pp. 221-255. (1965)
19.	R. Jaspel	Investigation of the trailing edge losses of a symmetrical, isolated aerofoil under transonic flow conditions. Thesis submitted for the Degree of M.Sc., Imperial College.
20.	T. H. Moulden	(unpublished N.P.L. work) 1962.
21.	P. W. Bearmen	Investigation into the effect of base bleed on the flow behind a two-dimensional model with a blunt trailing-edge. A.G.A.R.D. CP-4, pp.485-507. (1966)
22.	P. W. Bearmen	The effect of base bleed on the flow behind a two-dimensional model with a blunt trailing-edge. Aero. Quart., Vol.18, pp.207-214. (1967)
23.	C. J. Wood	The effect of base bleed on a periodic wake. J. R. Ae. Soc., Vol.68, pp. 477-482. (1964)
24.	F. Kadir	Transonic Base Flow. Ph.D. Thesis. The University of Liverpool.

Reference Number	Author	Title
25.	S. Weinbaum	Rapid expansion of a supersonic boundary layer and its application to near wake. A.I.A.A. Journal, Vol.4, pp. 217-226. (1966)
26.	J. L. Sproston J. C. Gibbings	The hodograph method of aerofoil and cascade design for incompressible flow. Part 5: The symmetrical aerofoil with blunt base. A.R.C. Report 35157/FM4463, Nov. 1973.
27.	E. P. Sutton	The development of slotted working section liners for transonic operation of RAE 3 ft. wind tunnel. A.R.C. R & M 3085.

TABLE 1

BOUNDARY LAYER DIMENSIONS AT 0·4" UPSTREAM OF THE TRAILING EDGE

($\dot{m}=0$. $\alpha=0°$)

SLOT , $w_d=0.092$

M_∞	δ	δ^*	θ
0·6	0·820"	0·161"	0·097"
1·0	0·293"	0·050"	0·023"
1·3	0·300"	0·042	0·023"

CIRCULAR HOLES . $w_d=0007"$

M_∞	δ	δ^*	θ
0·6	0·155"	0·025"	0·015"
1·0	0·105"	0·024"	0·011"
1·3	0·095"	0·021"	0·009"

FLARED HOLES , $w_d=0007"$

M_∞	δ	δ^*	θ
0·6	0·155"	0·025"	0·015"
1·0	0·105"	0·024"	0·011"
1 3	0·0 95"	0·021"	0·008"

TABLE 2

KADIR'S RESULTS FOR THE BOUNDARY LAYER DIMENSIONS AT 0.4" UPSTREAM OF THE TRAILING EDGE

($\dot{m}=0$, $\alpha=0^{\circ}$)

SLOT , $w_d = 0.024"$

M_∞	δ	δ^*	θ
0·6	0·32"	0·040"	0·028"
1·0	0·16"	0·033"	0·017"
1·3	0·15	0·027	0·015

SLOT , $w_d = 0.007"$

M_∞	δ	δ^*	θ
0·6	0·20"	0·029"	0·0174"
1·0	0·14"	0·027"	0·014"
1·3	0·12"	0·024"	0·0123"

TABLE 3

VISCOUS LOSS COEFFICIENTS FOR ZERO ANGLE OF INCIDENCE

CIRCULAR HOLES

M_∞	C_{VL}	C^*_{VL}	C_{Pb}	C^*_{Pb}
0·6	1·7	1·41	0·34	0·20
1·0	2·83	1·63	0·54	0·34
1·135	2·57	1·48	0·49	0·30
1·3	1·28	1·25	0·30	0·20

FLARED HOLES

M_∞	C_{VL}	C^*_{VL}	C_{Pb}	C^*_{Pb}
0·6	1·50	1·39	0·34	0·22
1·0	2·54	1·67	0·54	0·34
1·135	2·45	1·50	0·49	0·30
1·3	1·29	1·28	0·30	0·21

* With optimum base bleed

TABLE 4

VISCOUS LOSS COEFFICIENTS FOR CIRCULAR HOLES

$\alpha = 2°$

M_∞	C_{VL}	C^*_{VL}	C_{Pb}	C^*_{Pb}
0·6	1·74	1·51	0·29	0·18
1·0	2·75	1·72	0·54	0·35
1·3	1·47	1·26	0·28	0·19

$\alpha = 6°$

M_∞	C_{VL}	C^*_{VL}	C_{Pb}	C^*_{Pb}
0·6	2·24	2·37	0·15	0·18
1·0	2·36	1·45	0·42	0·29
1·3	1·38	1·20	0·26	0·18

* With optimum bleed

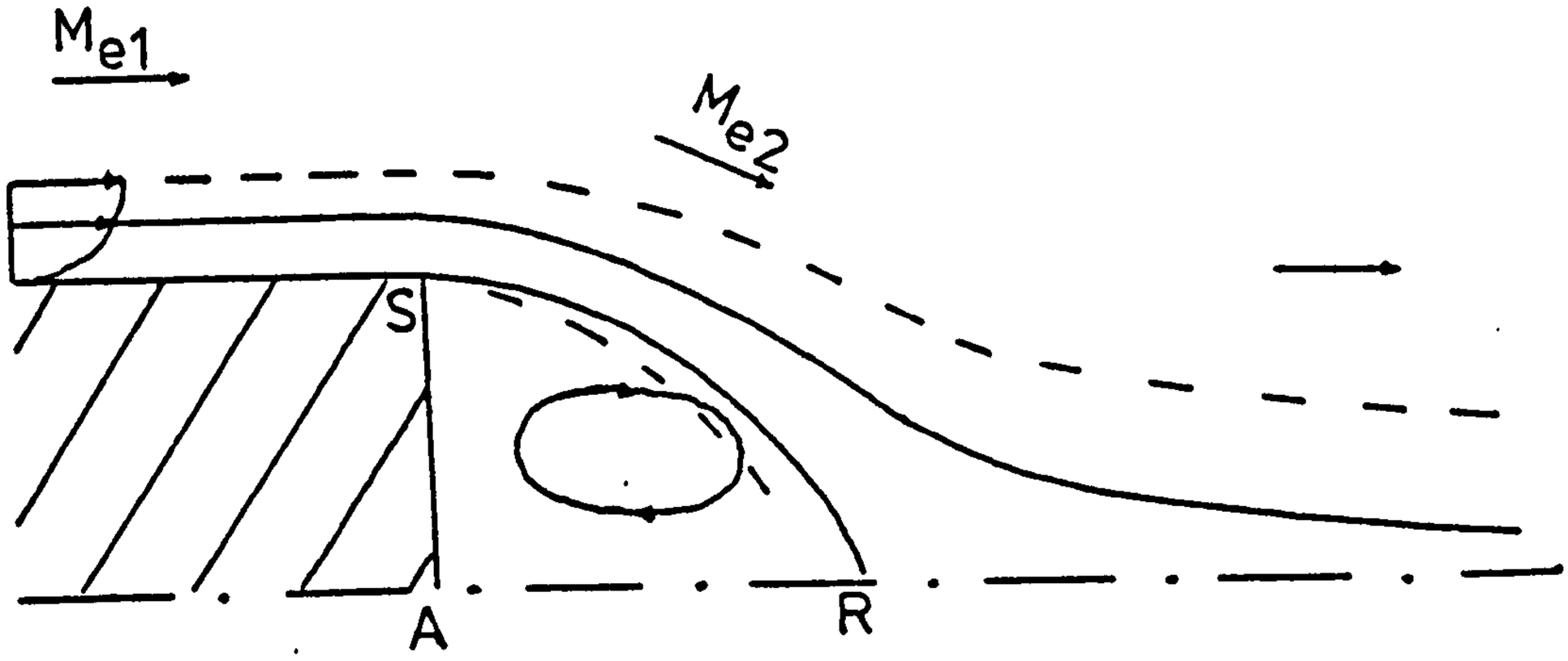

(A) Subsonic flow

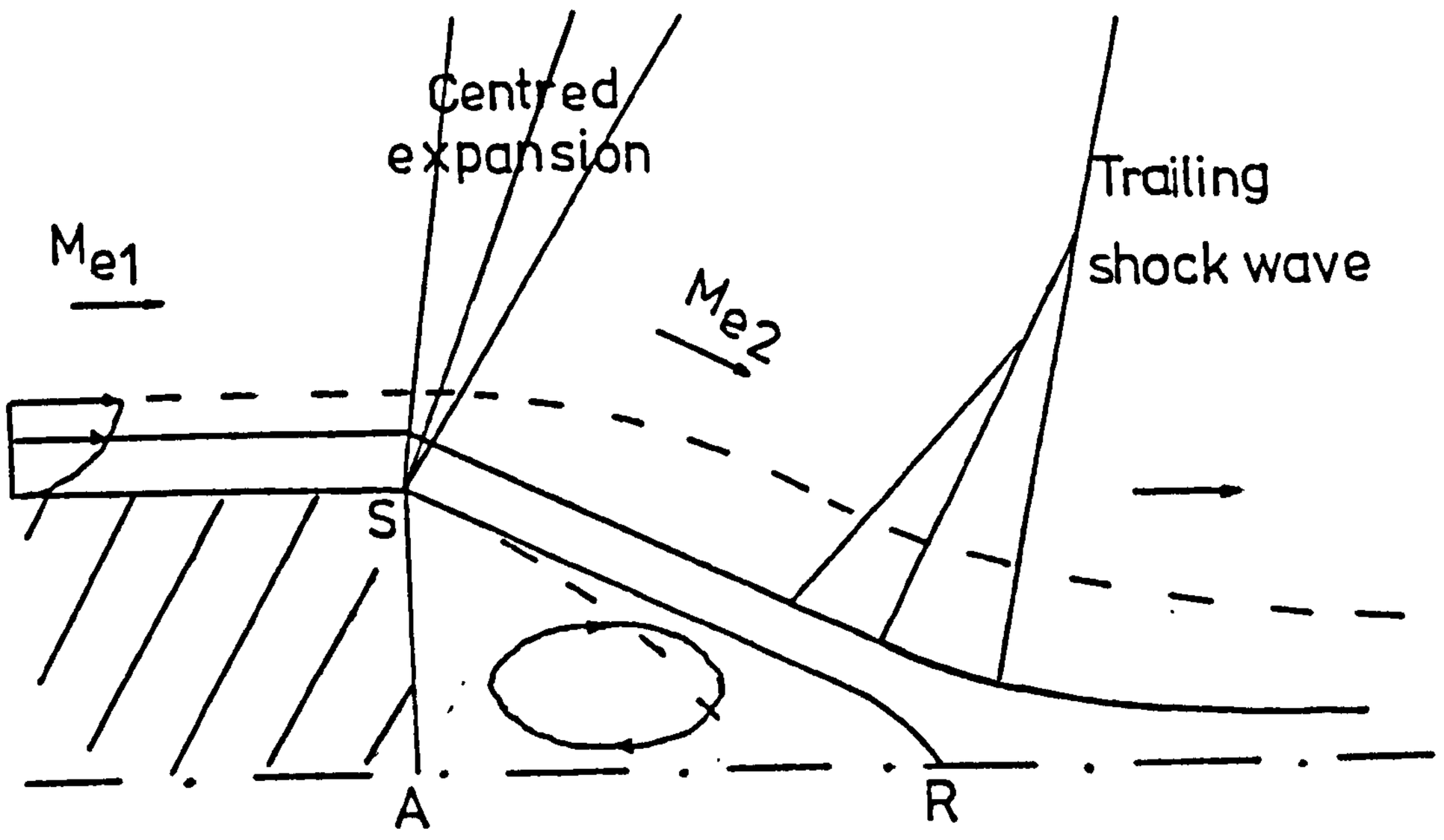

(B) Supersonic flow

— — — — shear layer edge

FIG1 SKETCH OF THE HYPOTHETICAL STEADY BASE FLOW

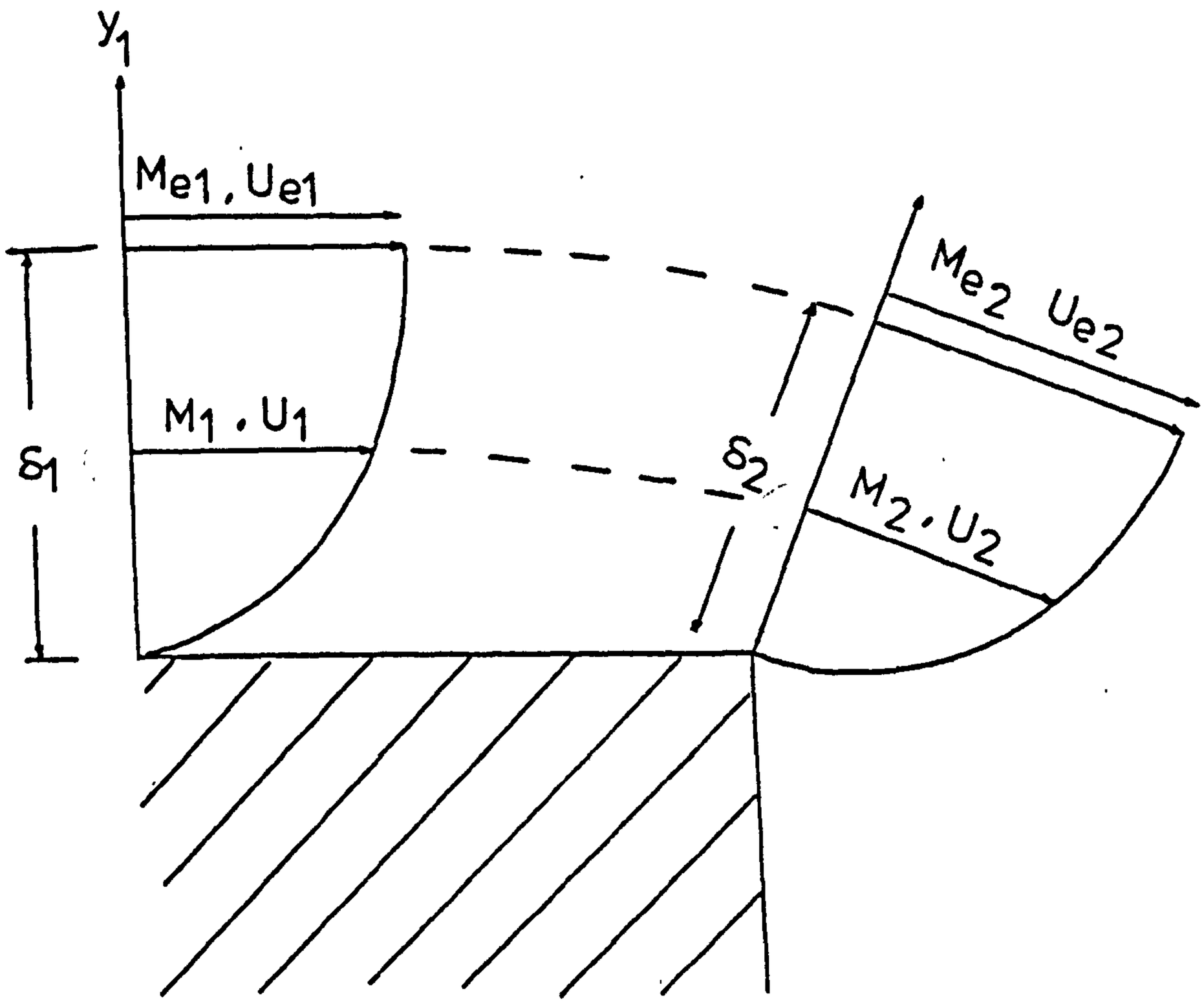

FIG 2 FLOW MODEL AT THE EXPANSION CORNER

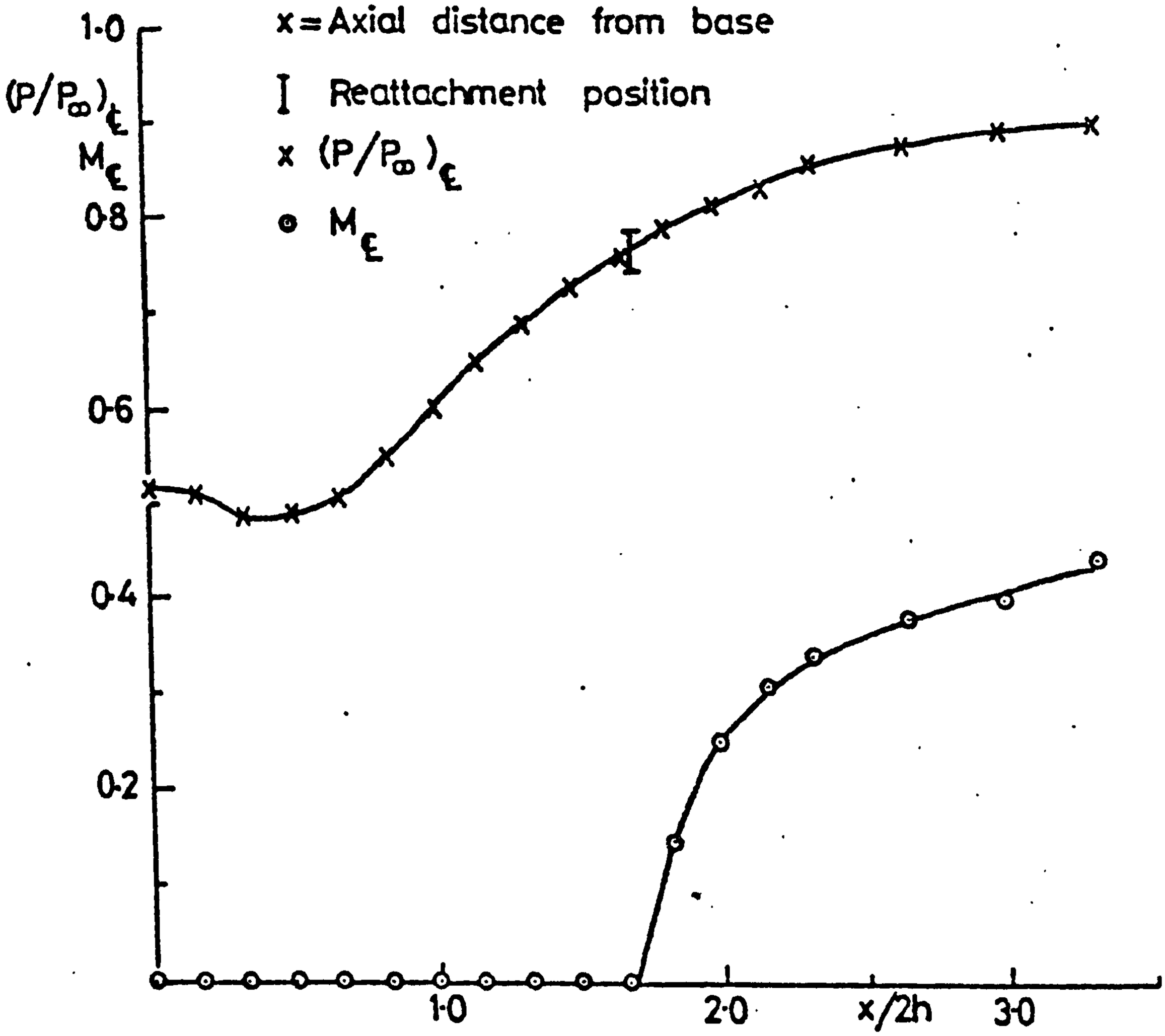

FIG. 3. AXIAL PRESSURE AND MACH Nº DISTRIBUTION FOR $M_{e,\infty}$=1·0 (d=·024", $\dot{m}$=0, α=0)

FIG.4. EFFECT OF MACH Nº ON BASE PRESSURE

$\alpha = 0$, $m = 0$, $d = \cdot 024$".

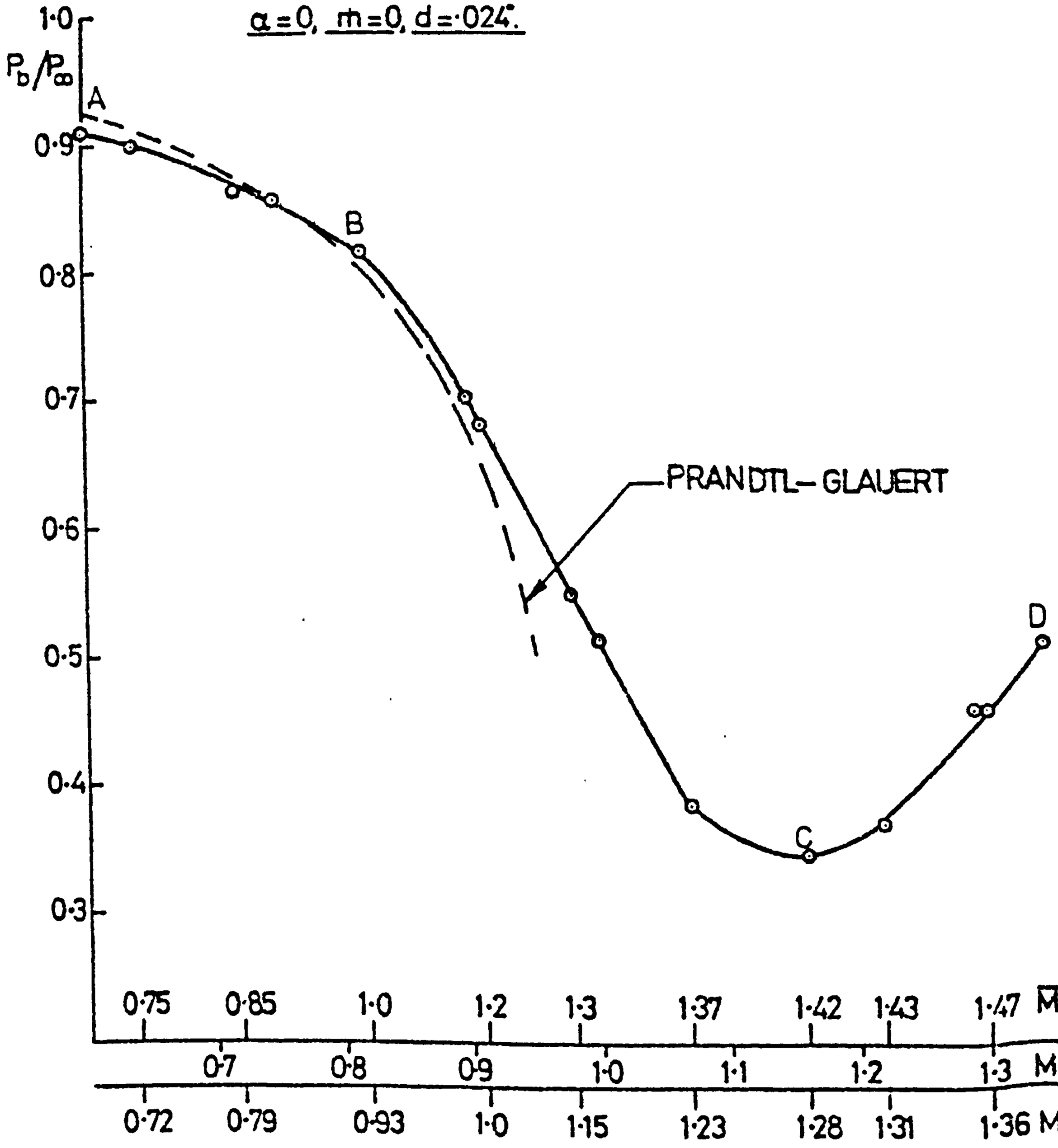

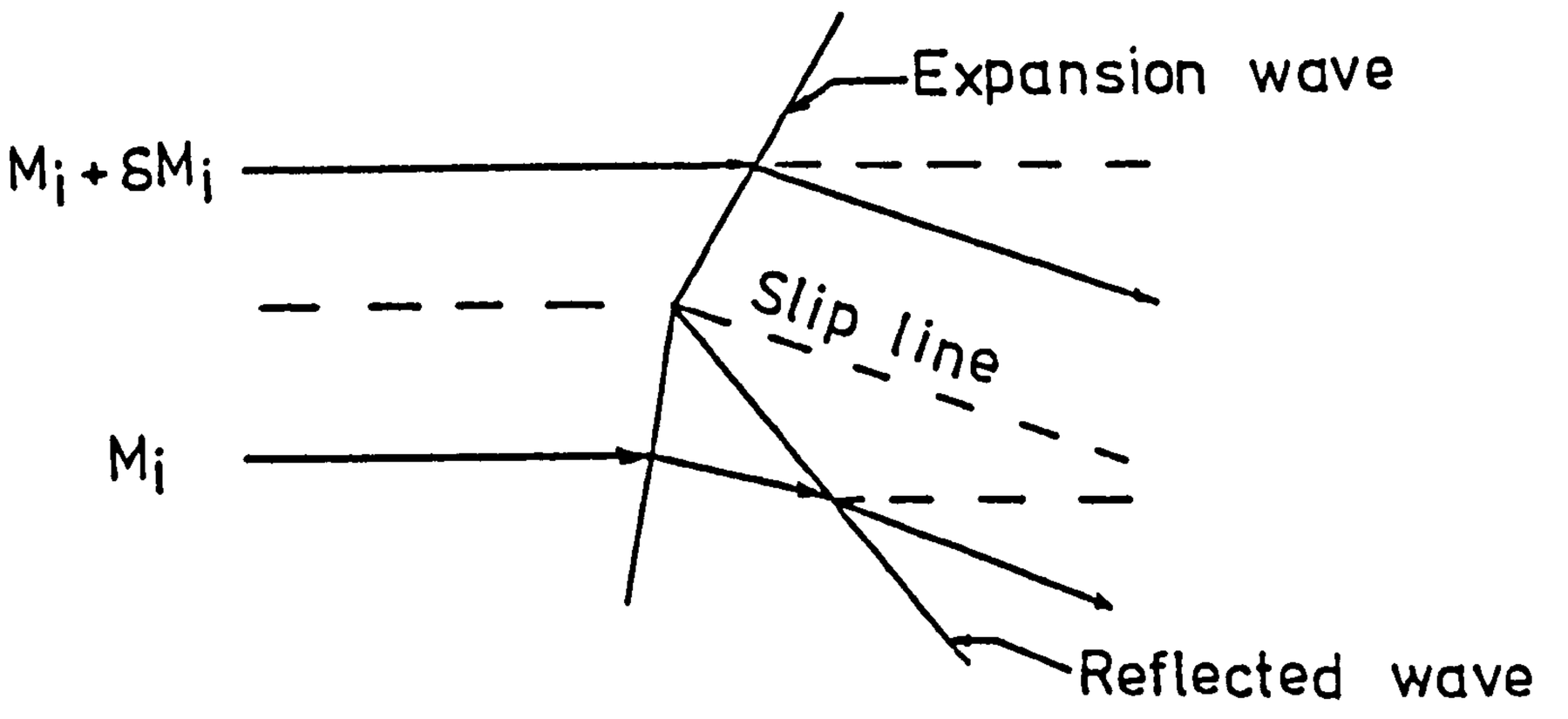

FIG.5. SCHEMATIC DIAGRAM FOR THE INTERACTION OF AN EXPANSION WAVE AT A WEAK MACH NUMBER DISCONTINUITY. (REF.25)

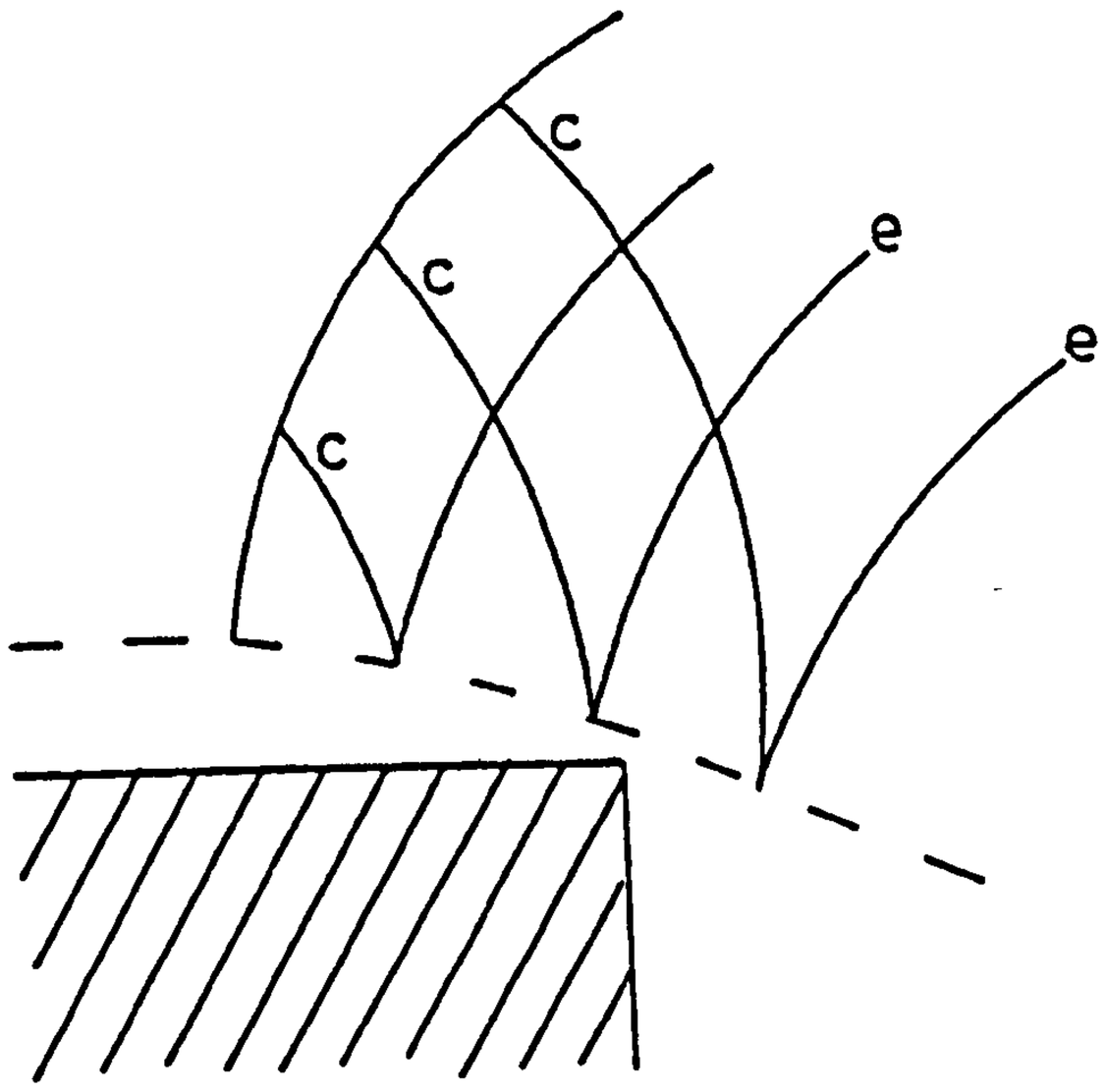

(A) $M_i < \sqrt{2}$

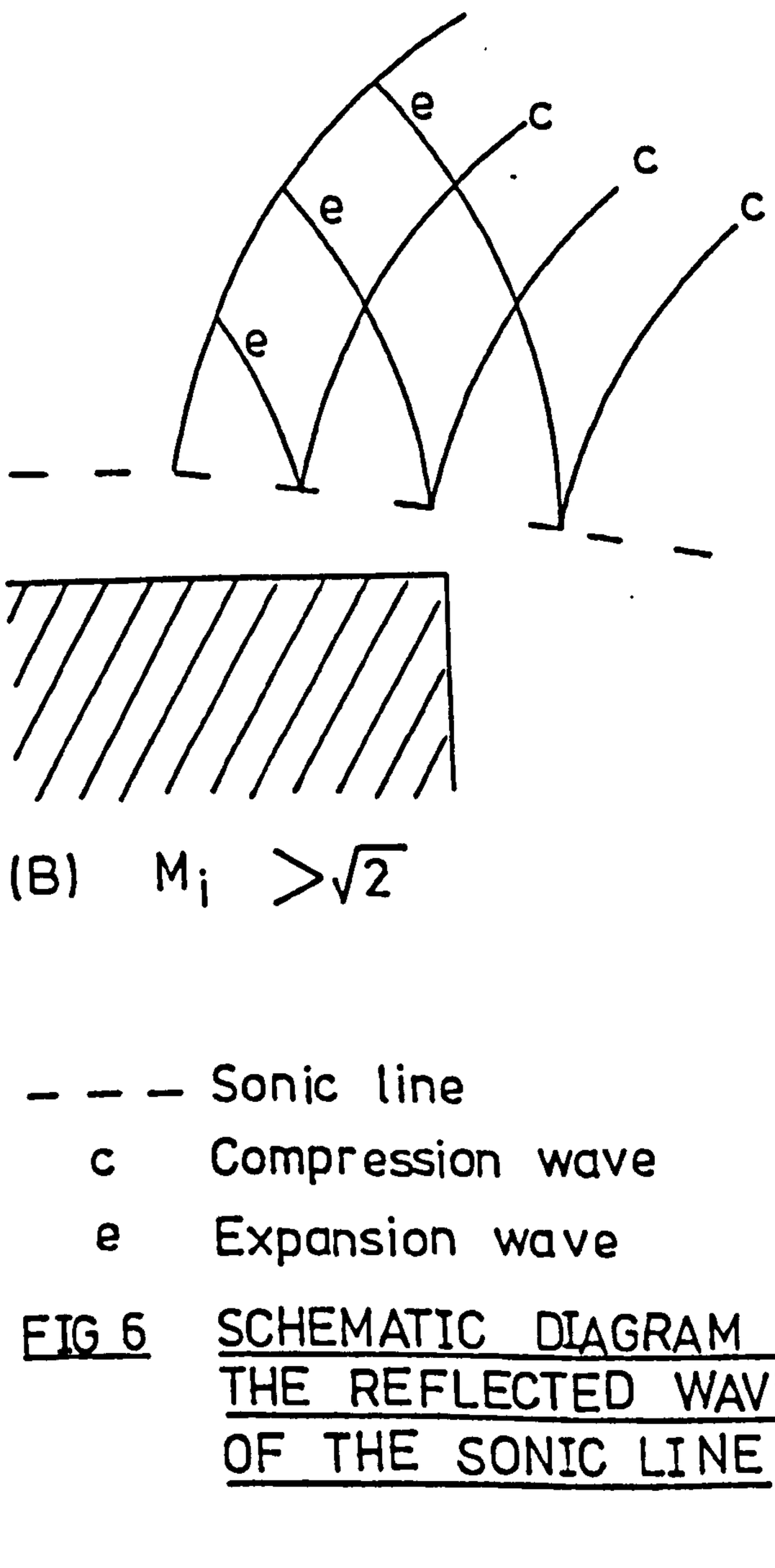

(B) $M_i > \sqrt{2}$

— — — Sonic line

c Compression wave

e Expansion wave

FIG 6 SCHEMATIC DIAGRAM OF THE EFFECT OF THE REFLECTED WAVES ON THE SHAPE OF THE SONIC LINE

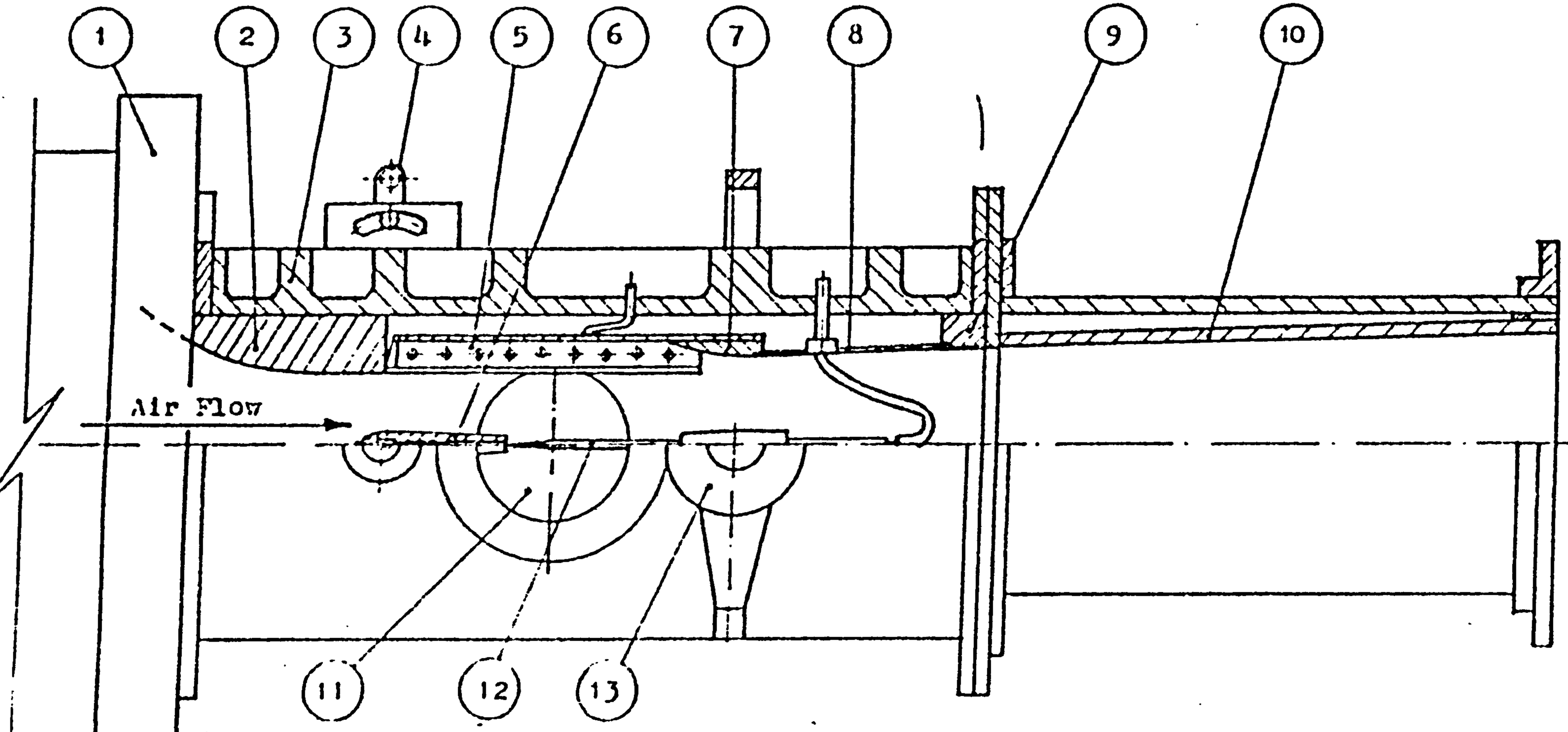

1) Settling Chamber. 2) Subsonic Linear. 3) Housing. 4) Blade Adjustment Gear.

5) Slotted Test Section. 6) Blade. 7) Slotted Wedge. 8) Transition Plate.

9) Transition Linear. 10) Diffuser. 11) Schlieren Glass Window. 12) Probe.

13) Traverse Gear.

GENERAL LAYOUT OF 4" HIGH SPEED WIND TUNNEL

FIG. 7

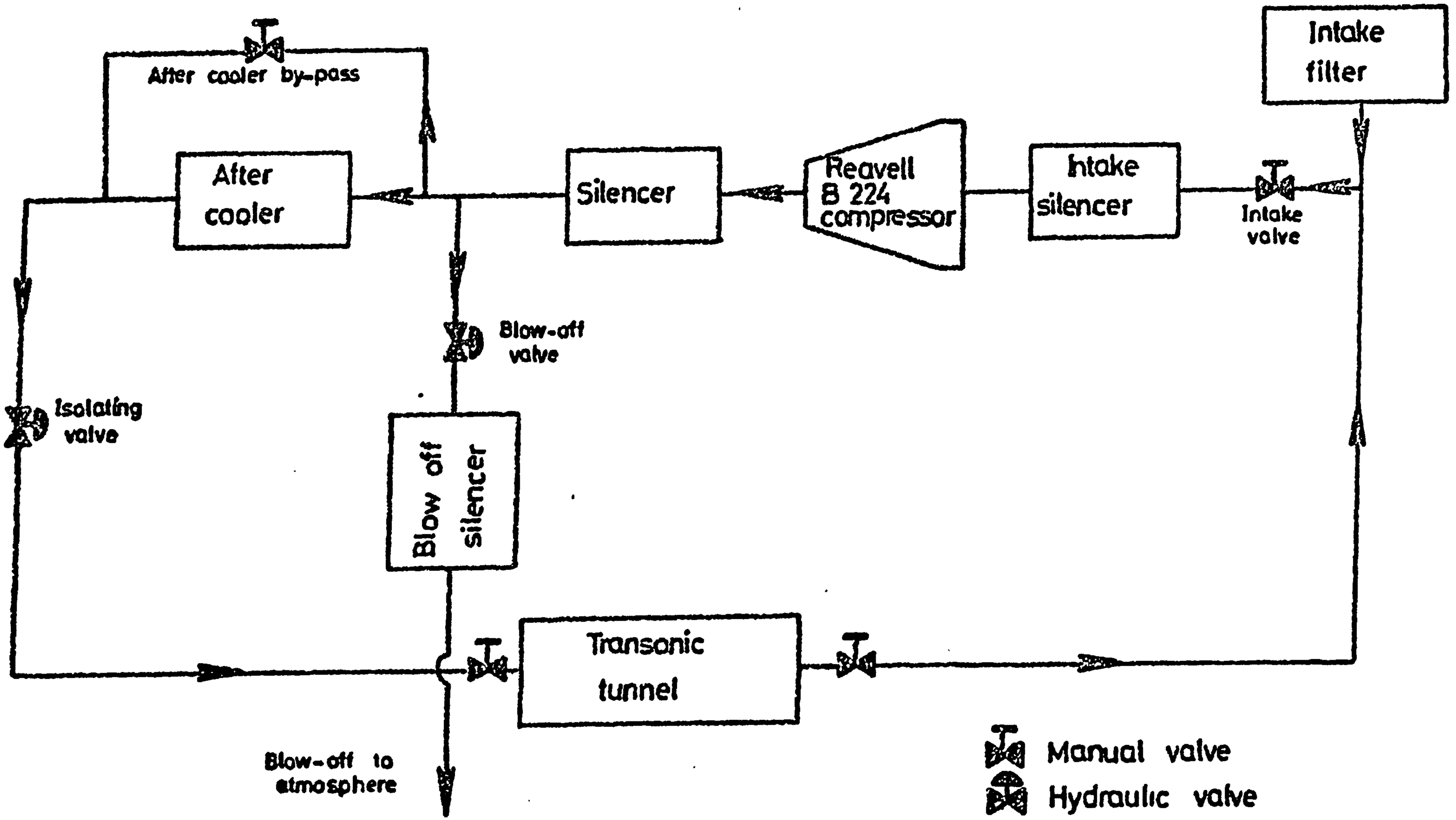

FIG. 8. TRANSONIC TUNNEL AIR CIRCUIT.

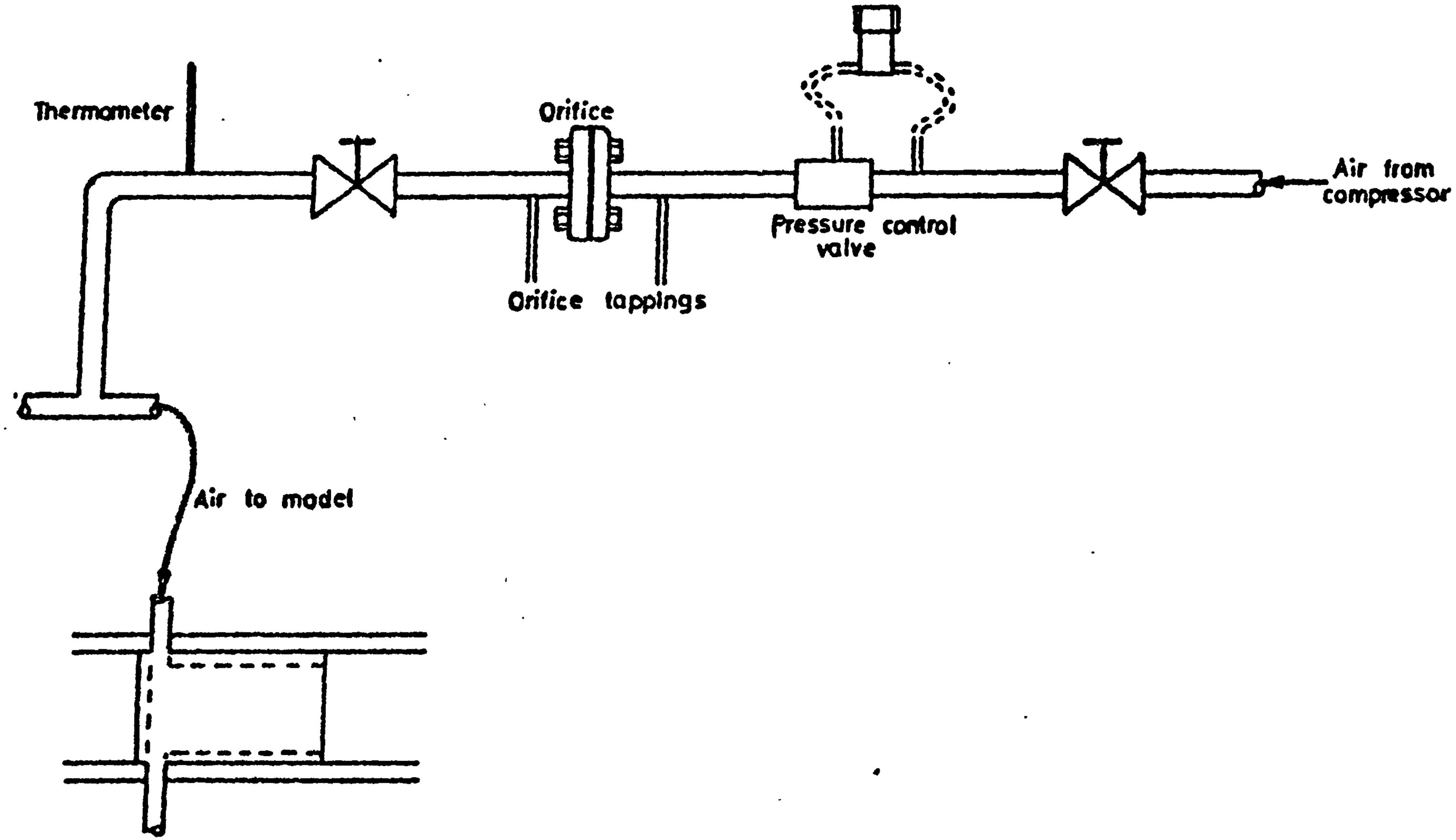

FIG. 9 AIR BLEED CIRCUIT

FIG. 10. THE BASIC MODEL

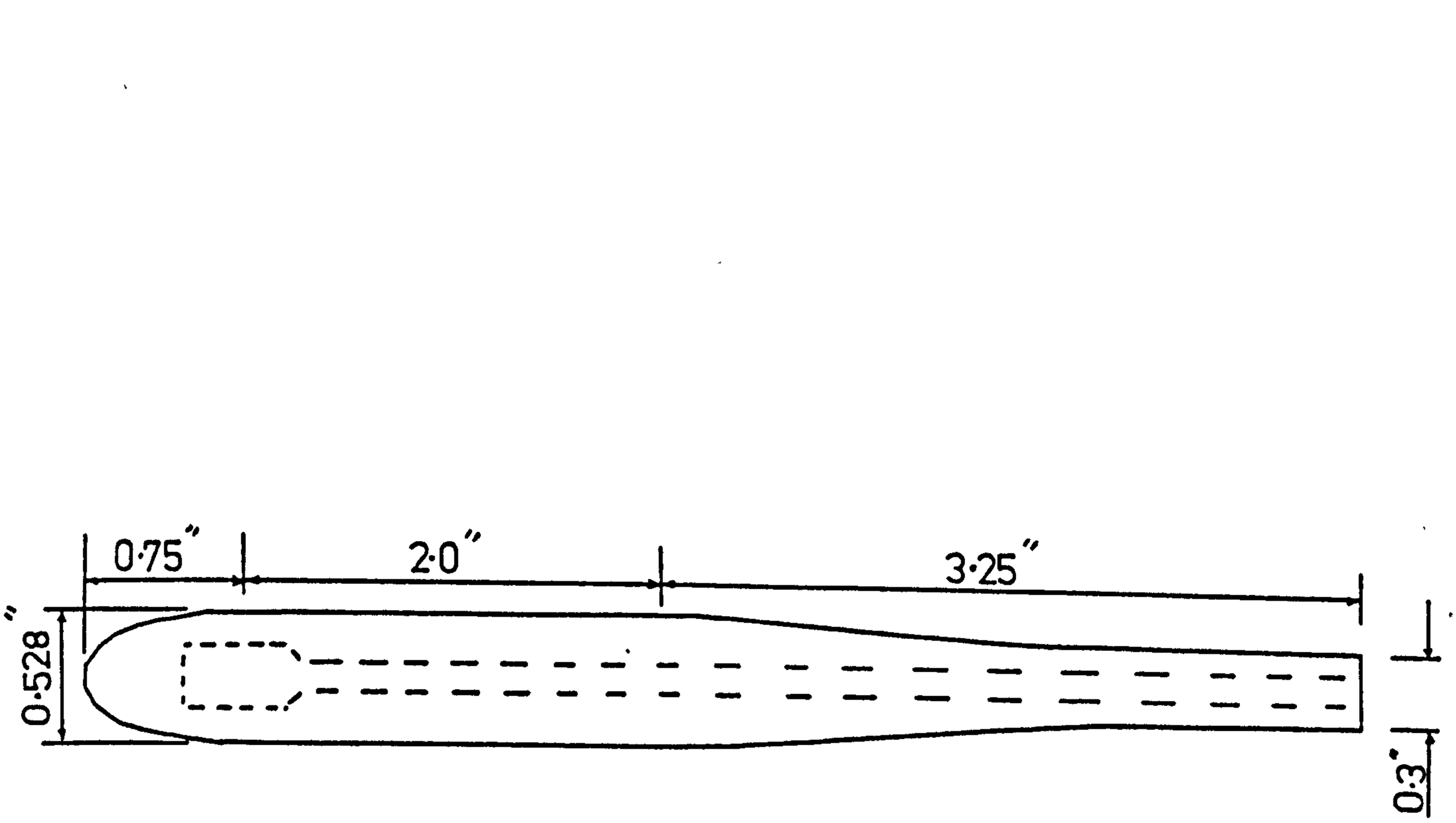

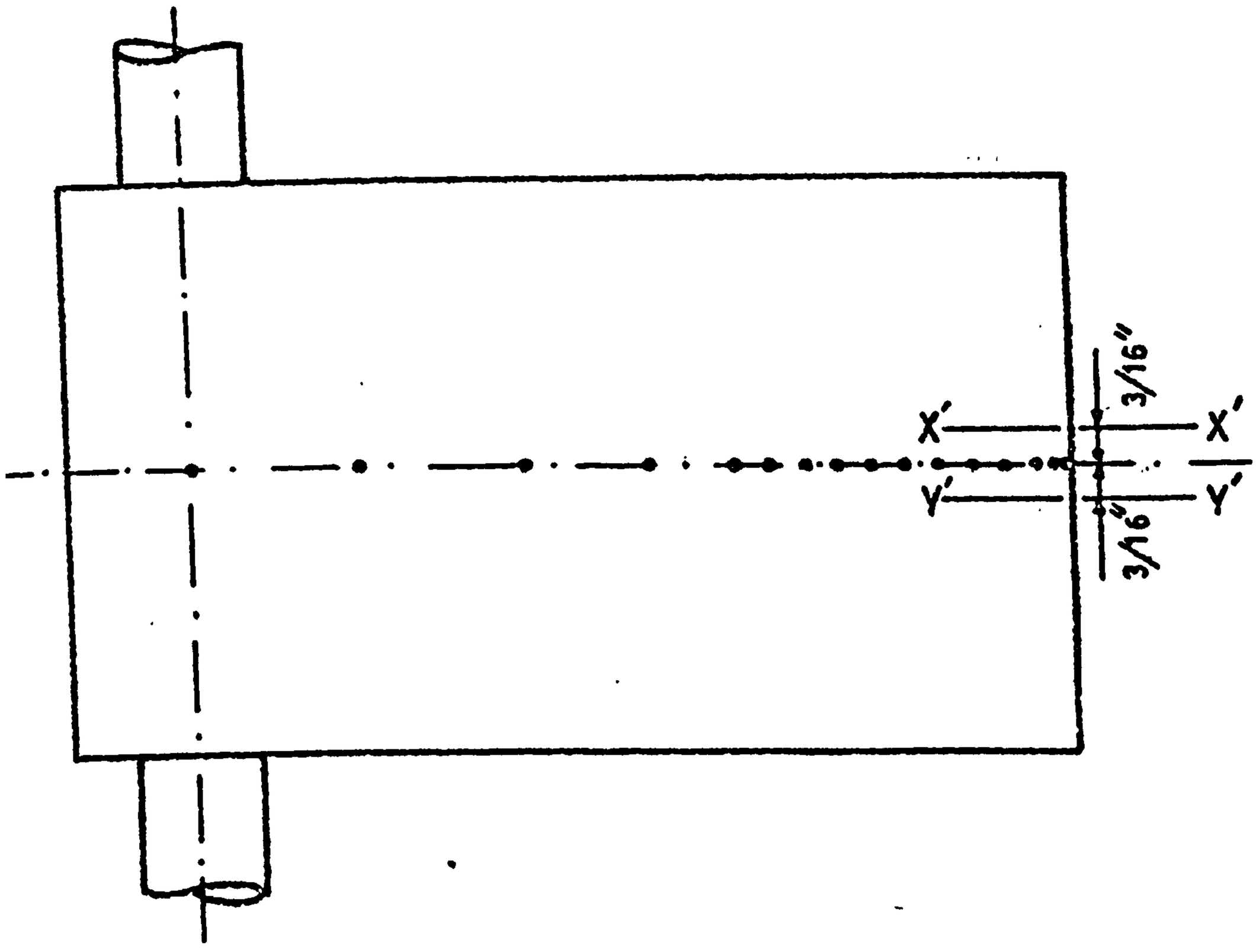

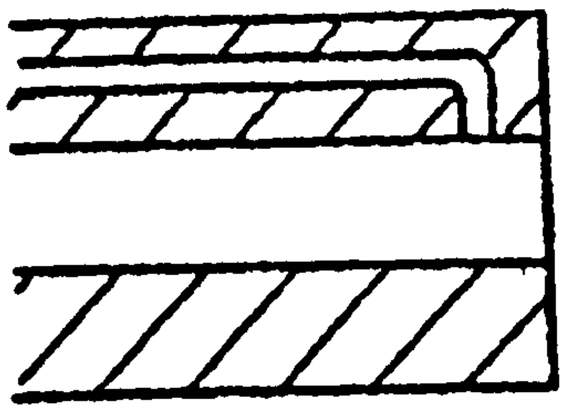

Y'Y' view showing slot tapping.

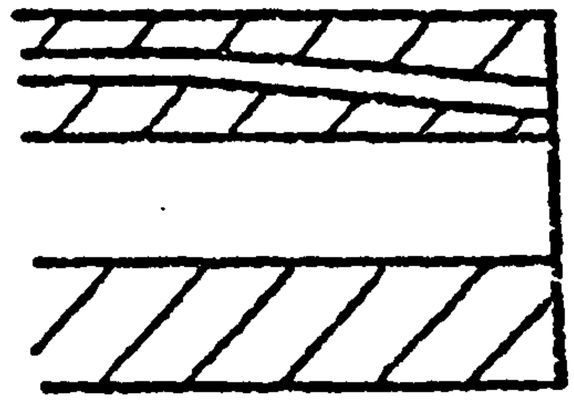

X'X' view showing base tapping.

Upper surface				Lower surface	
Tapping No.	Distance from base in.	Tapping No.	Distance from base in.	Tapping No.	Distance from base in.
1	0·03	9	1·4	1	0·03
2	0·1	10	1·6	2	0·1
3	0·2	11	1·8	3	1·0
4	0·4	12	2·0	4	2·0
5	0·6	13	2·5	5	3·25
6	0·8	14	3·25	6	5·25
7	1·0	15	4·25		
8	1·2	16	5·25		

FIG.11. PRESSURE TAPPING ARRANGEMENT.

BASE CONFIGURATIONS

SLOT

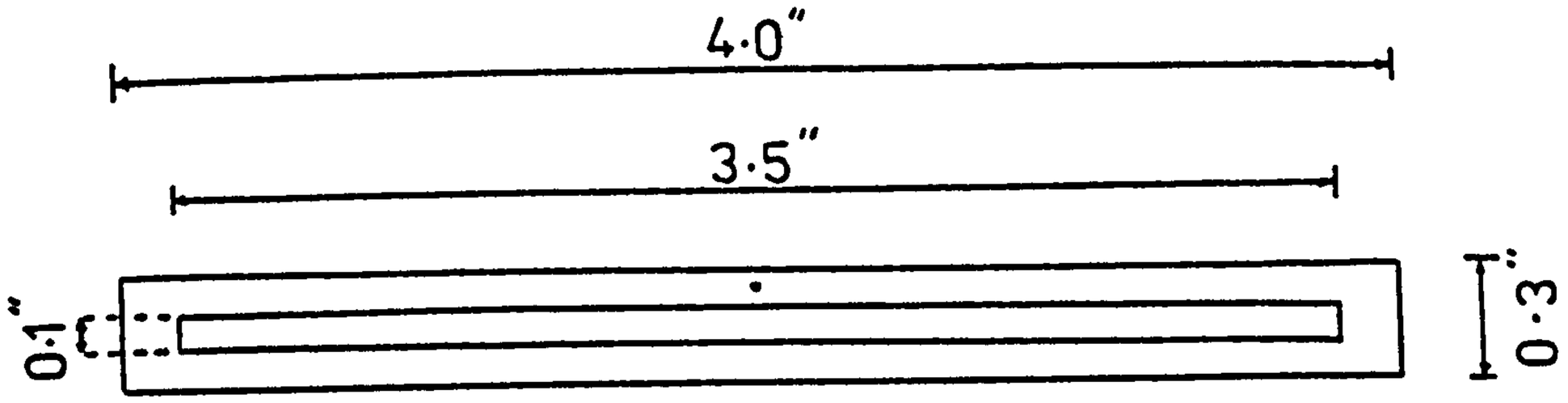

CIRCULAR HOLES

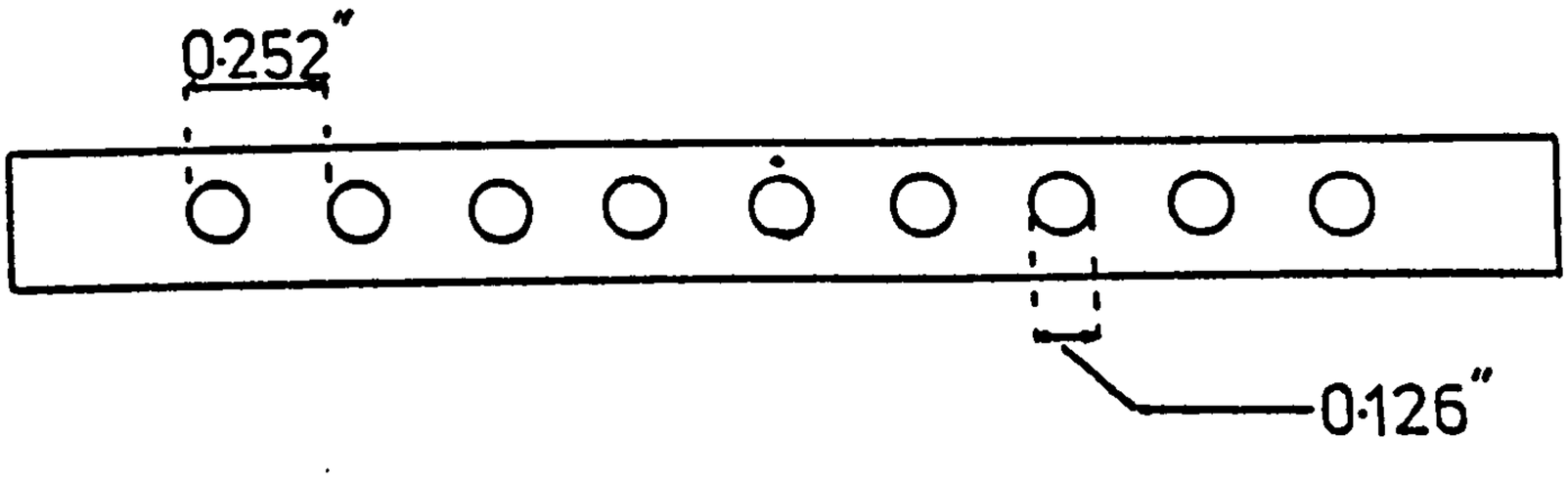

FLARED HOLES

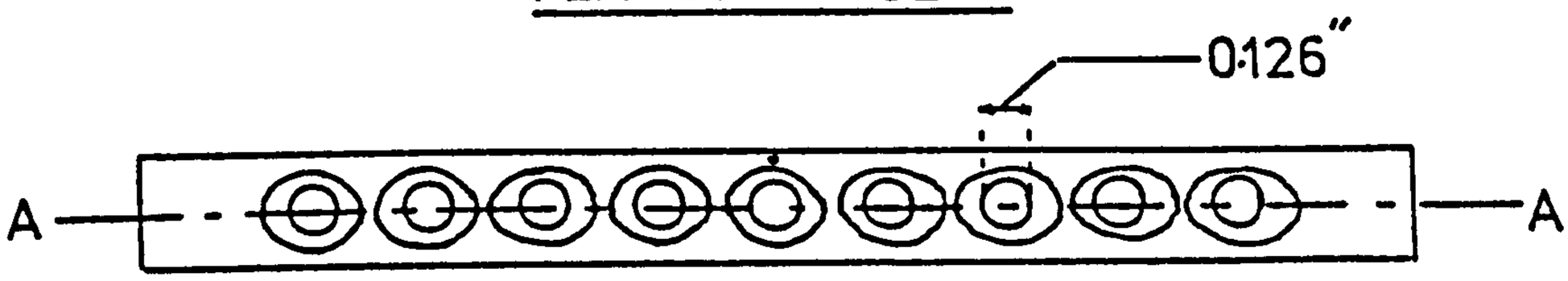

SECTION A—A

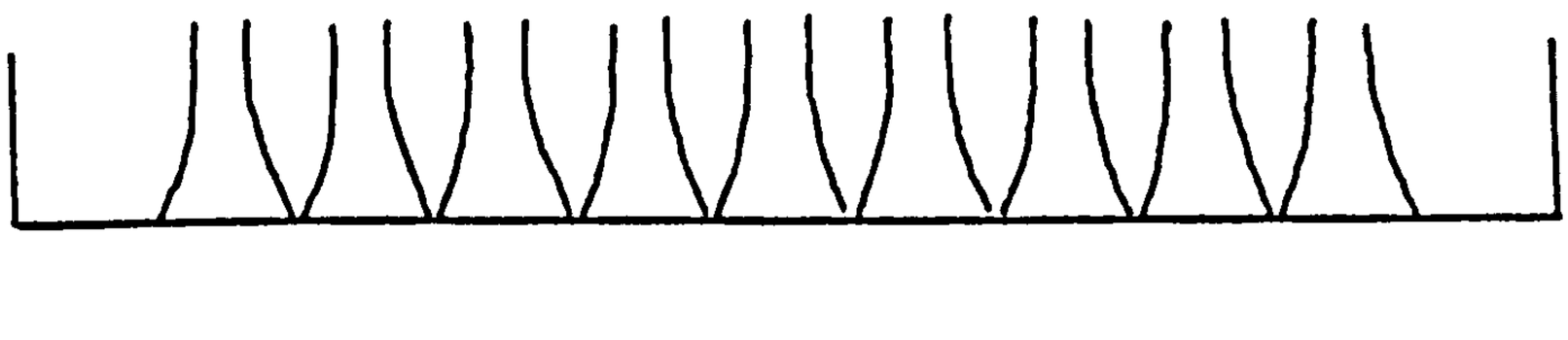

FIG. 12.

FIG. 13. PITOT-STATIC TUBE

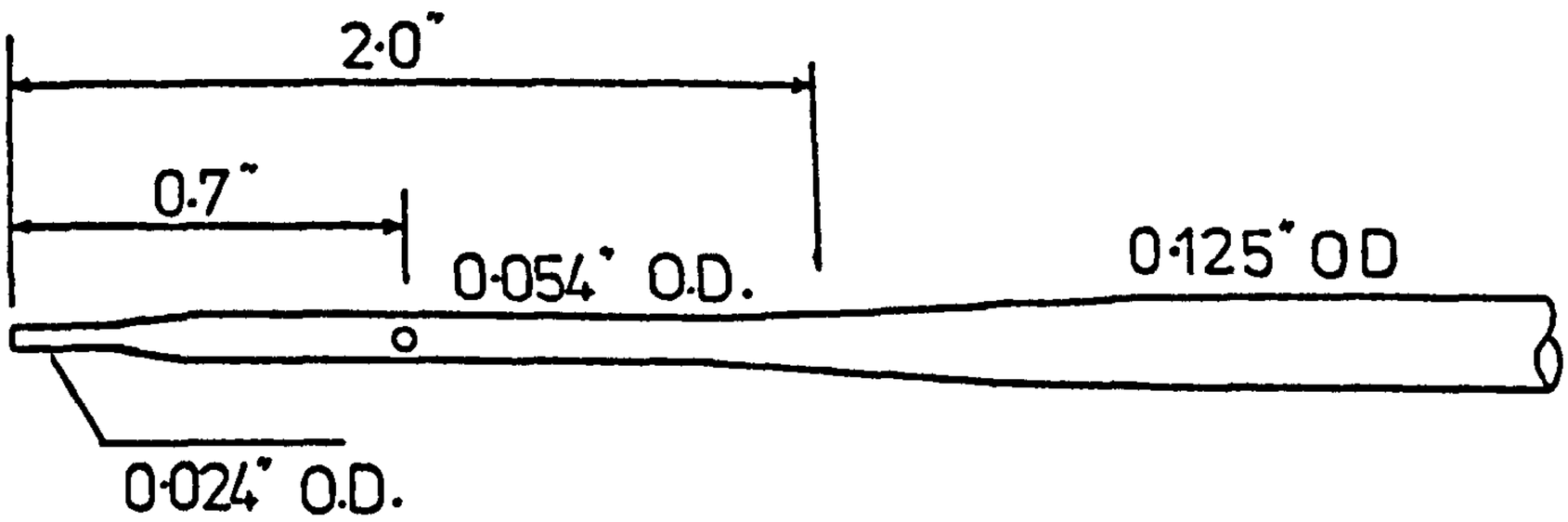

FIG.14. PITOT STATIC PROBE CALIBRATION CURVE

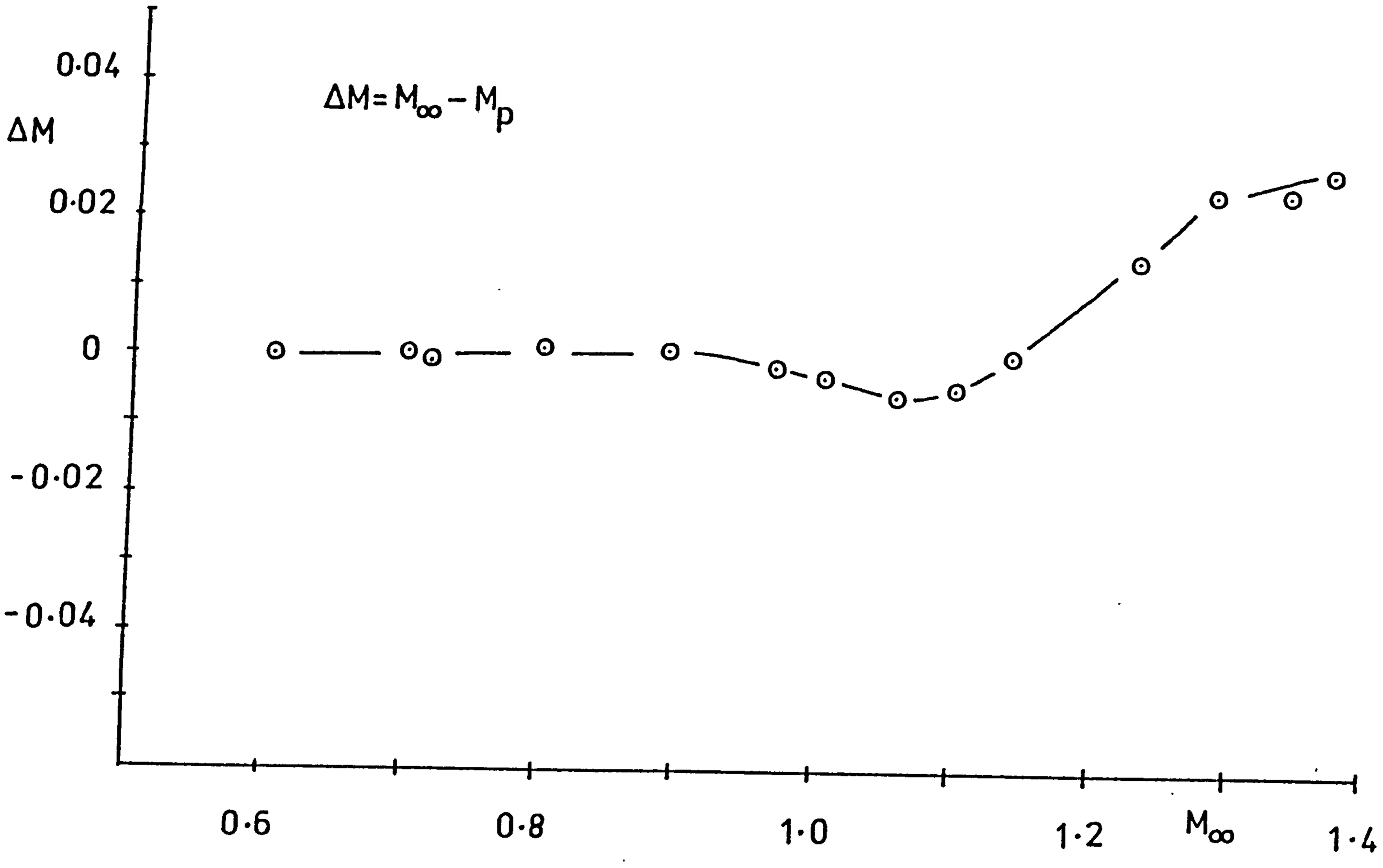

FIG.15a. UPPER SURFACE MACH Nº DISTRIBUTION

$\alpha = 0°$, $w_d = 0.092"$, $\dot{m} = 0$, SLOT

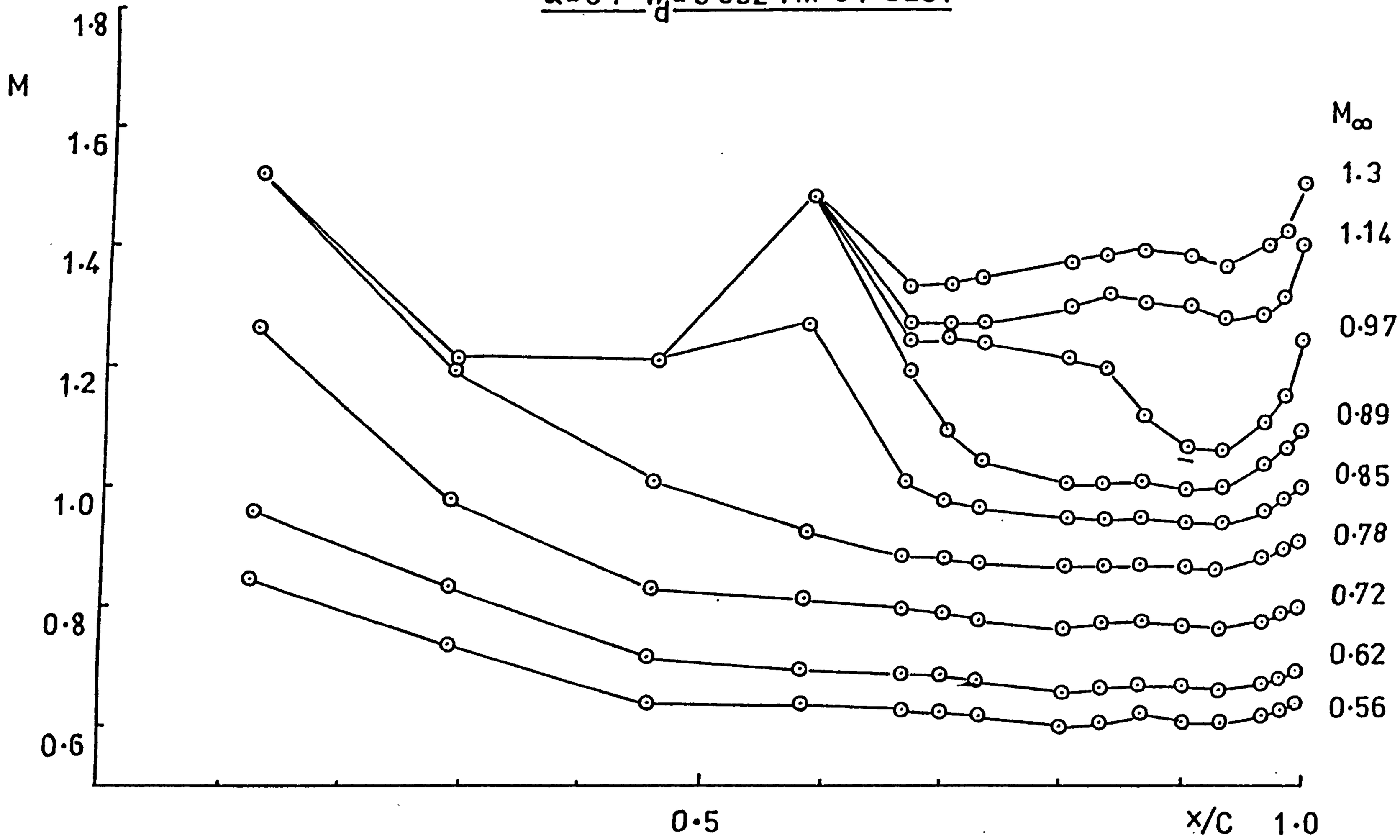

FIG.15b. SUCTION SURFACE MACH Nº DISTRIBUTION

$\alpha = 2°$, $w_d = 0.092"$, $\dot{m} = 0$, SLOT

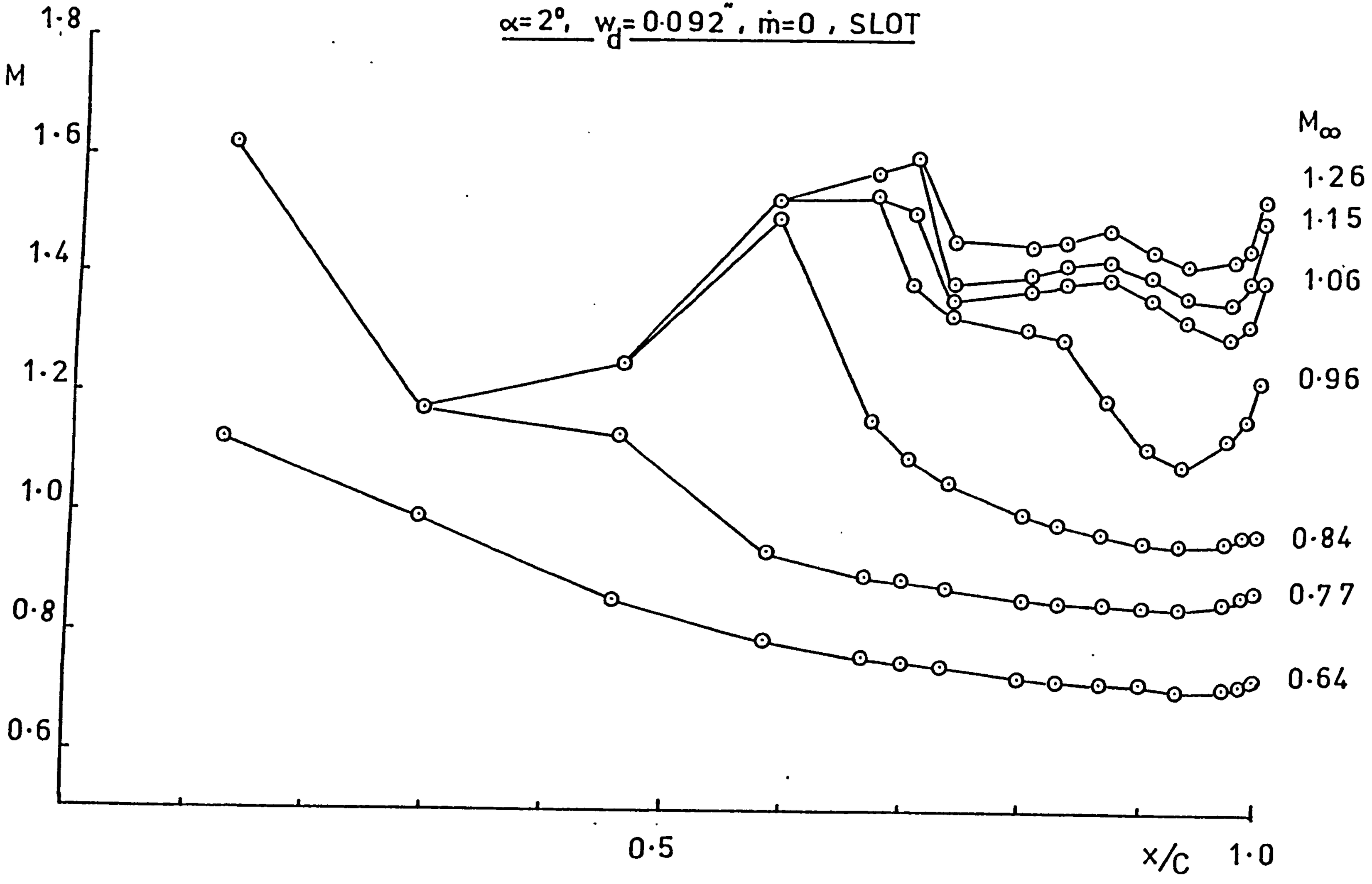

FIG.15c. SUCTION SURFACE MACH Nº DISTRIBUTION

$\alpha = 4°$, $w_d = 0{\cdot}092''$, $\dot{m} = 0$, SLOT

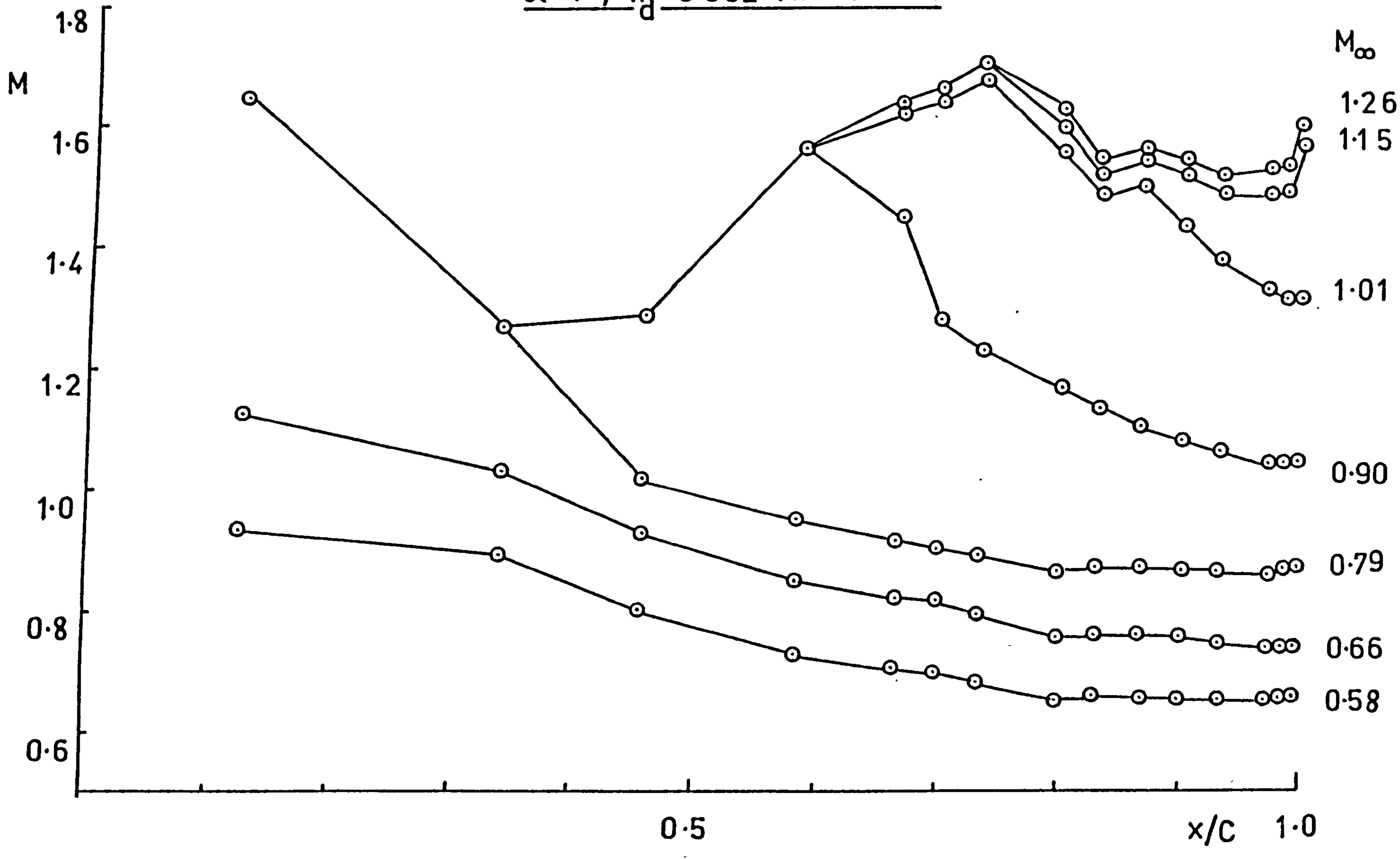

FIG.15d. SUCTION SURFACE MACH Nº DISTRIBUTION

$\alpha = 6^{\circ}$, $w_d = 0.092''$, $\dot{m}=0$, SLOT

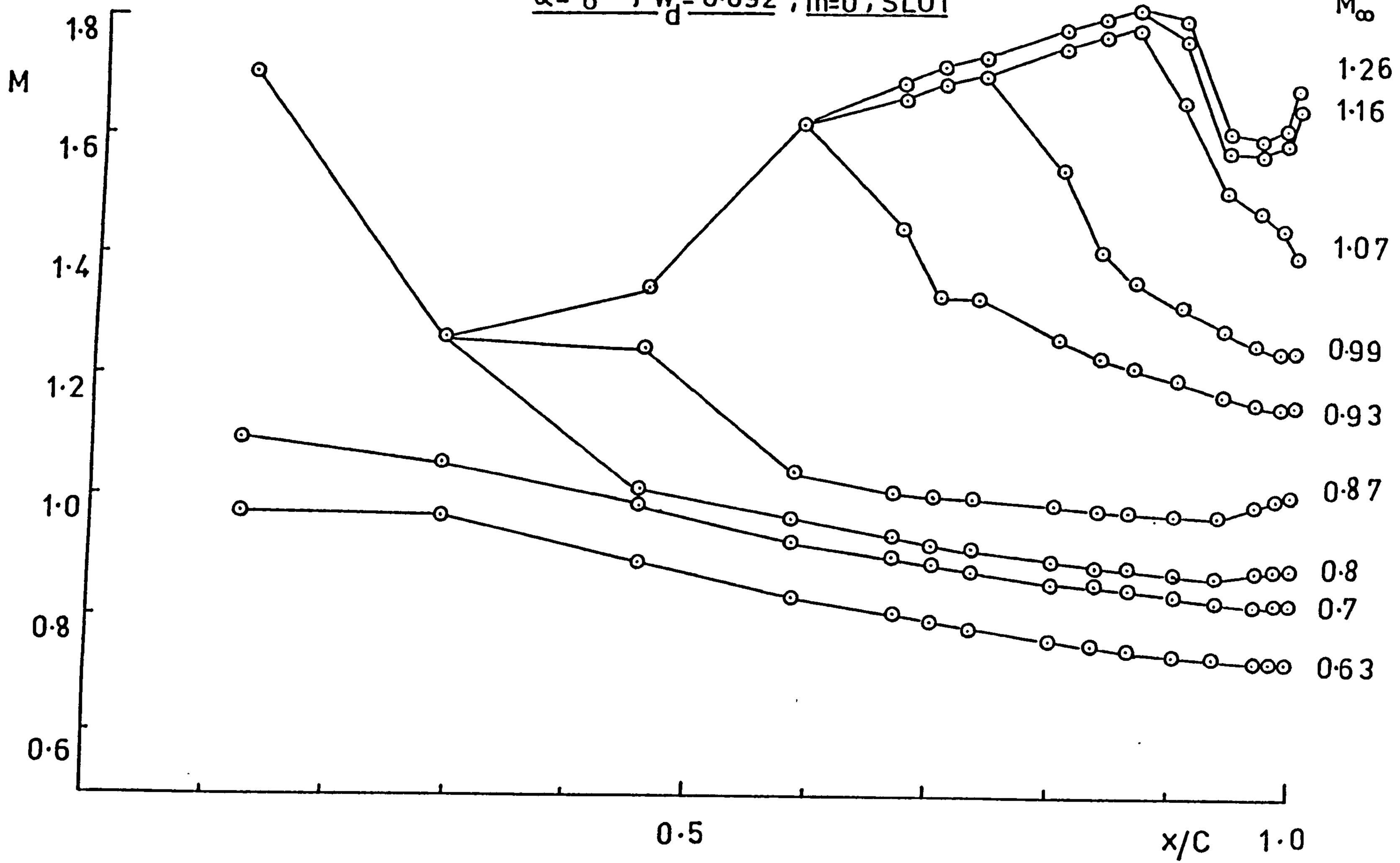

FIG.16a. SUCTION SURFACE MACH Nº DISTRIBUTION

$\alpha = 0°$; $w_d = 0.007''$, $\dot{m} = 0$, CIRCULAR

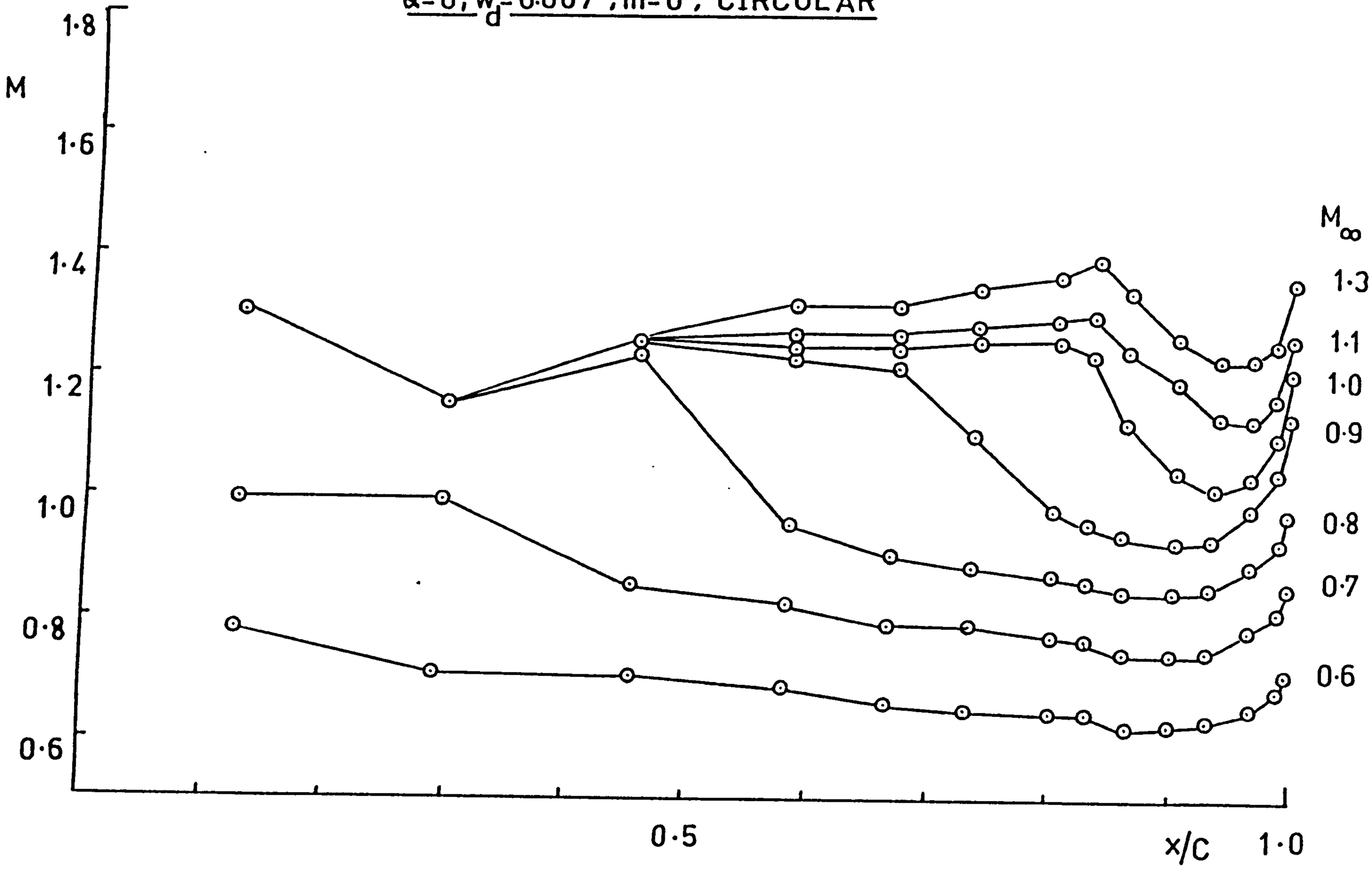

FIG.16b. SUCTION SURFACE MACH Nº DISTRIBUTION

$\alpha = 2°$, $w_d = 0.007''$, $\dot{m} = 0$, CIRCULAR

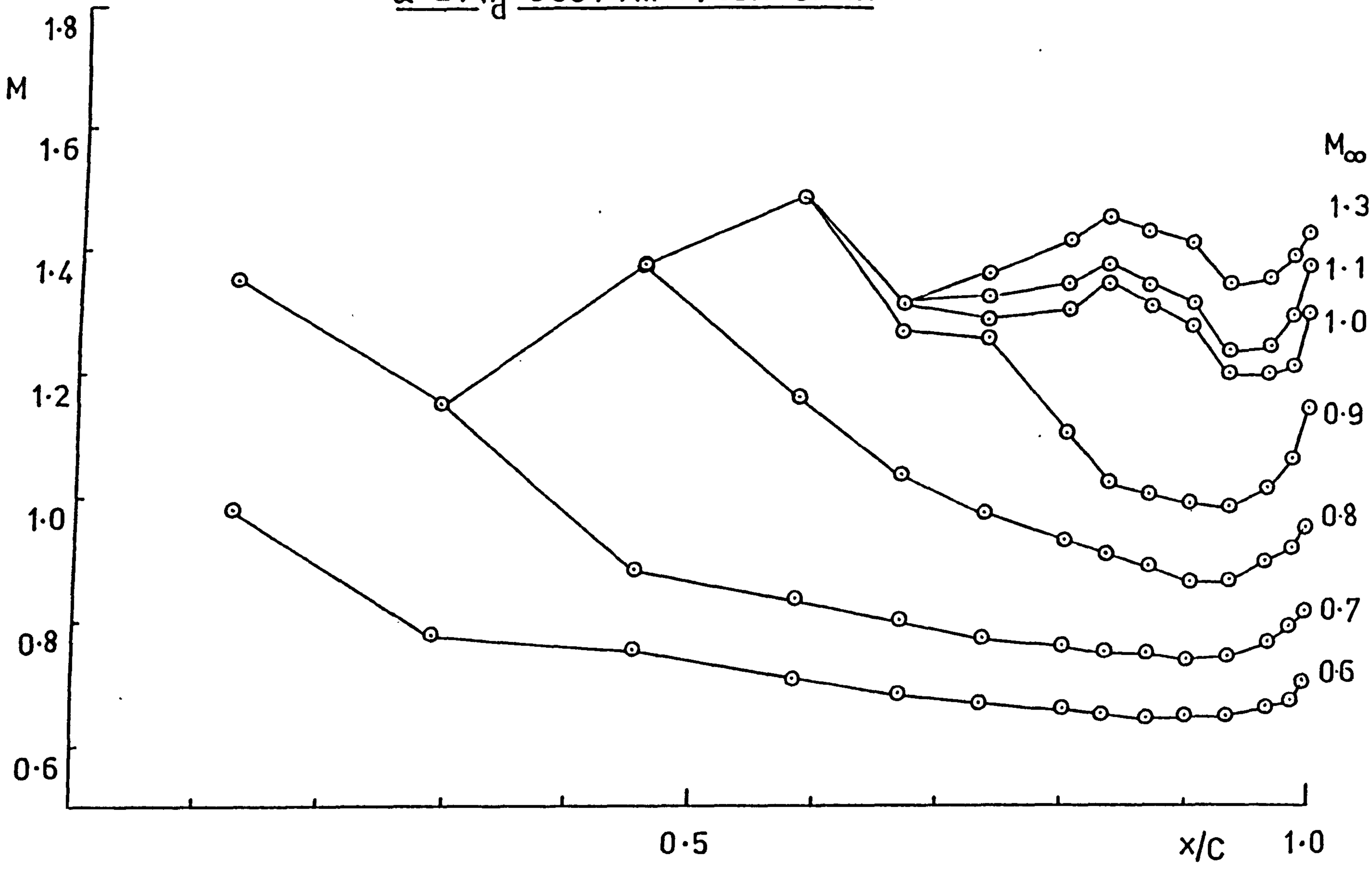

FIG.16c. SUCTION SURFACE MACH Nº DISTRIBUTION

$\alpha = 4°$, $w_d = 0{\cdot}007''$, $\dot{m} = 0$, CIRCULAR

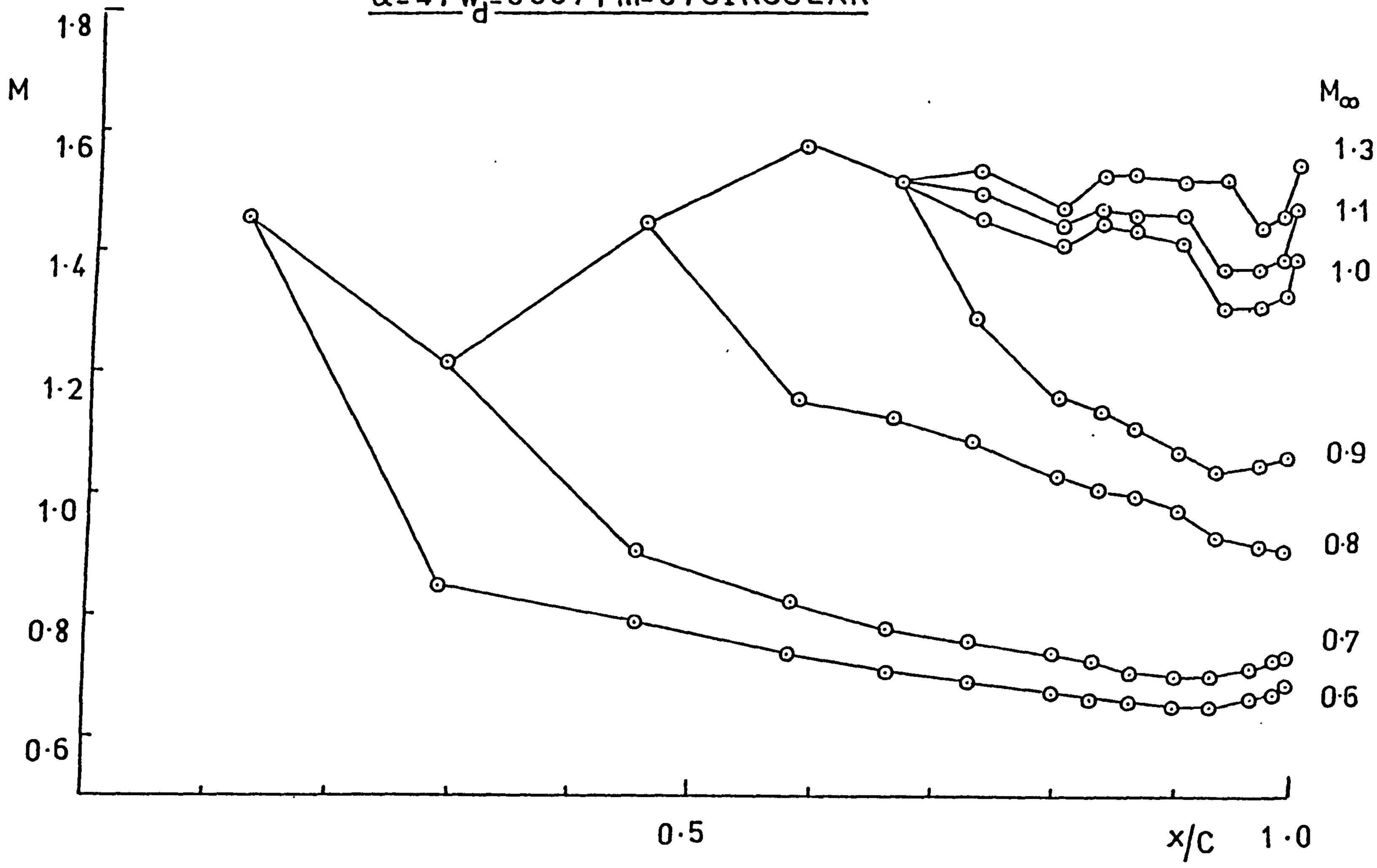

FIG.16 d. SUCTION SURFACE MACH Nº DISTRIBUTION

$\alpha = 6°$, $w_d = 0.007''$, $\dot{m} = 0$. CIRCULAR

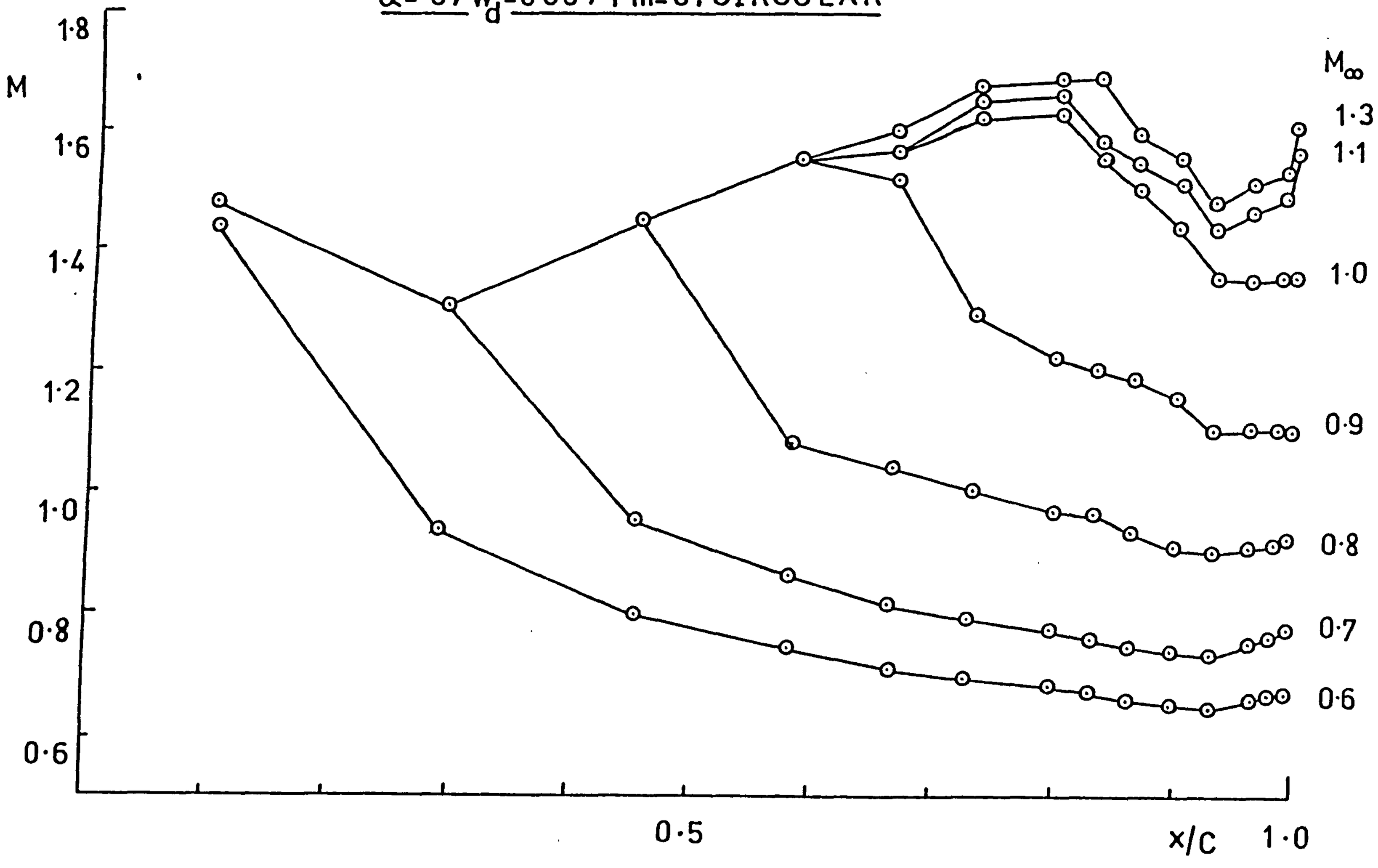

FIG.17. SUCTION SURFACE MACH Nº DISTRIBUTION

$\alpha = 0°$, $w_d = 0.007"$, $\dot{m} = 0$, FLARED

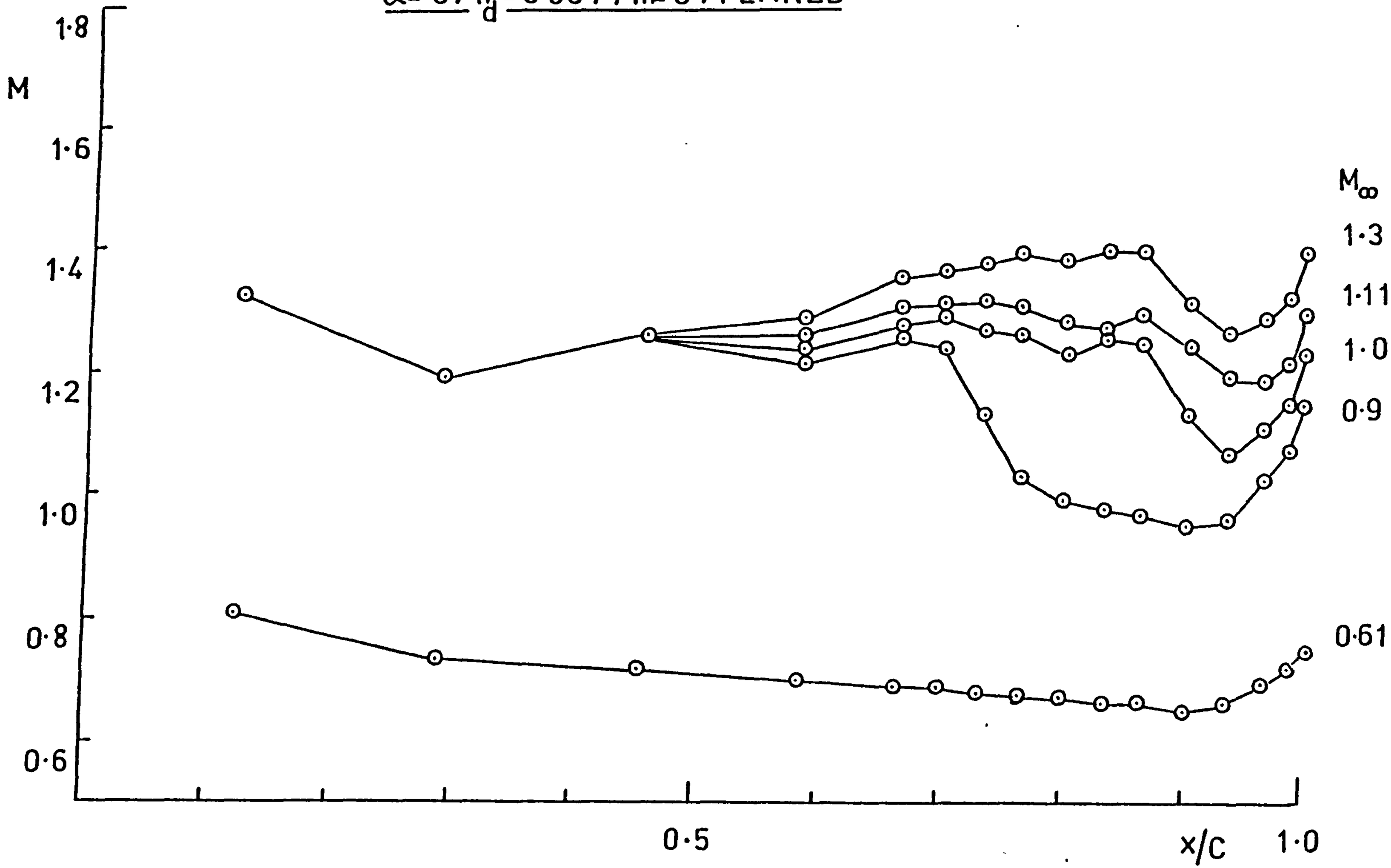

FIG.18a. BOUNDARY LAYER TRAVERSE AT 0·4" BEFORE T.E.

$\alpha = 0°$; $w_d = 0.092"$, SLOT

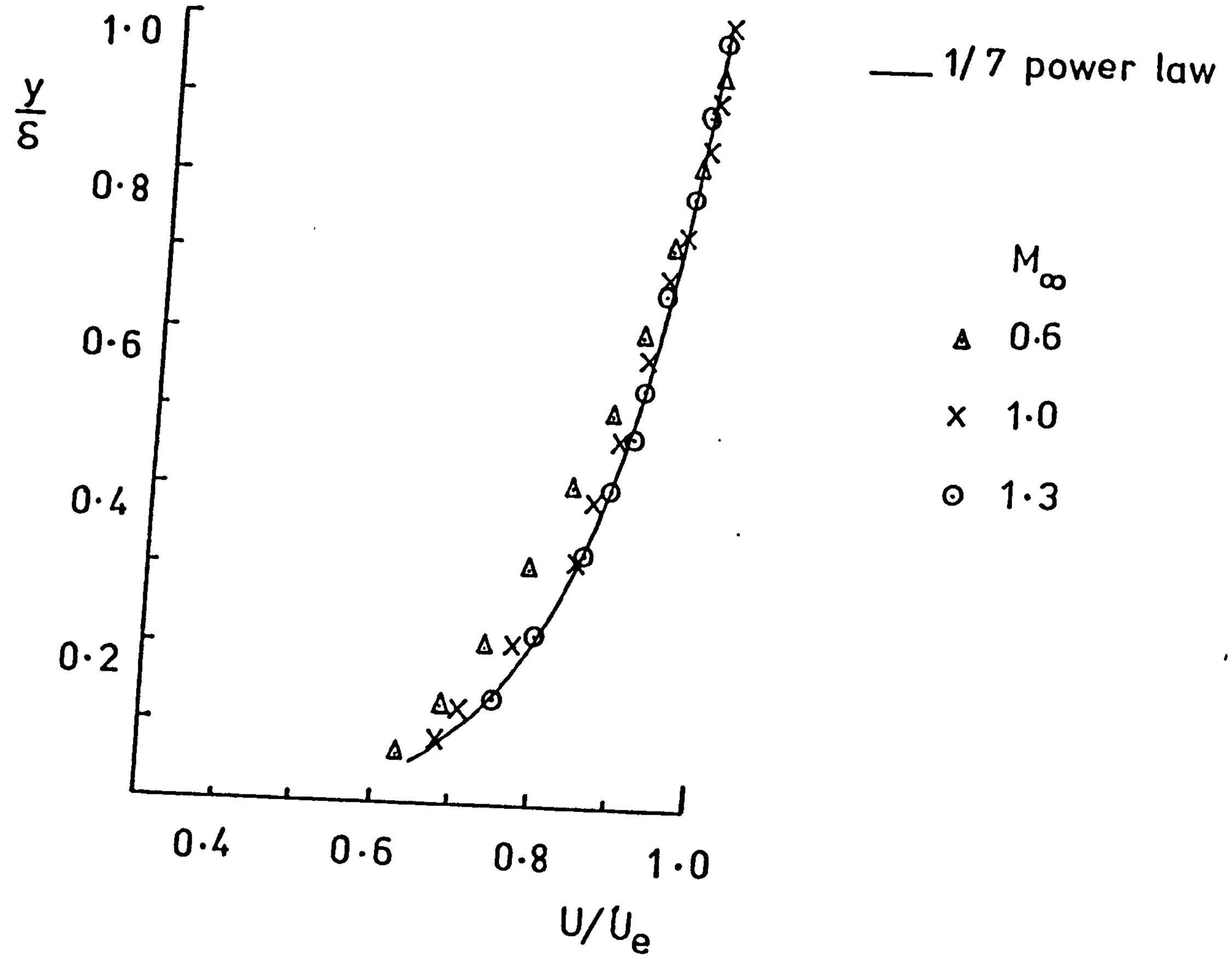

FIG.18b. BOUNDARY LAYER TRAVERSE AT 0·4" BEFORE T. E.

$\alpha = 0°$; $w_d = 0{\cdot}007"$, CIRCULAR

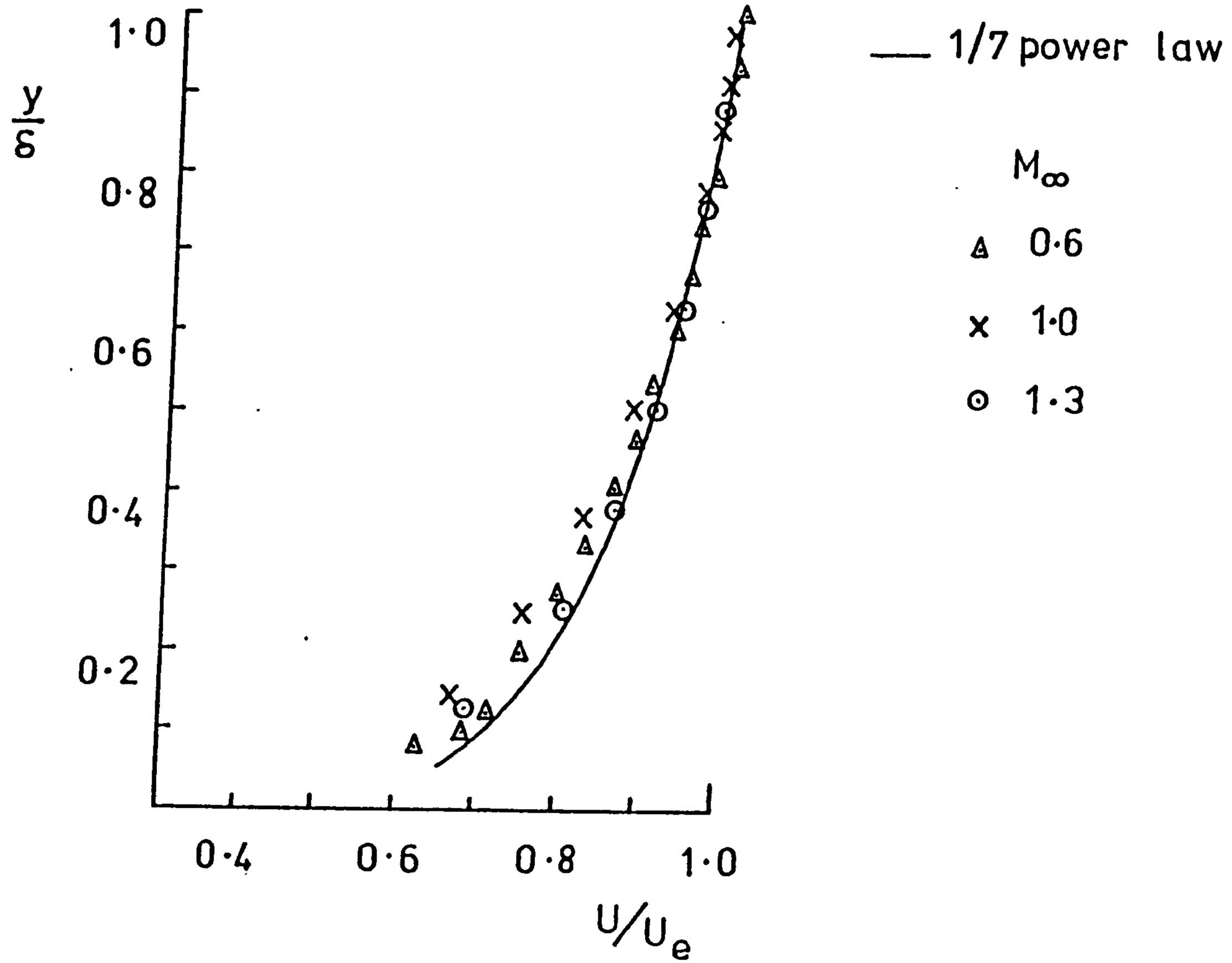

FIG.18c. BOUNDARY LAYER TRAVERSE AT 0·4" BEFORE T.E.

$\alpha = 0°$, $w_d = 0{\cdot}007"$, FLARED

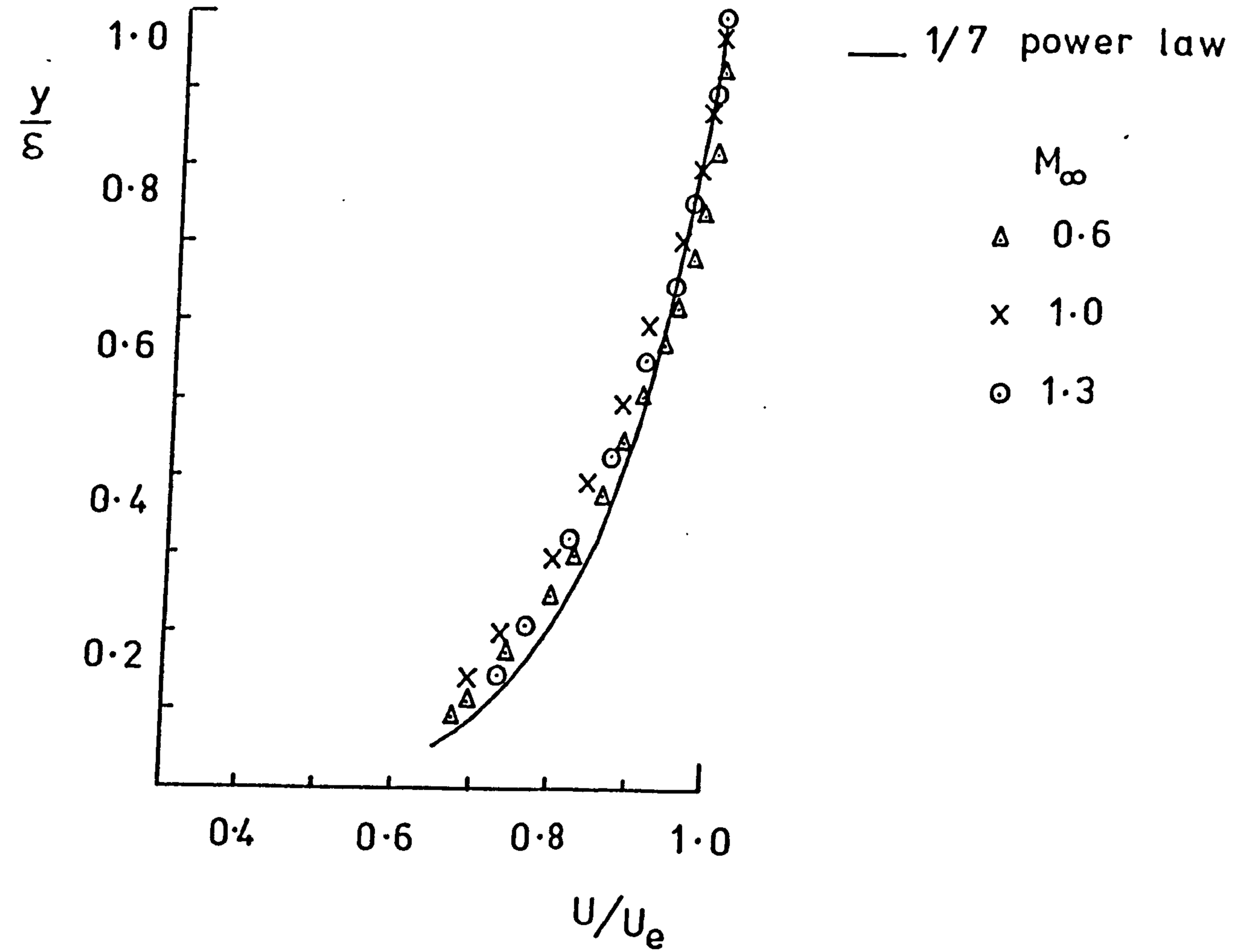

THE VARIATION OF P_b/P_∞ WITH M_∞

$\alpha = 0°; \dot{m} = 0$

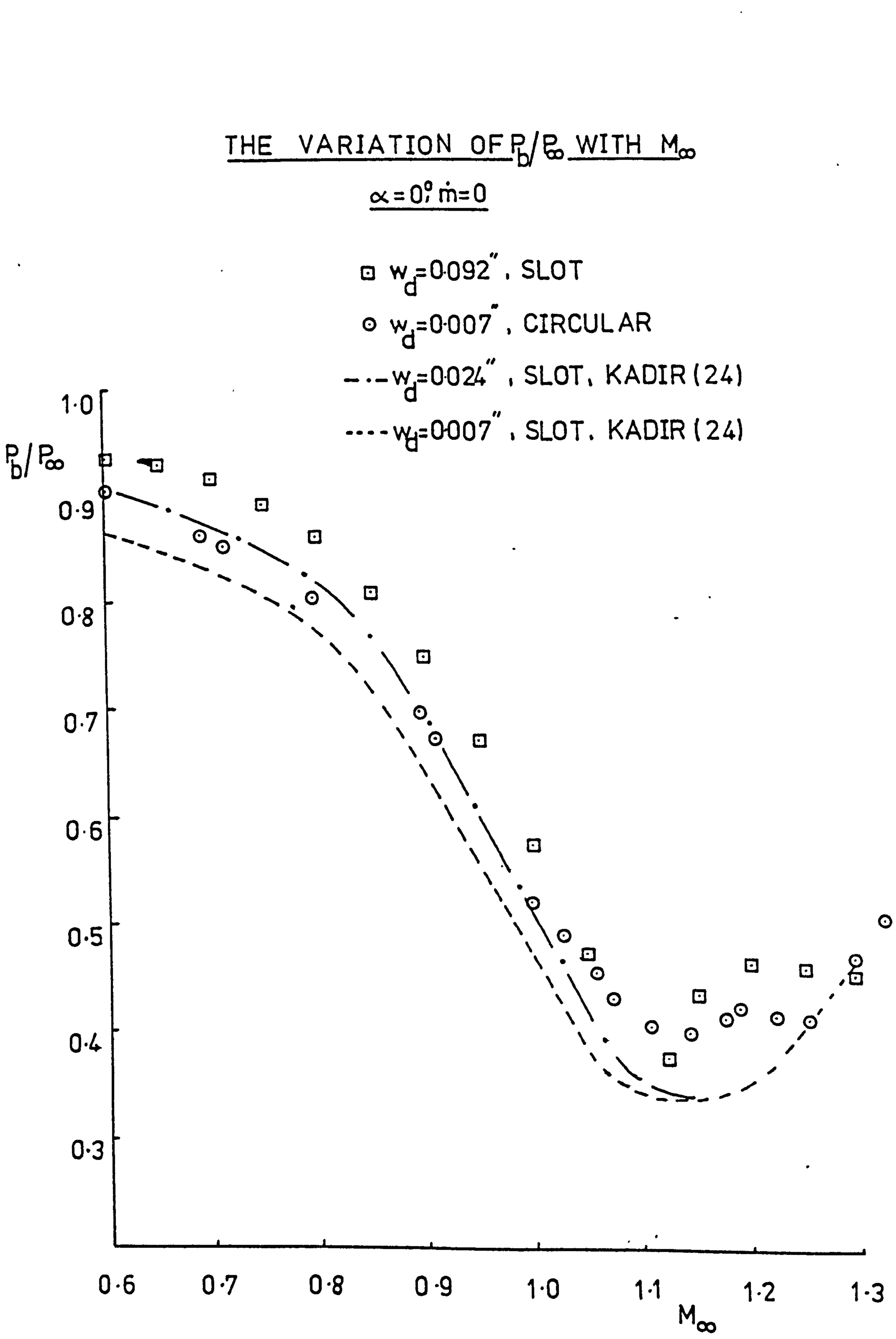

FIG. 19a.

THE VARIATION OF P_b/P_∞ WITH M_∞

$\alpha = 2°$; $\dot{m} = 0$

⊡ $w_d = 0.092"$, SLOT

⊙ $w_d = 0.007"$, CIRCULAR

—·— $w_d = 0.024"$ and $w_d = 0.007"$, SLOT, KADIR (24)

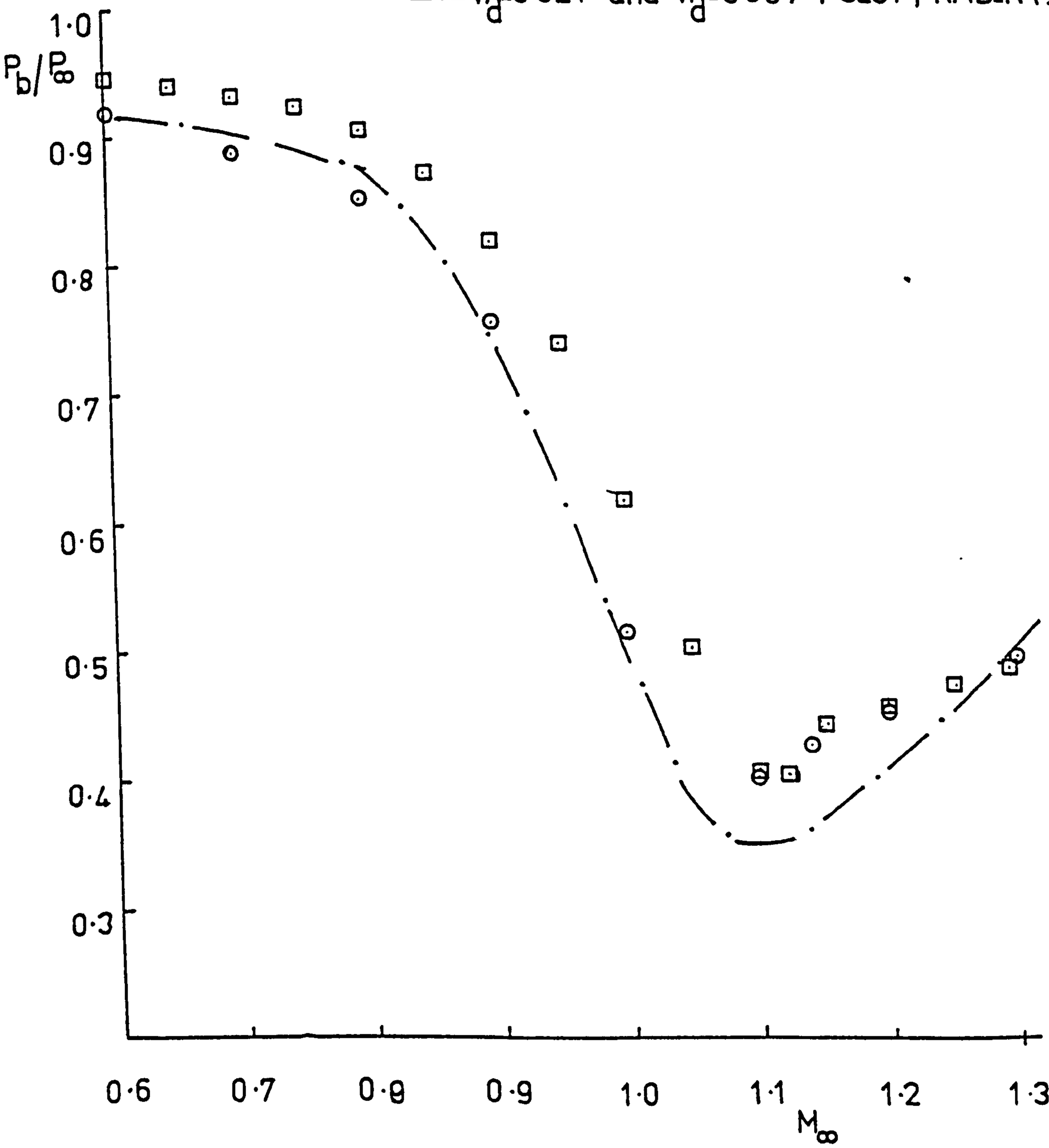

FIG.19b.

THE VARIATION OF P_b/P_∞ WITH M_∞

$\alpha = 4°$; $\dot{m} = 0$

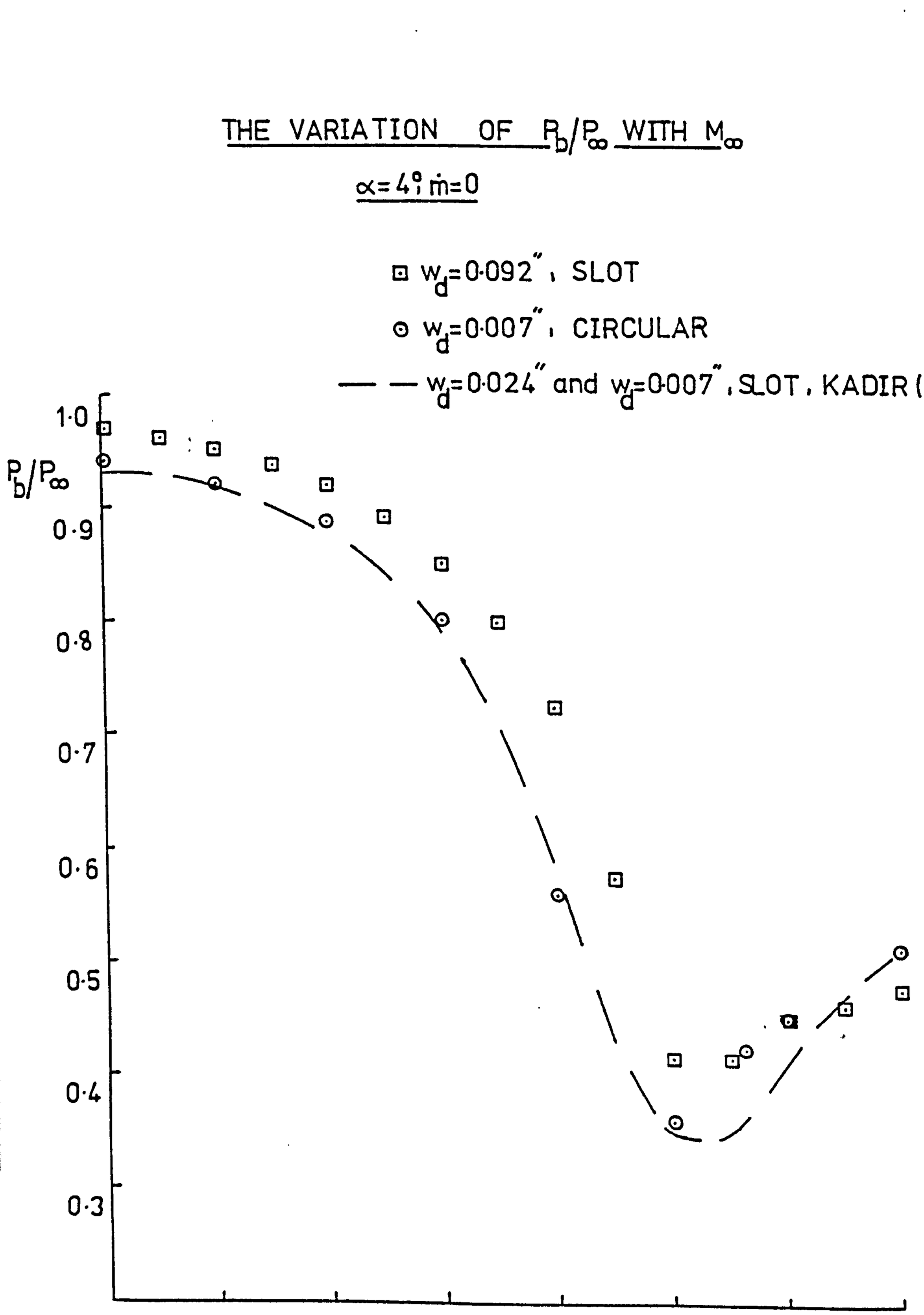

FIG.19c.

THE VARIATION OF P_b/P_∞ WITH M_∞

$\alpha=6^\circ$, $\dot{m}=0$

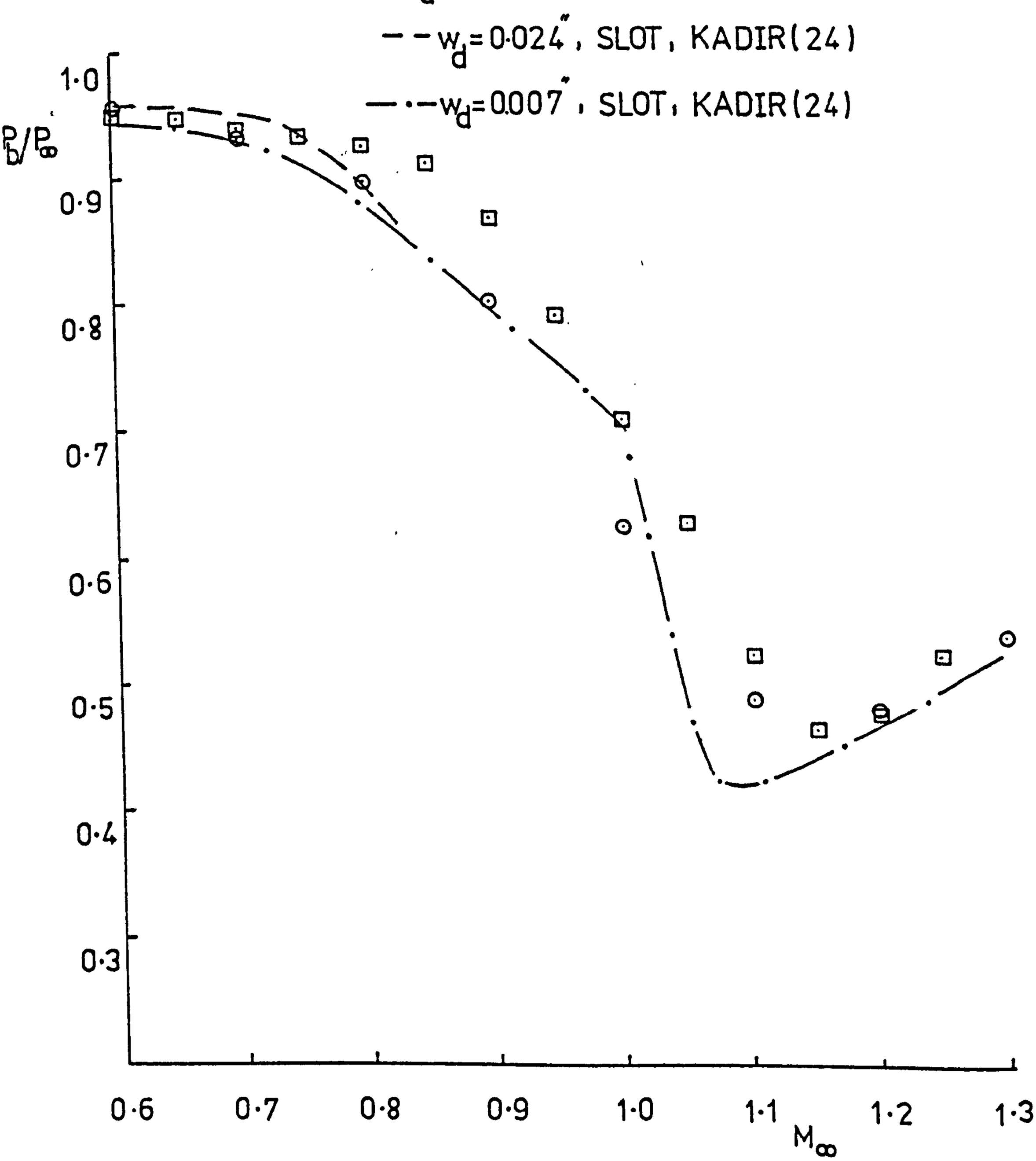

FIG.19d.

THE VARIATION OF P_b/P_∞ WITH M_∞

$\alpha = 0^\circ, \dot{m} = 0$

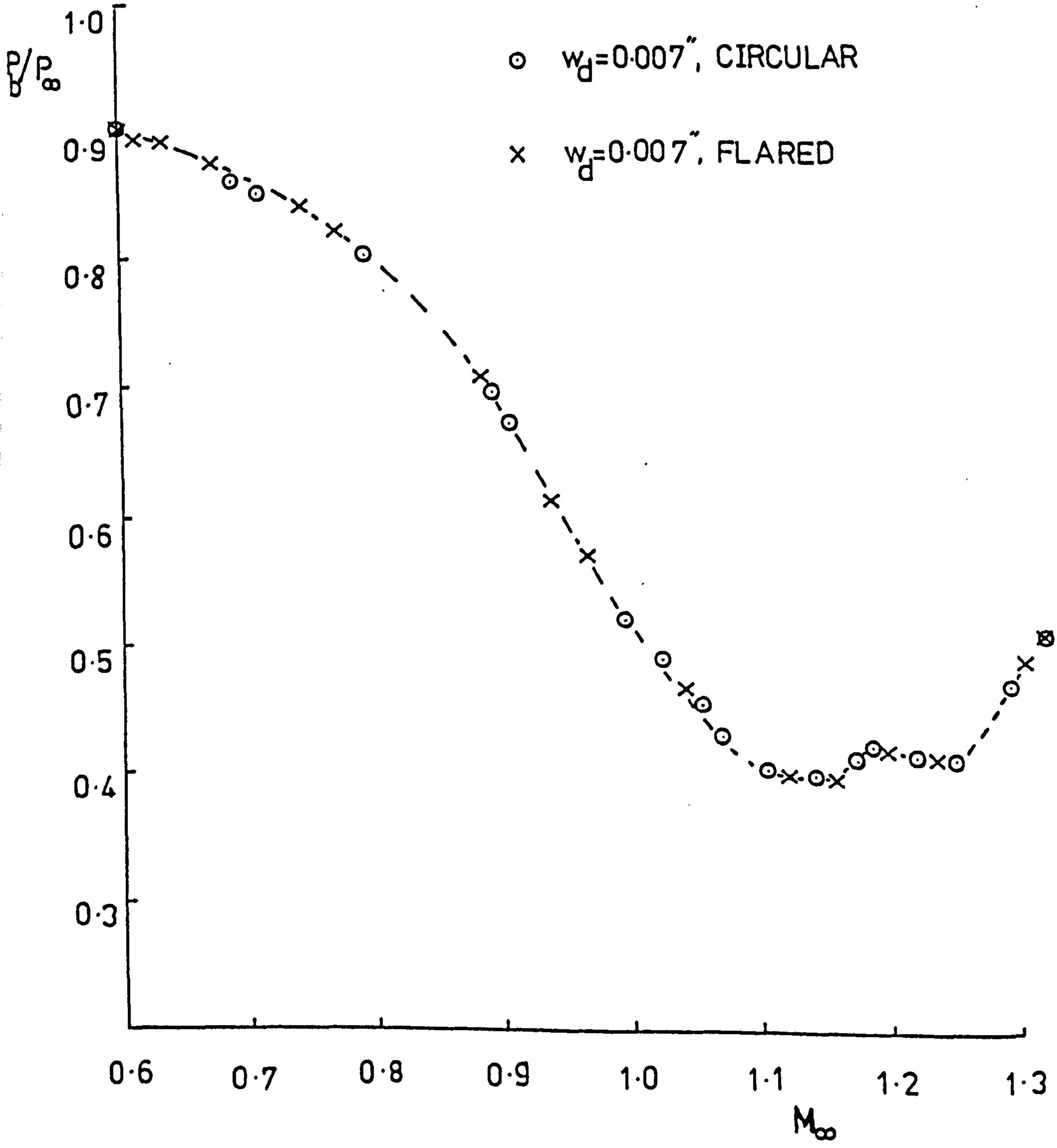

FIG. 20.

FIG.21a. EFFECT OF BASE BLEED ON BASE PRESSURE

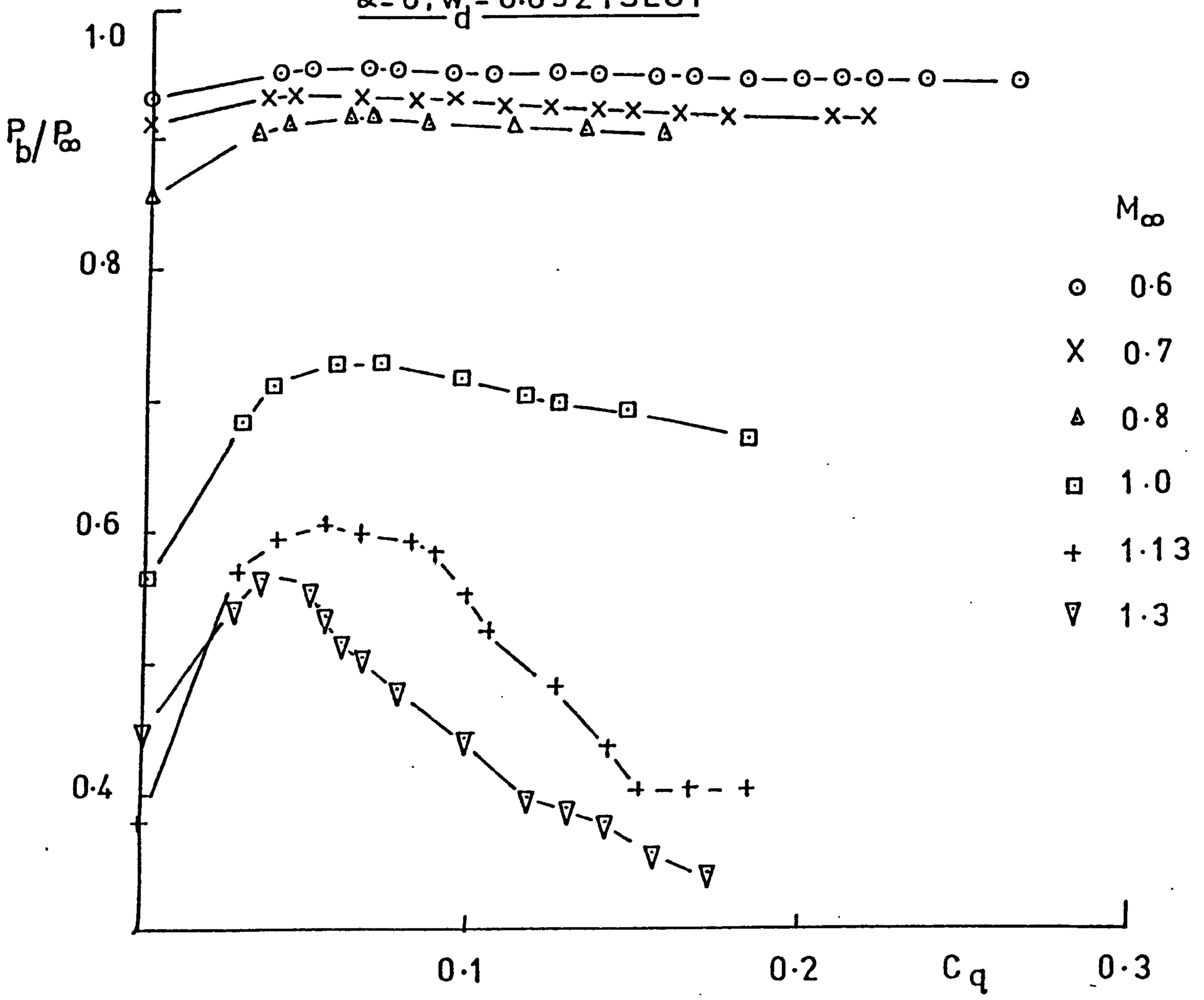

FIG.21b. EFFECT OF α ON THE VARIATION OF P_b/P_∞ WITH BASE BLEED

$M_\infty = 0.6$, $w_d = 0.092''$, SLOT

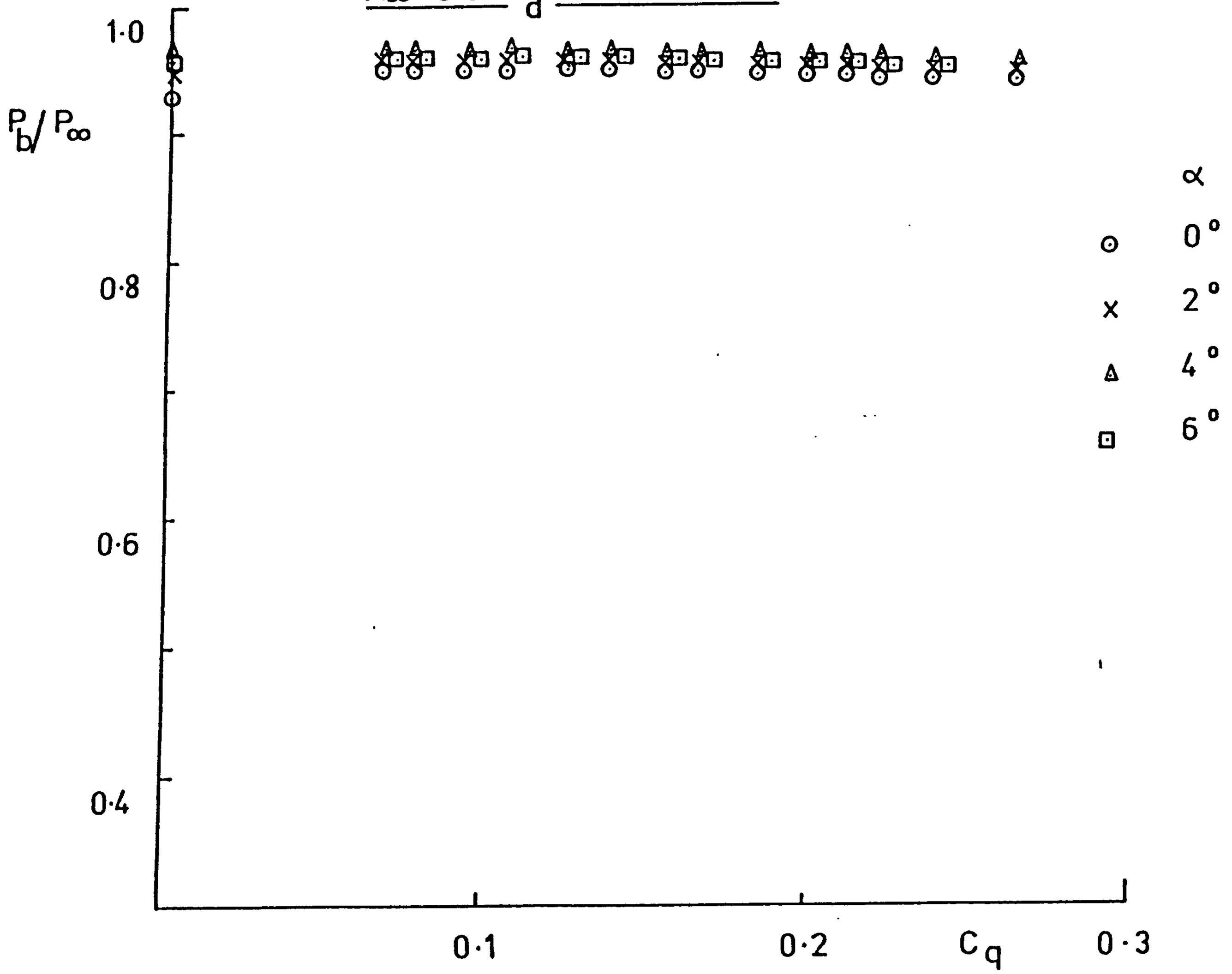

FIG.21c. EFFECT OF α ON THE VARIATION OF P_b/P_∞ WITH BASE BLEED

$M_\infty = 1.0$, $w_d = 0.092''$, SLOT

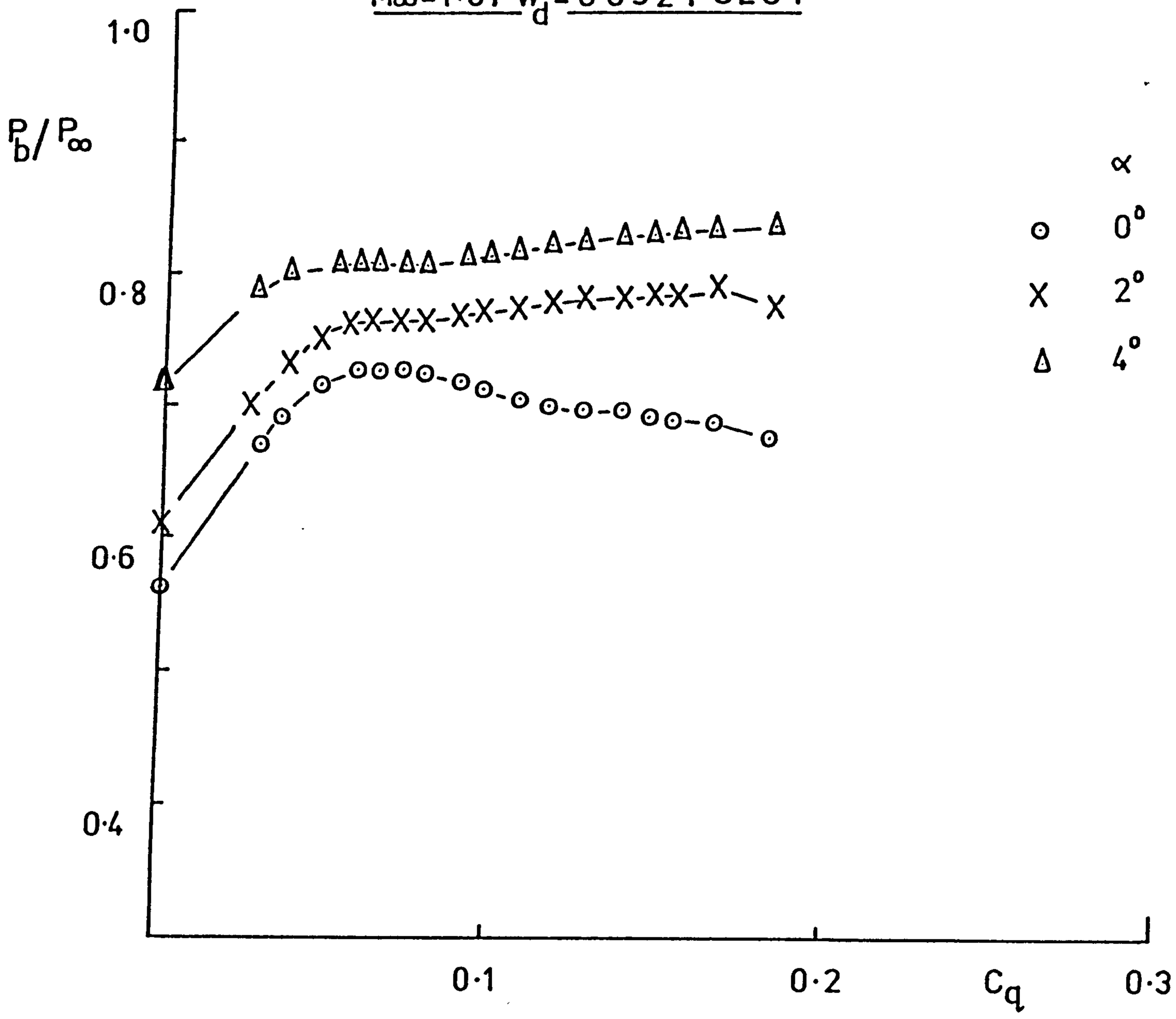

FIG.21d. EFFECT OF α ON THE VARIATION OF P_b/P_∞ WITH BASE BLEED

$M_\infty = 1.3$, $w_d = 0.092''$, SLOT

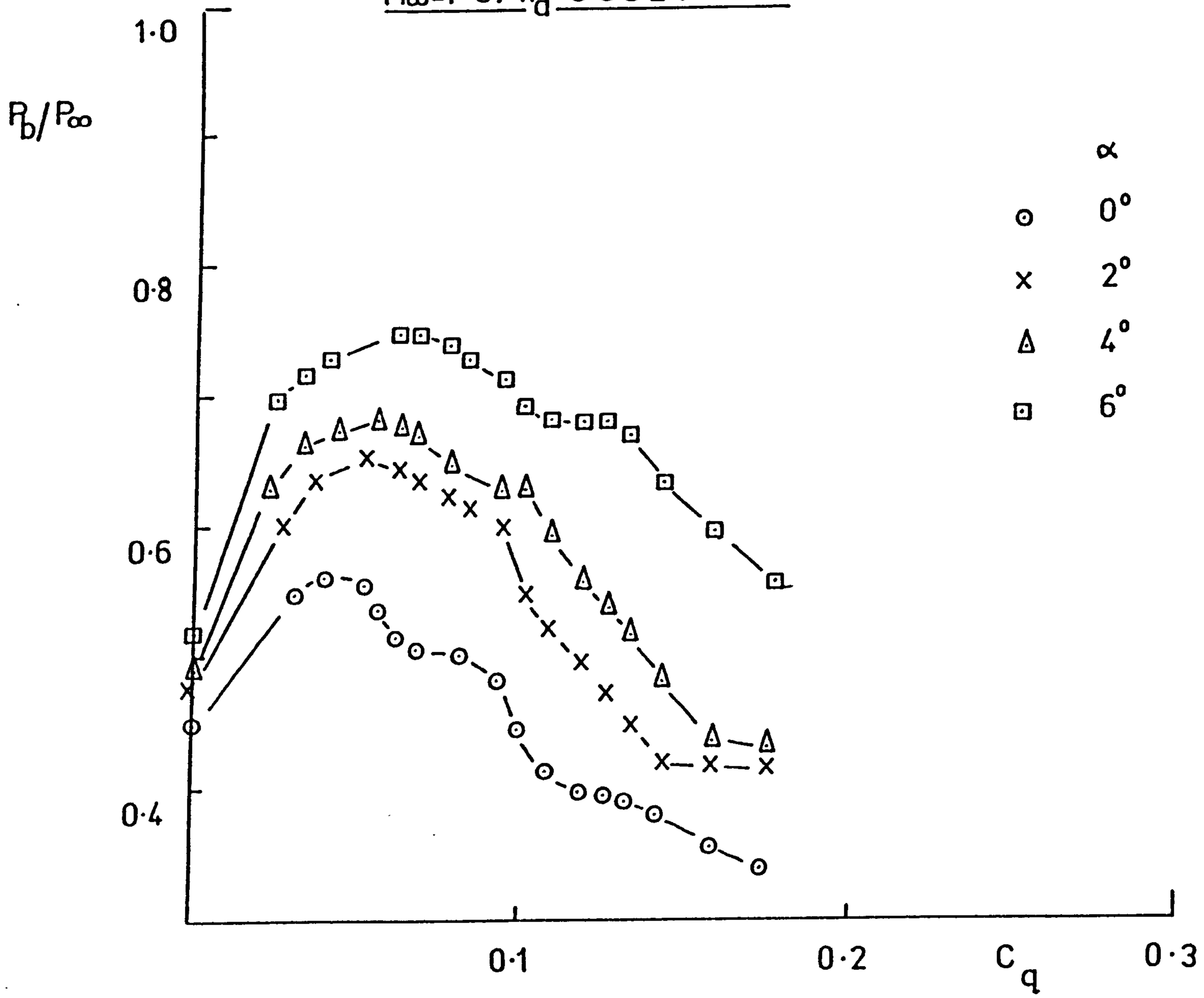

FIG. 22. DIAGRAMS SHOWING EFFECT OF BLEED AIR

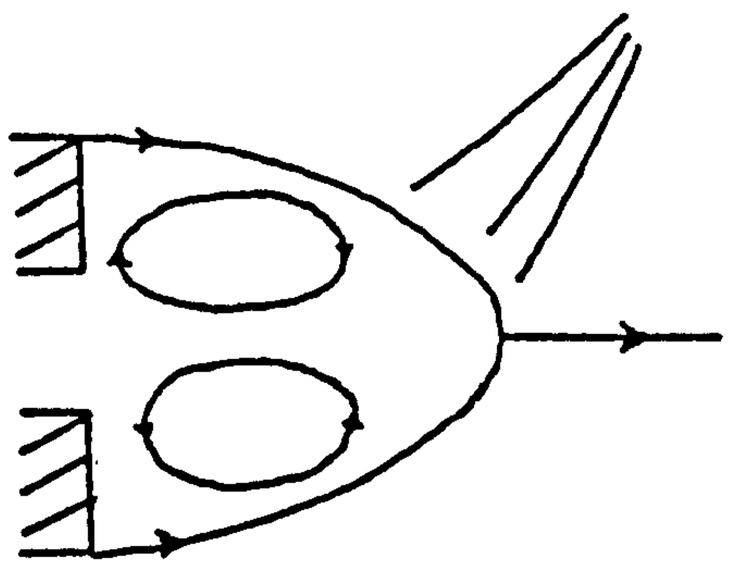

a) ZERO BLEED FLOW

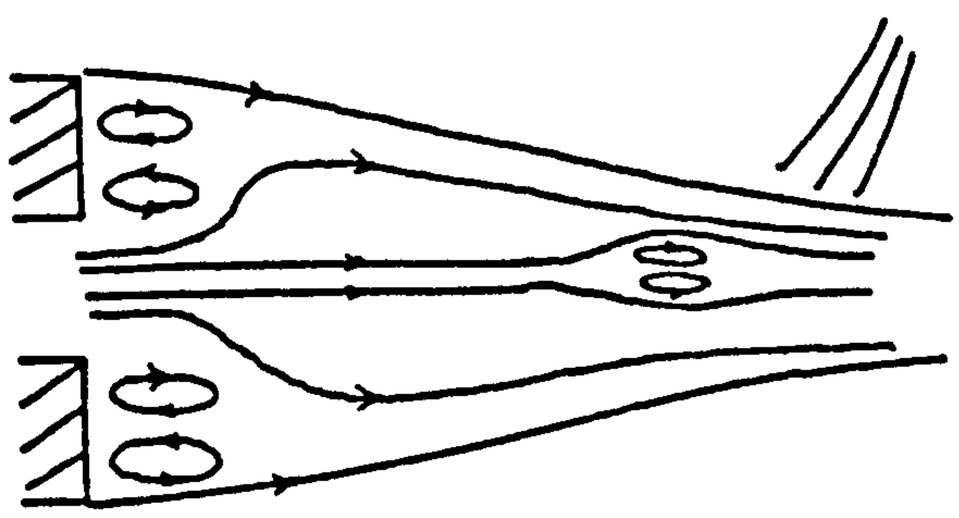

b) BLEED FLOW FOR $(P_b/P_\infty)_{max.}$

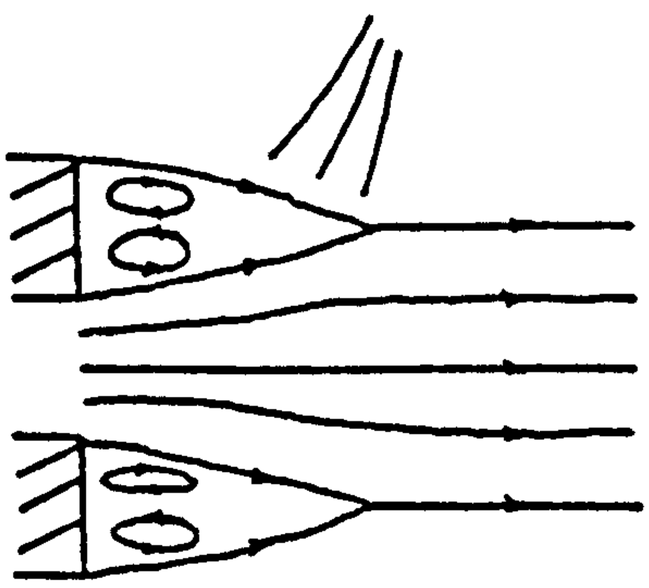

c) BLEED FLOW FOR $C_q > C_q$ FOR $(P_b/P_\infty)_{max.}$

FIG.23a. EFFECT OF BASE BLEED ON BASE PRESSURE

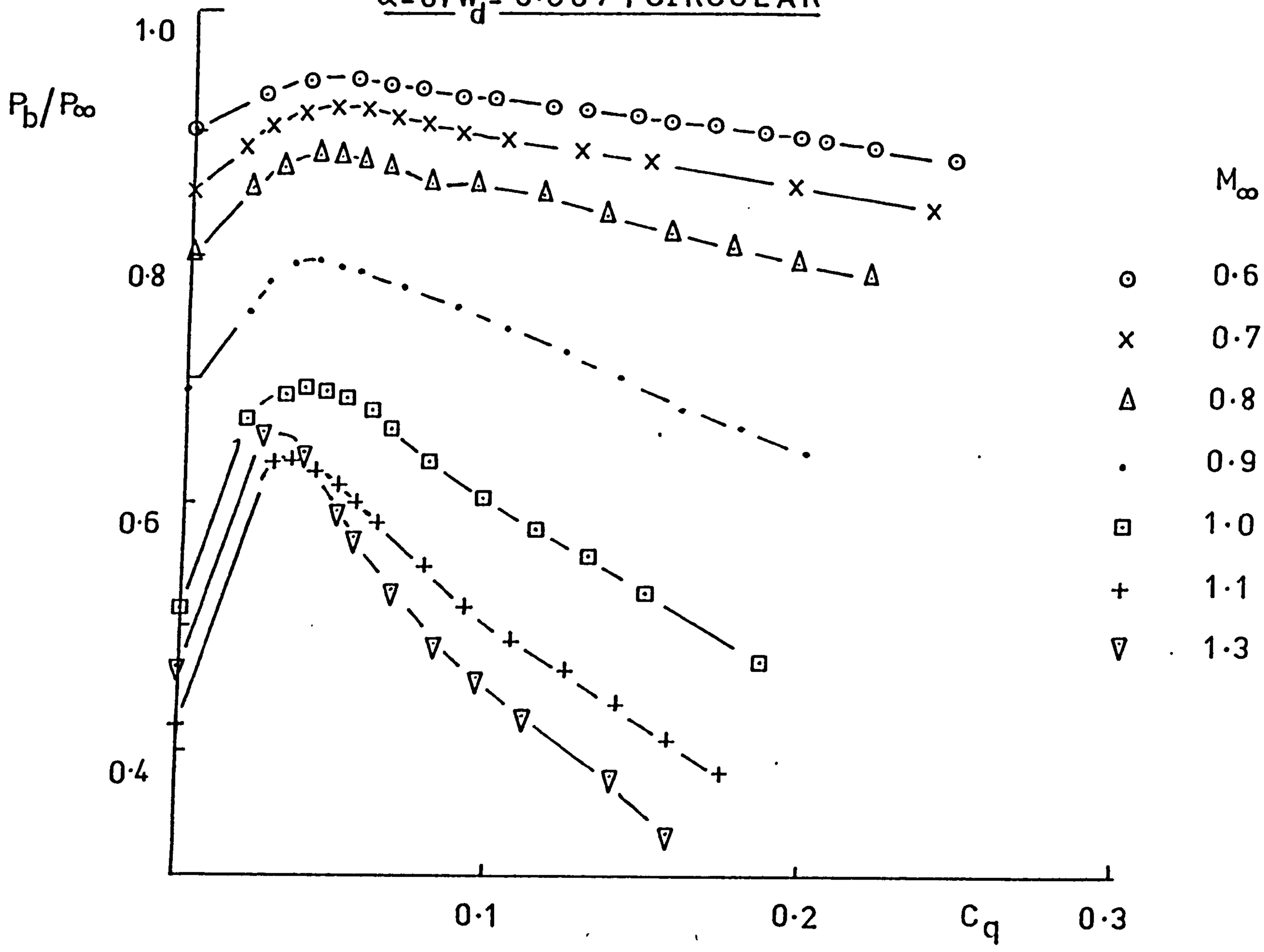

FIG.23b. EFFECT OF α ON THE VARIATION OF P_b/P_∞ WITH BASE BLEED

$M_\infty = 0.6$, $w_d = 0.007''$, CIRCULAR

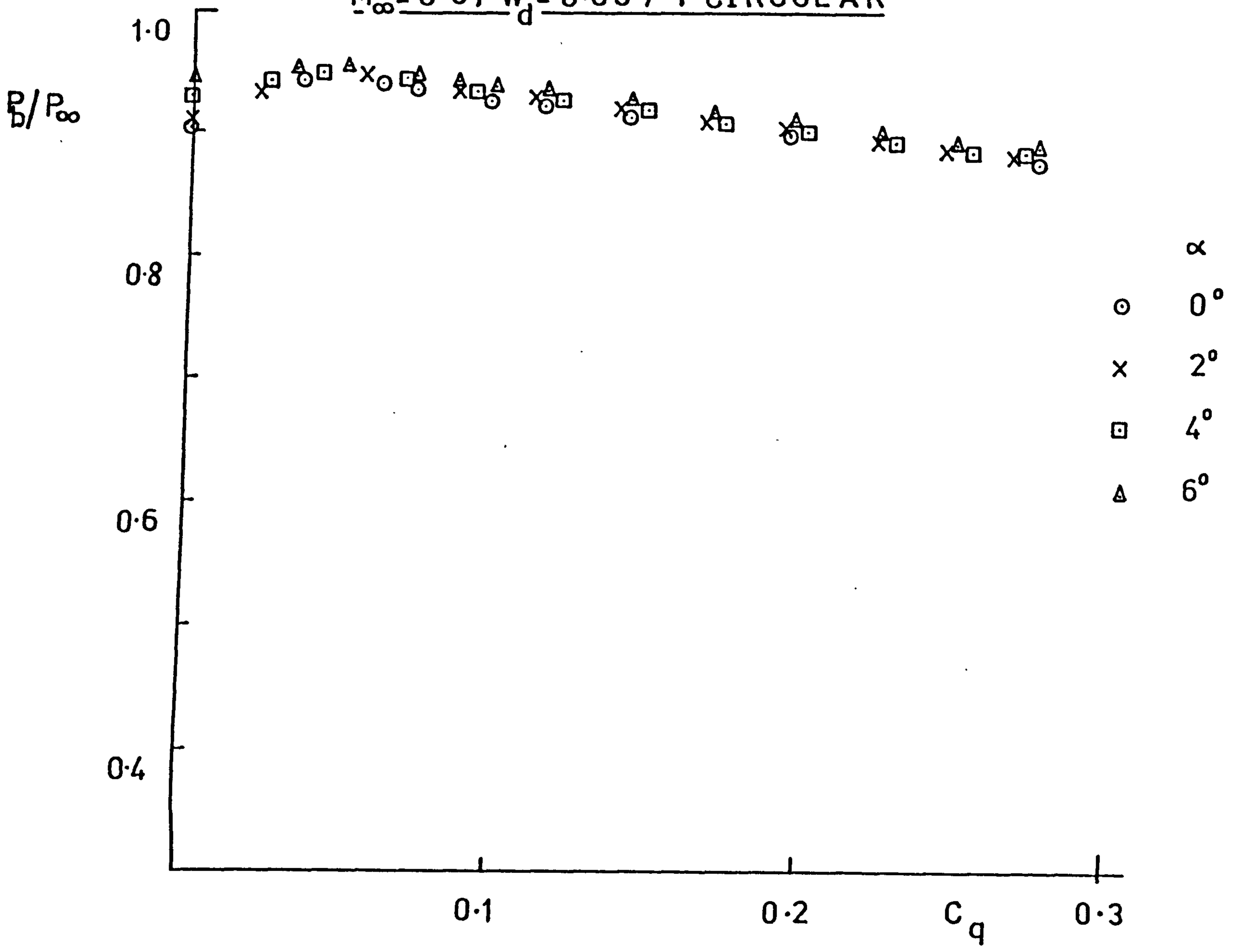

FIG.23c. EFFECT OF α ON THE VARIATION OF P_b/P_∞ WITH BASE BLEED

$M_\infty = 1.0$, $w_d = 0.007''$, CIRCULAR

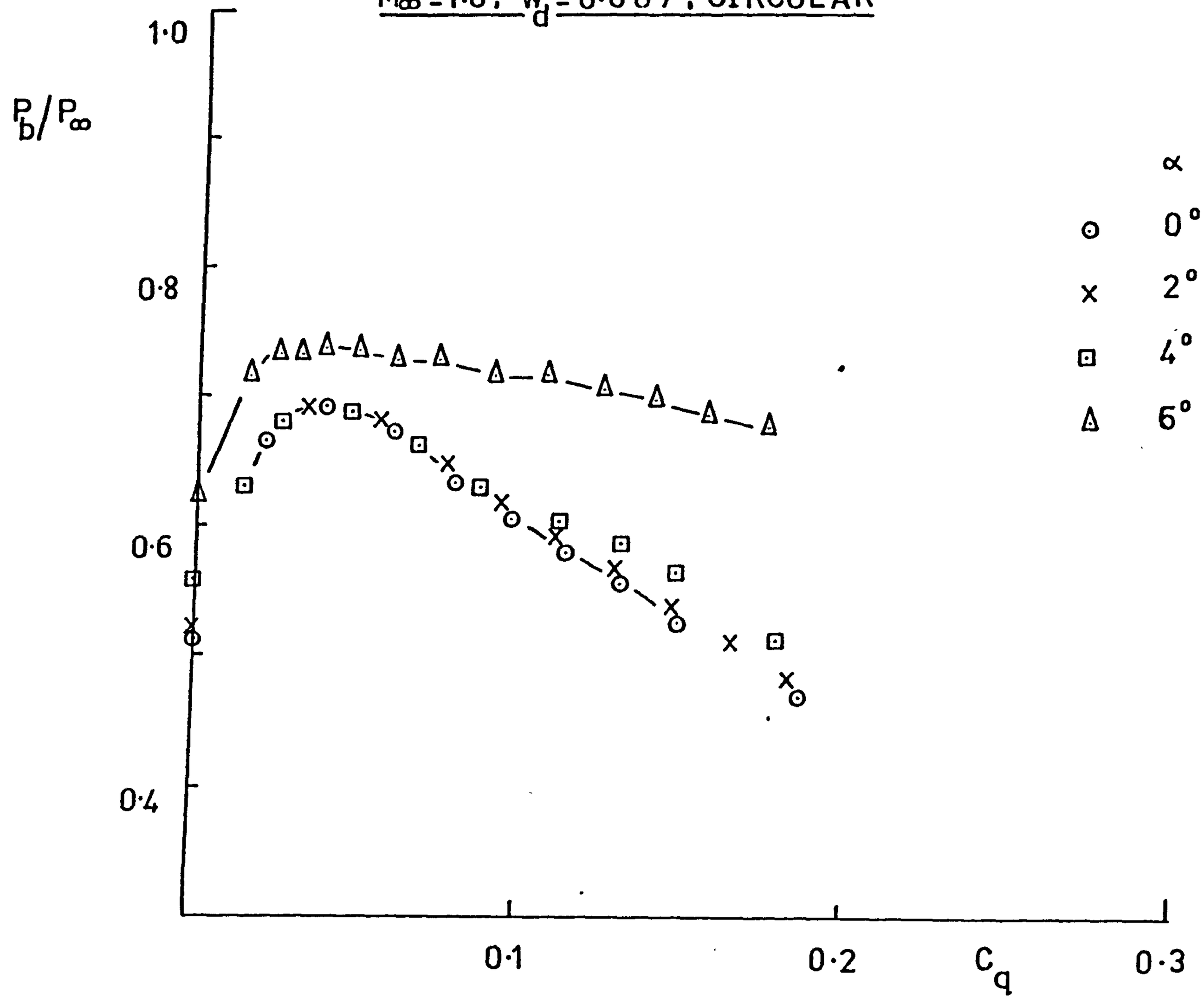

FIG.23d. EFFECT OF α ON THE VARIATION OF P_b/P_∞ WITH BASE BLEED

$M_\infty = 1.3$, $w_d = 0.007''$, CIRCULAR

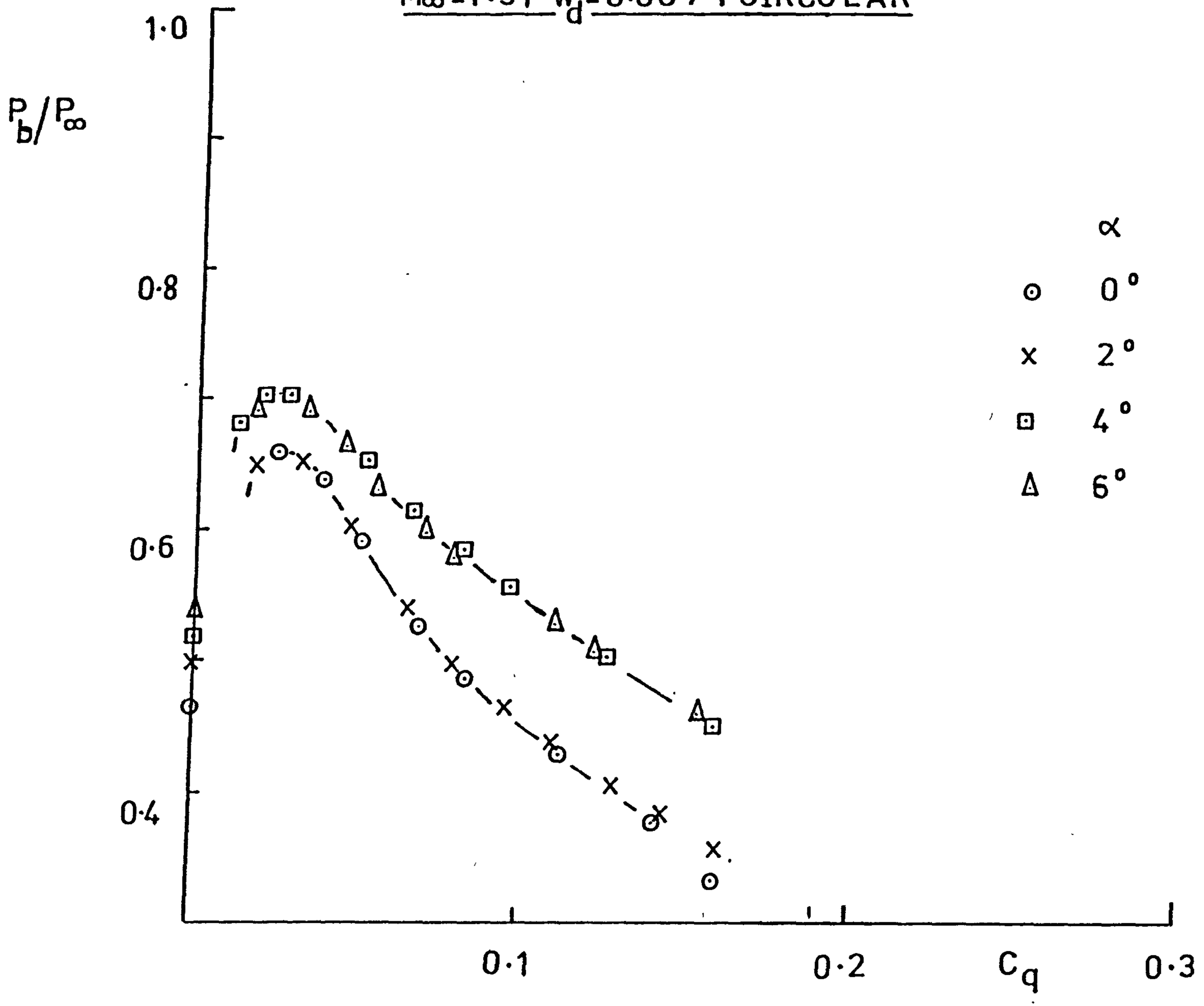

FIG. 24. EFFECT OF BASE BLEED ON BASE PRESSURE

$\alpha = 0°$, $w_d = 0.007''$, FLARED

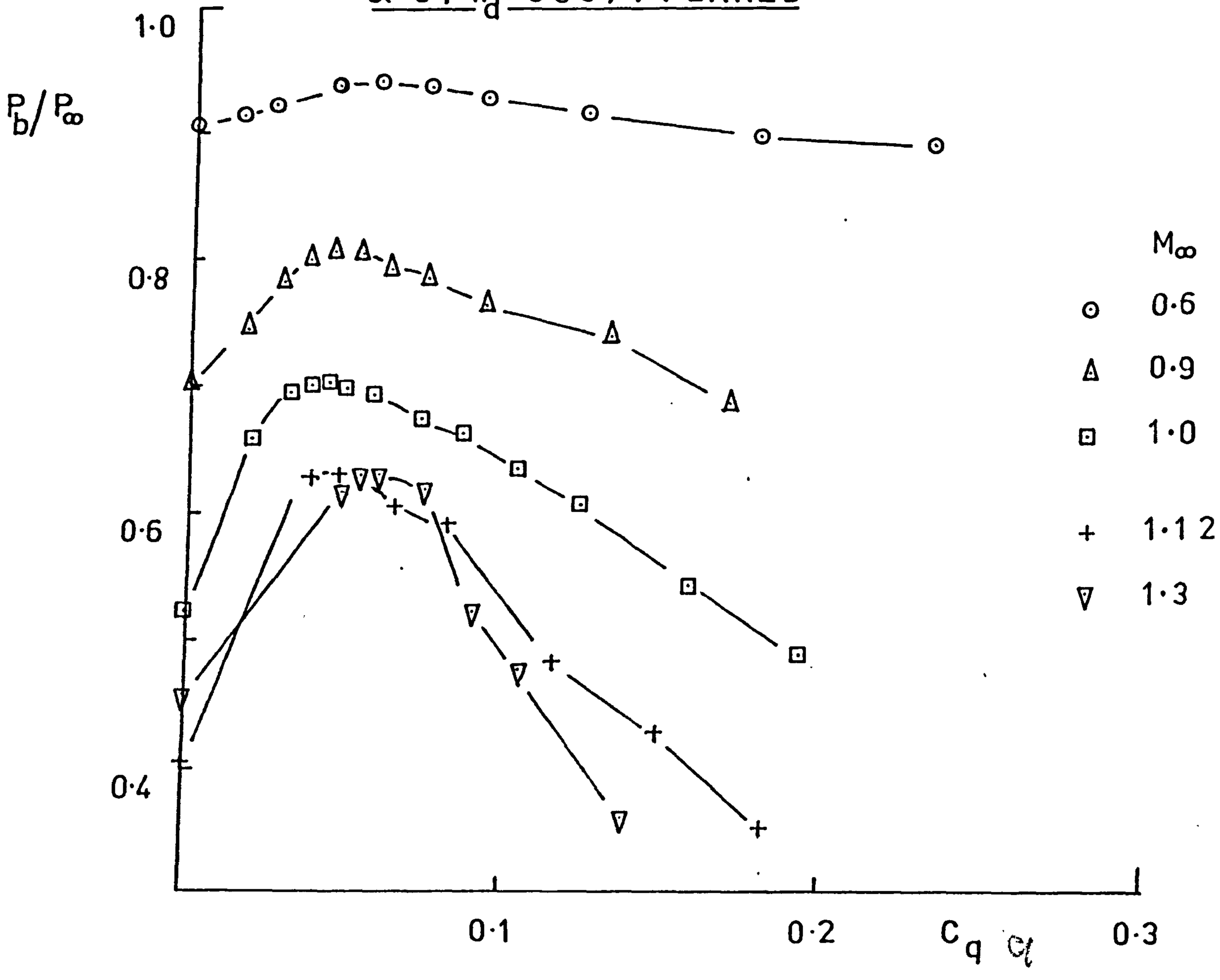

FIG.25a.WAKE PROFILE

$M_\infty = 0.6$, $\alpha = 0°$, CIRCULAR HOLES

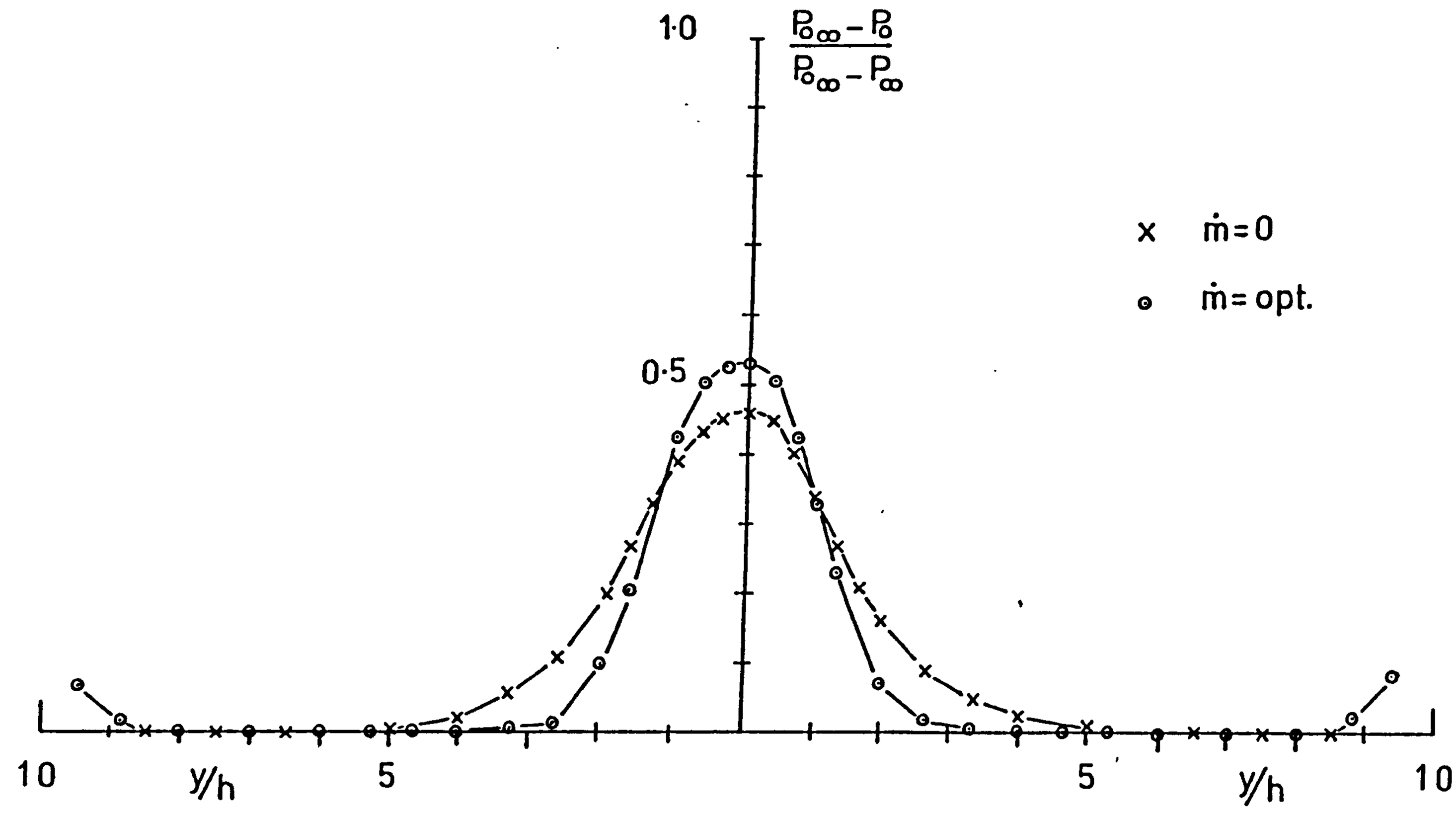

FIG25b. WAKE PROFILE

$M_\infty = 1{\cdot}0$, $\alpha = 0°$, CIRCULAR HOLES

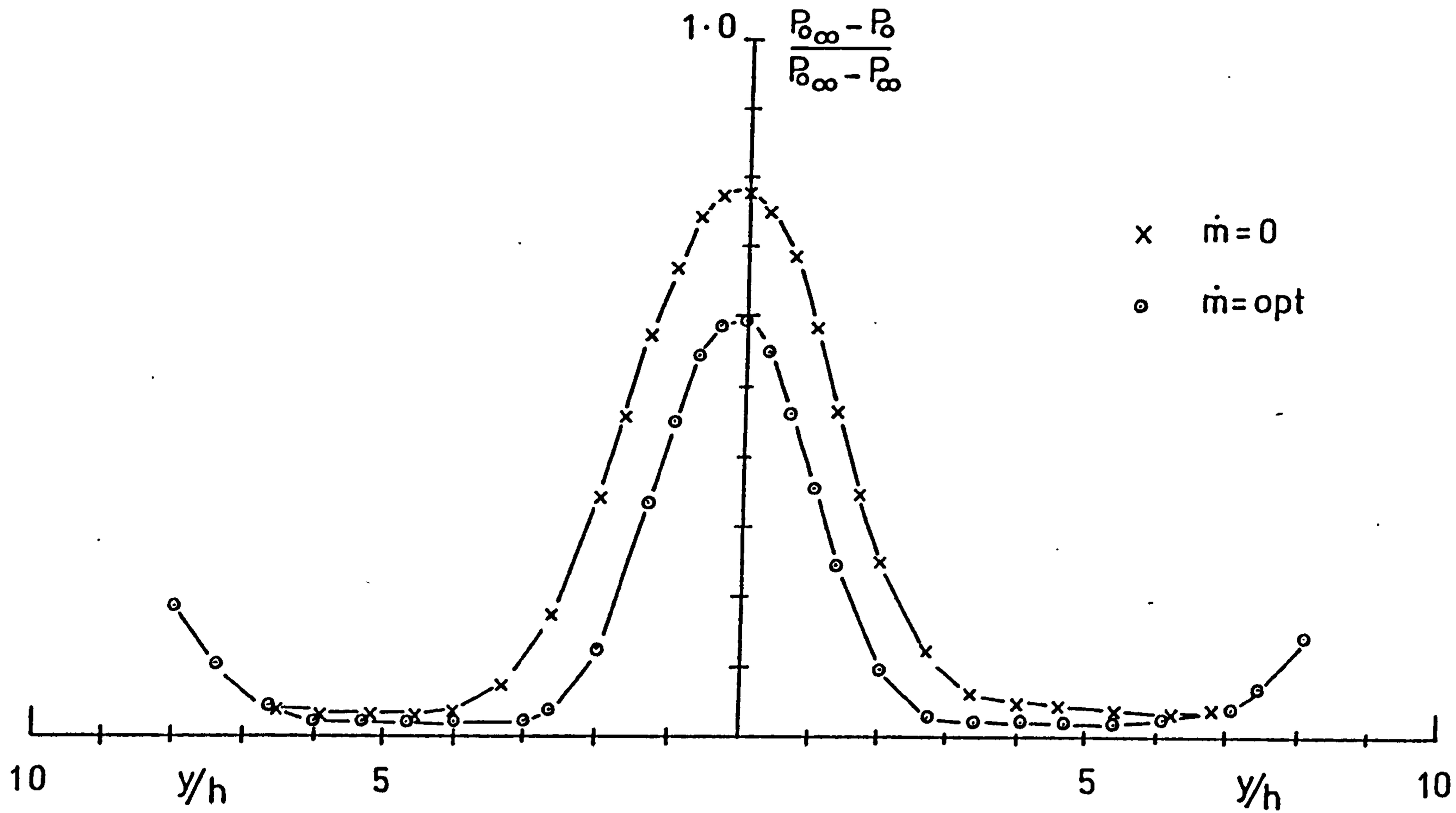

FIG.25c. WAKE PROFILE

M_∞=1·135, α=0°; CIRCULAR HOLES

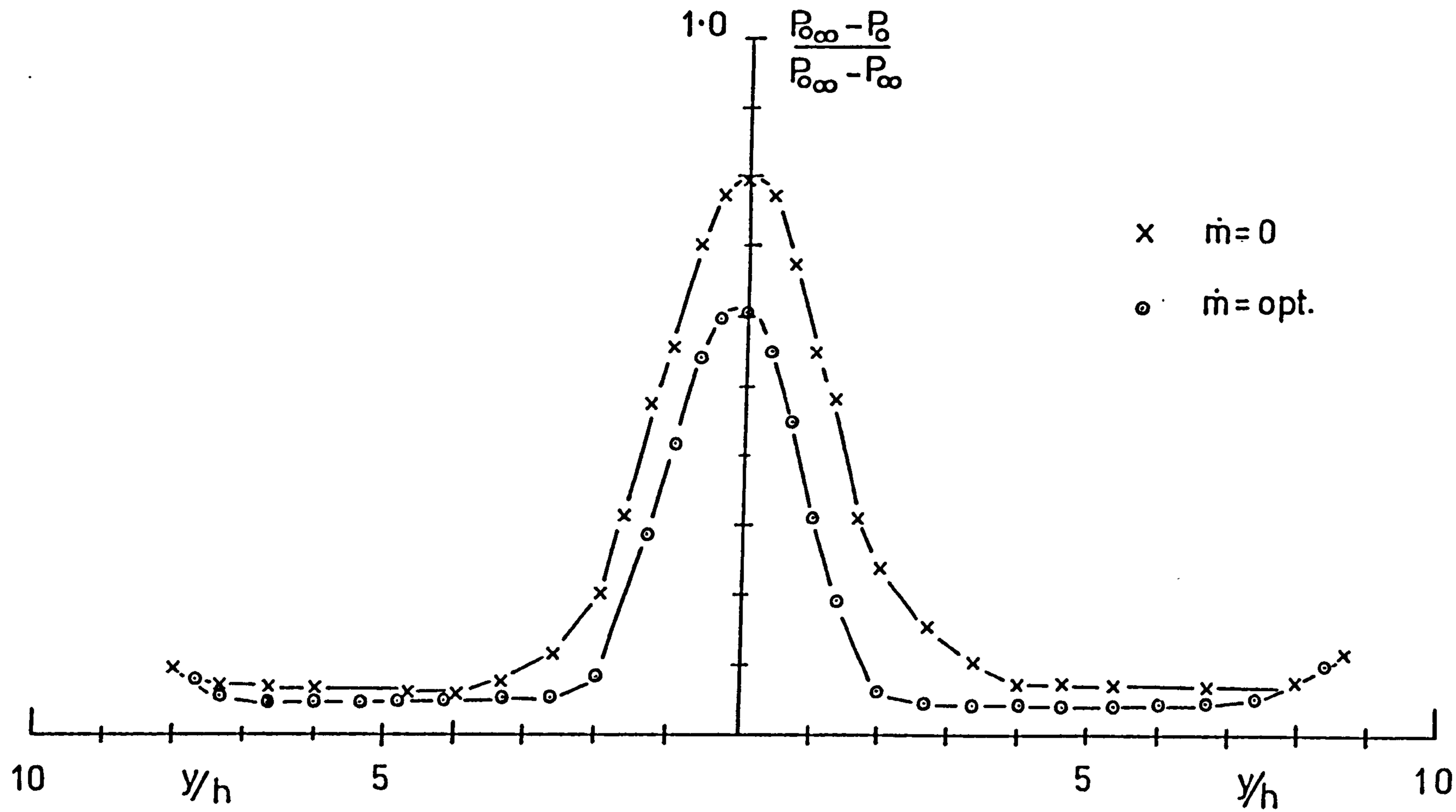

FIG.25d. WAKE PROFILE

M_∞=1·3, α=0°; CIRCULAR HOLES

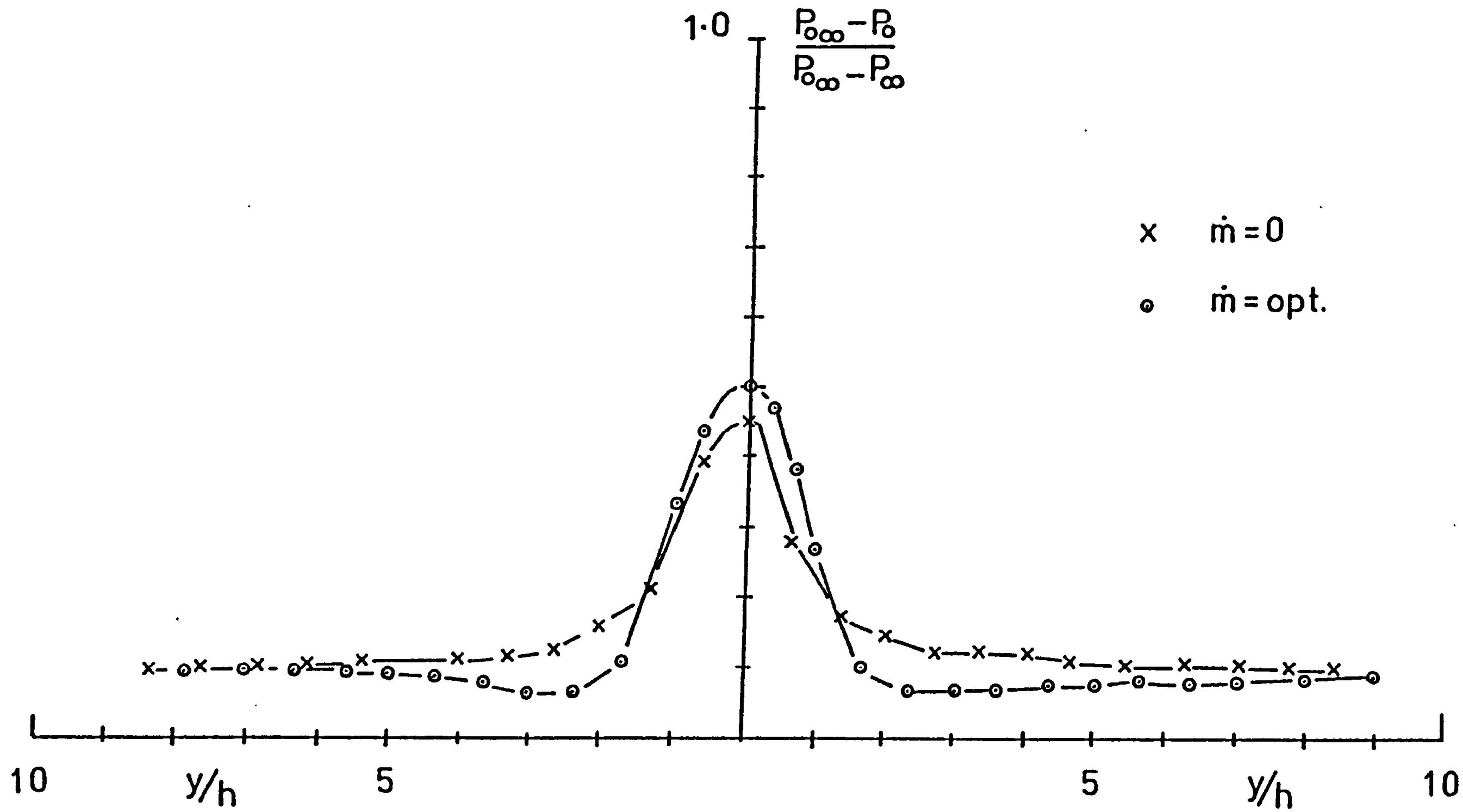

FIG.26a. WAKE PROFILE

$M_\infty = 0.6$, $\alpha = 2°$; CIRCULAR HOLES

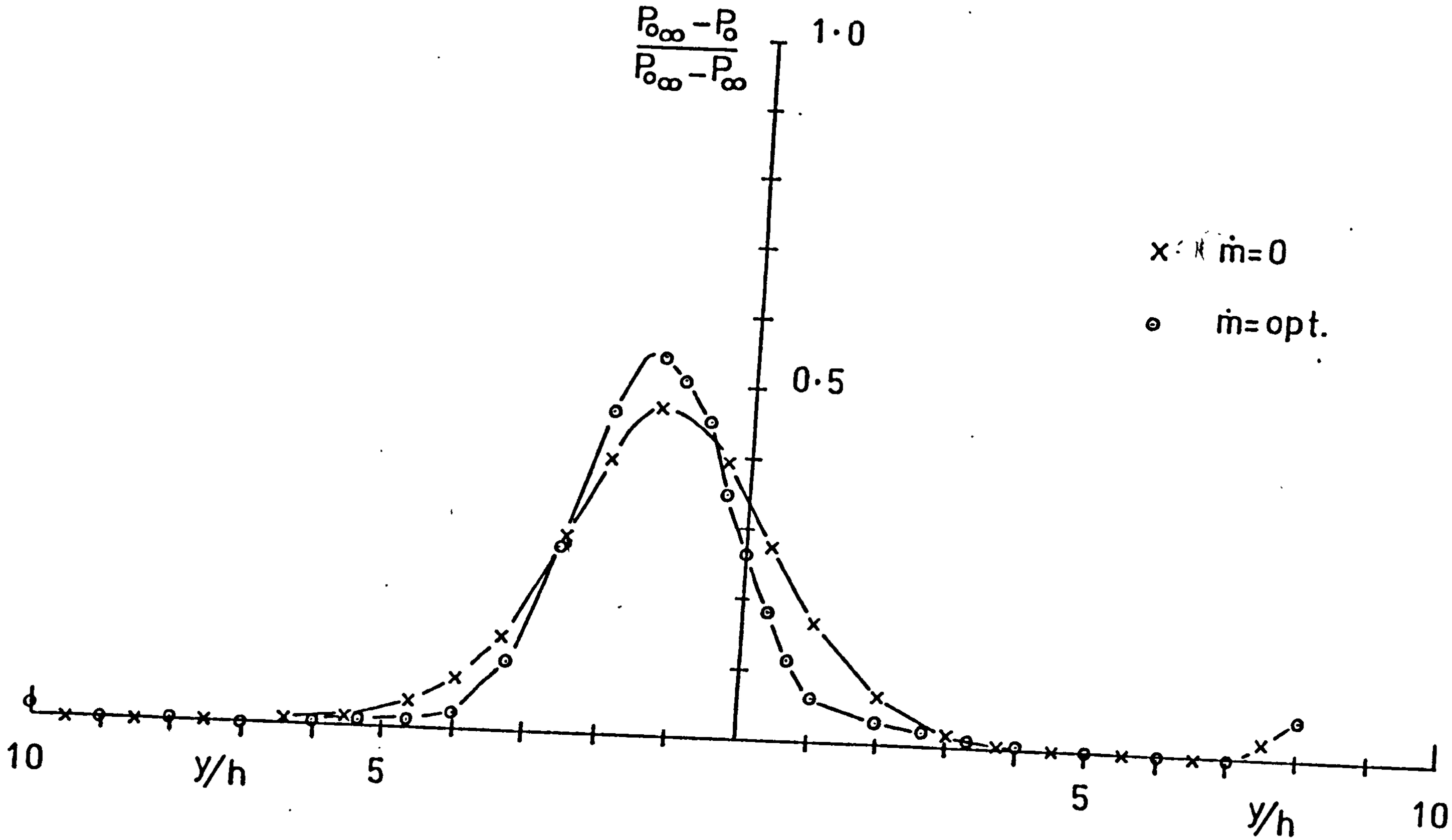

FIG26b. WAKE PROFILE

$M_\infty = 0{\cdot}6$, $\alpha = 6°$; CIRCULAR HOLES

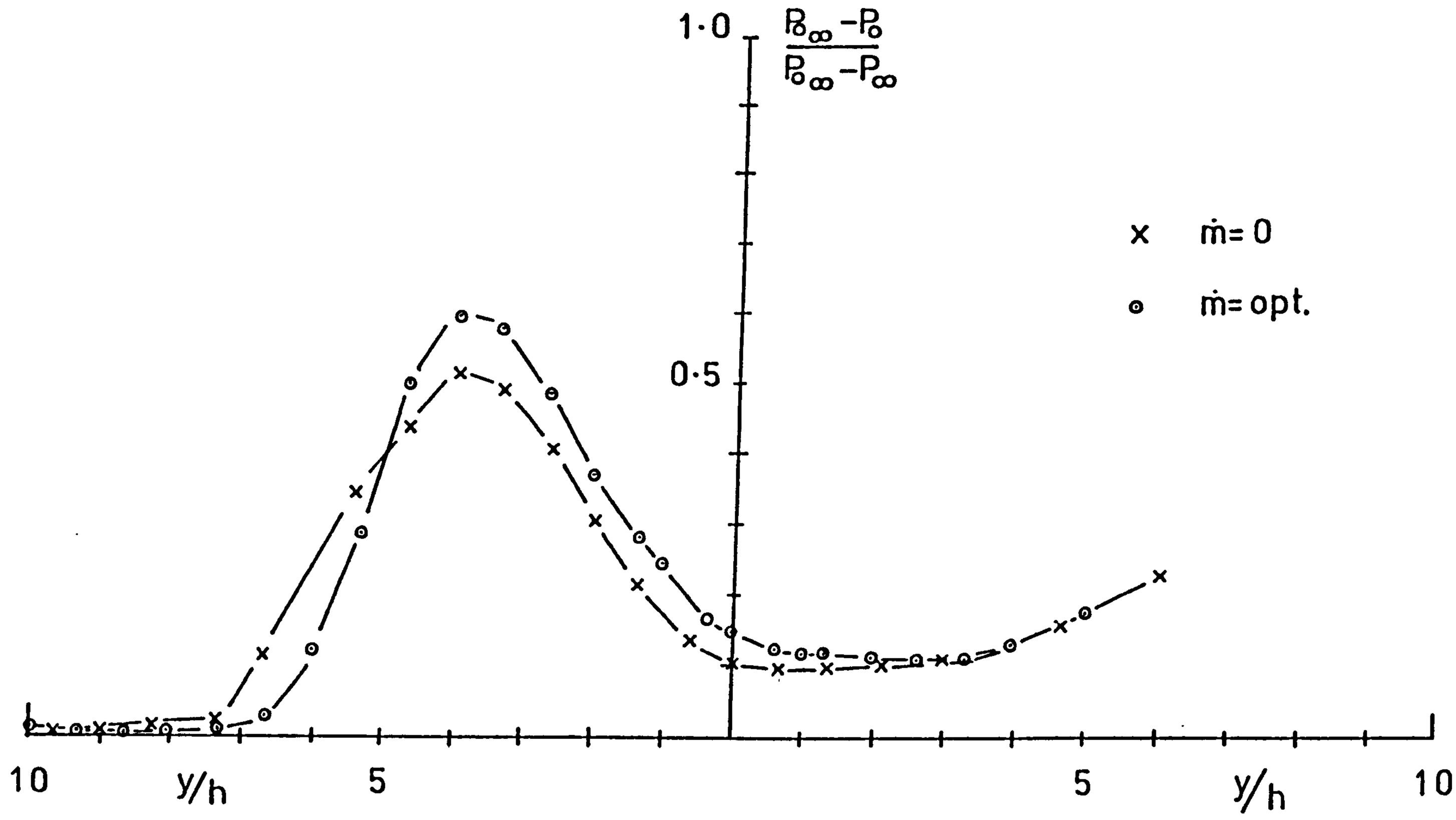

FIG.27a. WAKE PROFILE

$M_\infty = 1{\cdot}0$, $\alpha = 2°$; CIRCULAR HOLES

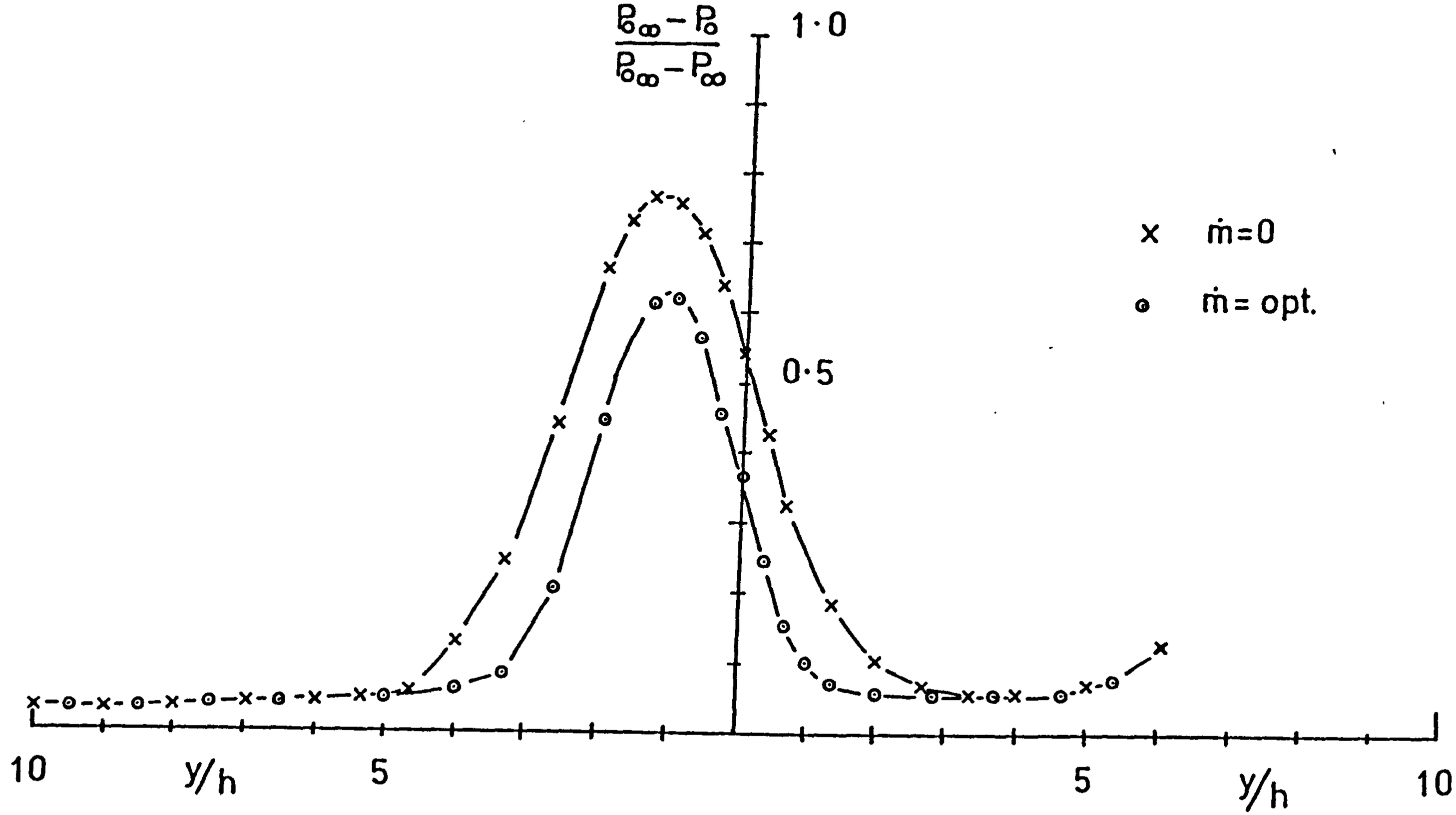

FIG27b. WAKE PROFILE

$M_\infty = 1{\cdot}0$, $\alpha = 6°$ CIRCULAR HOLES

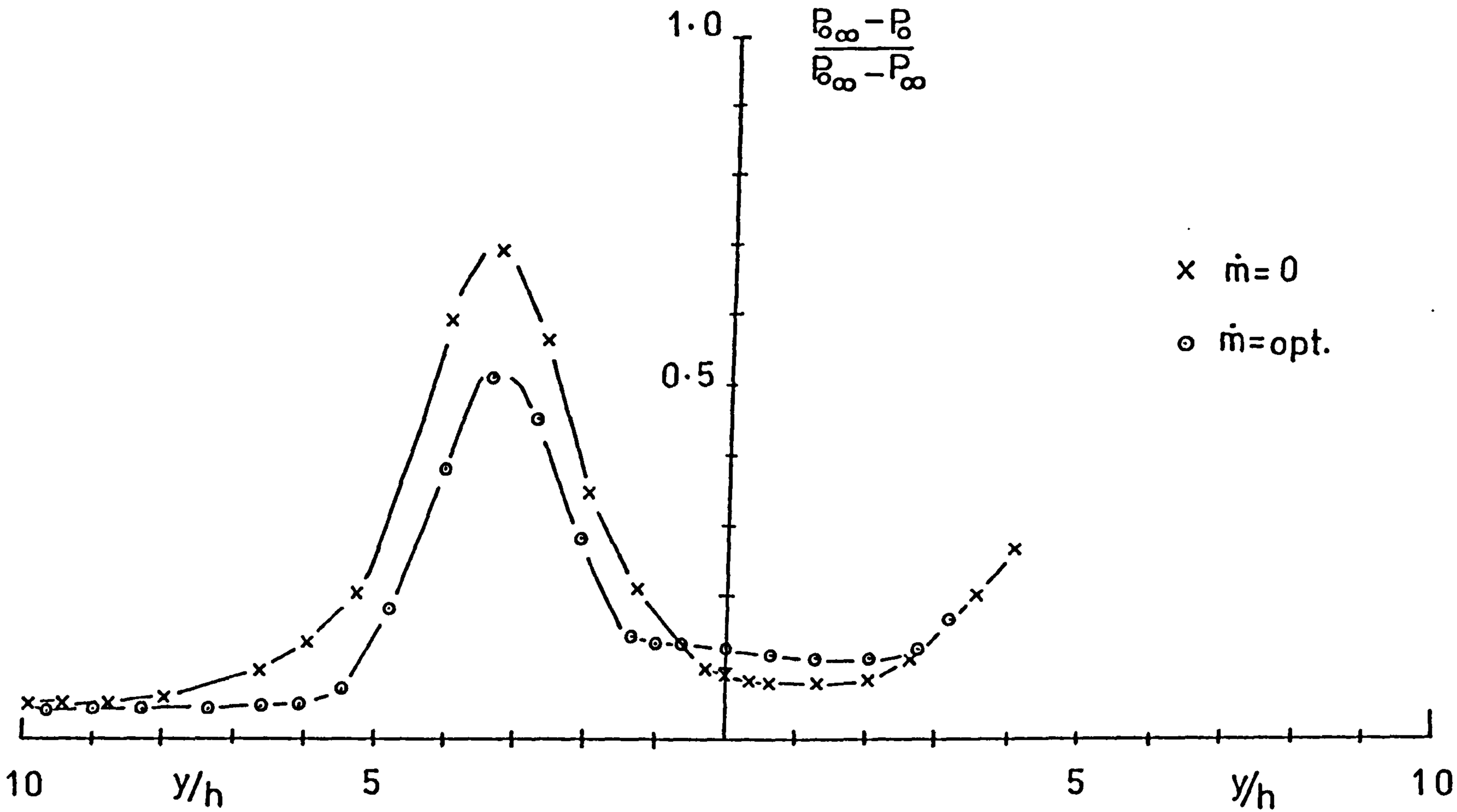

FIG.28a. WAKE PROFILE

M_∞=1·3, α= 2°, CIRCULAR HOLES

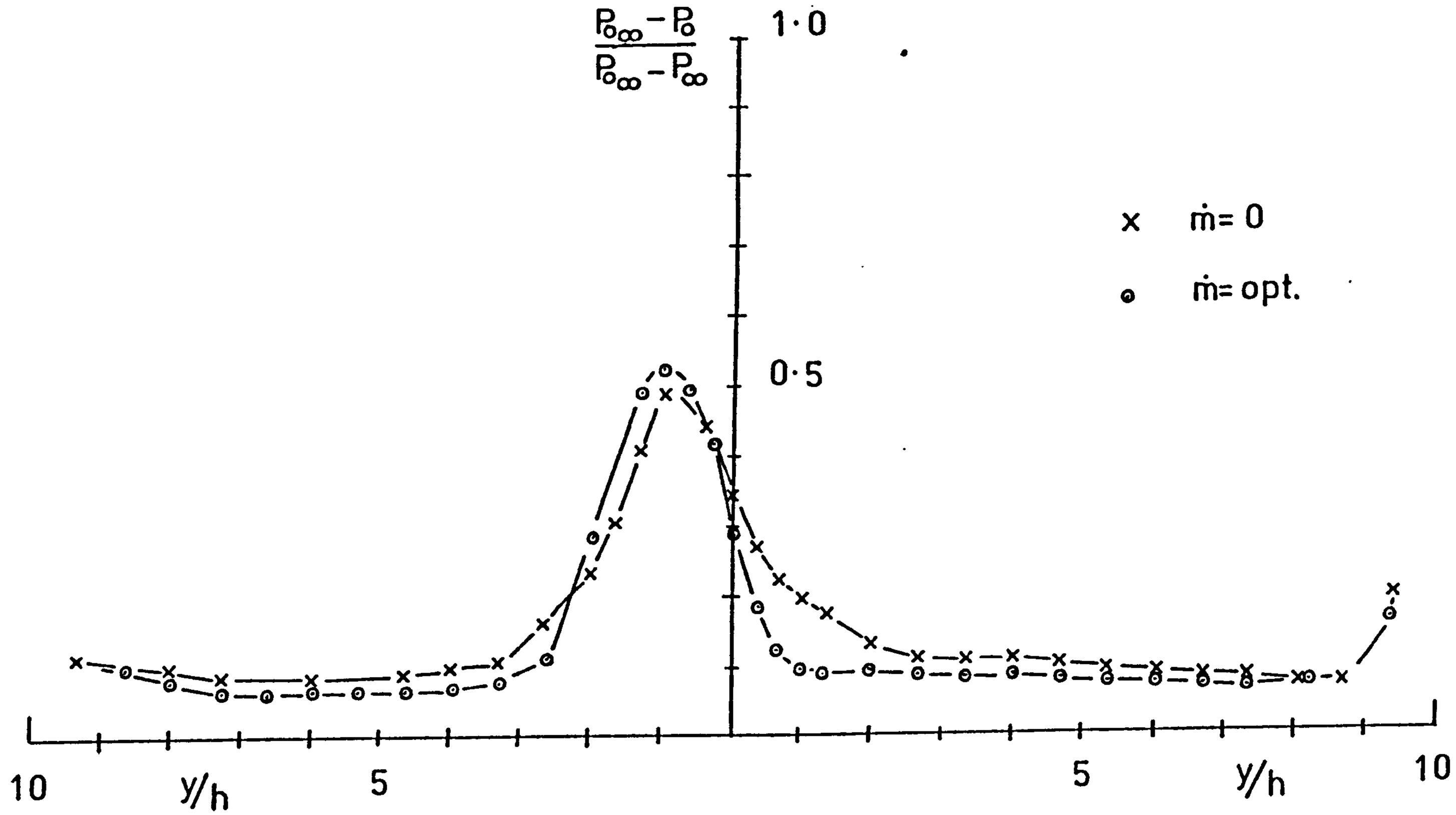

FIG.28b. WAKE PROFILE

M_∞=1·3, α=6°; CIRCULAR HOLES

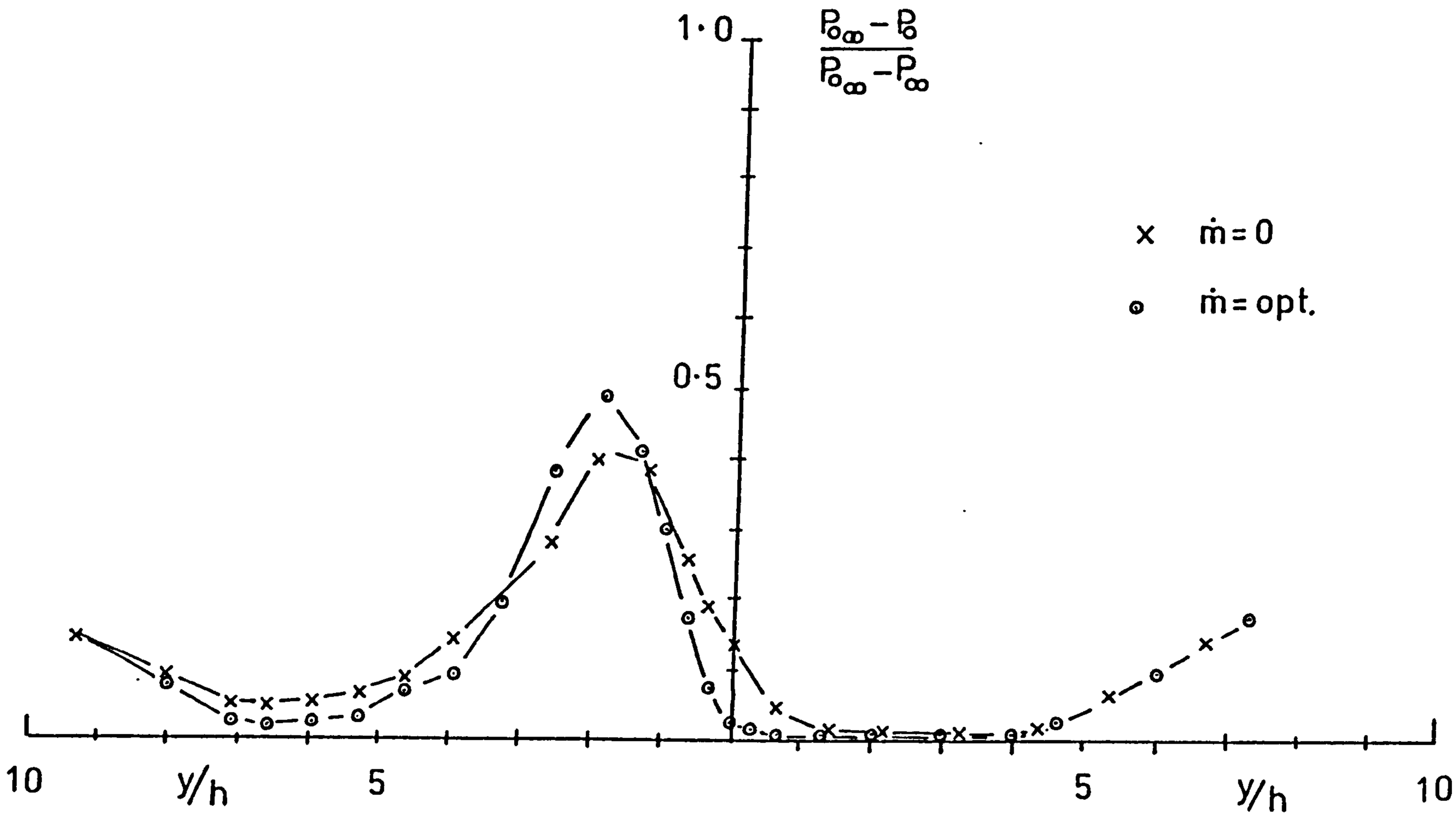

FIG29a. WAKE PROFILE

$M_\infty = 0.6$, $\alpha = 0°$, FLARED HOLES

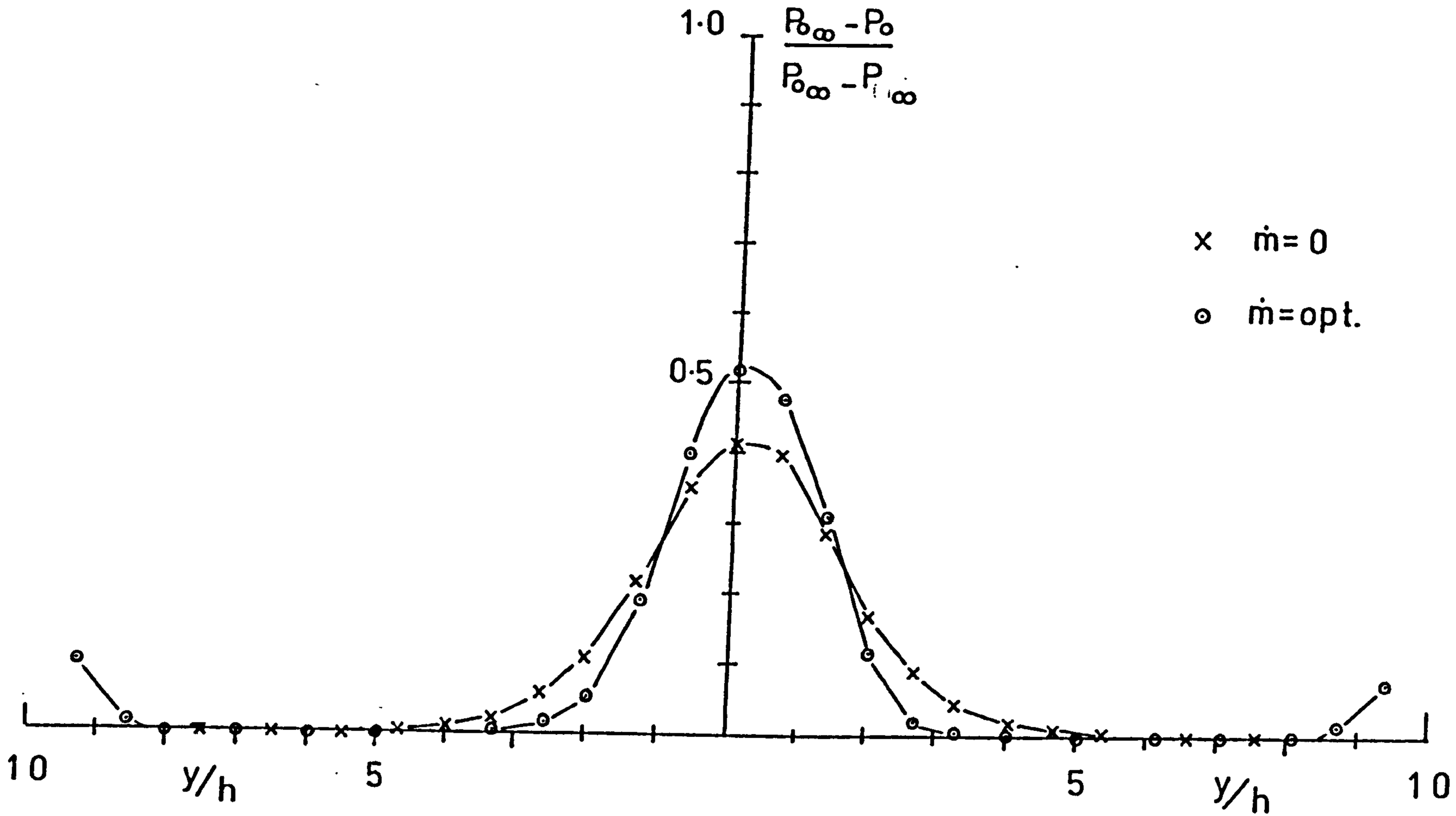

FIG29b.WAKE PROFILE

$M_\infty = 1{\cdot}0, \alpha = 0°$ FLARED HOLES

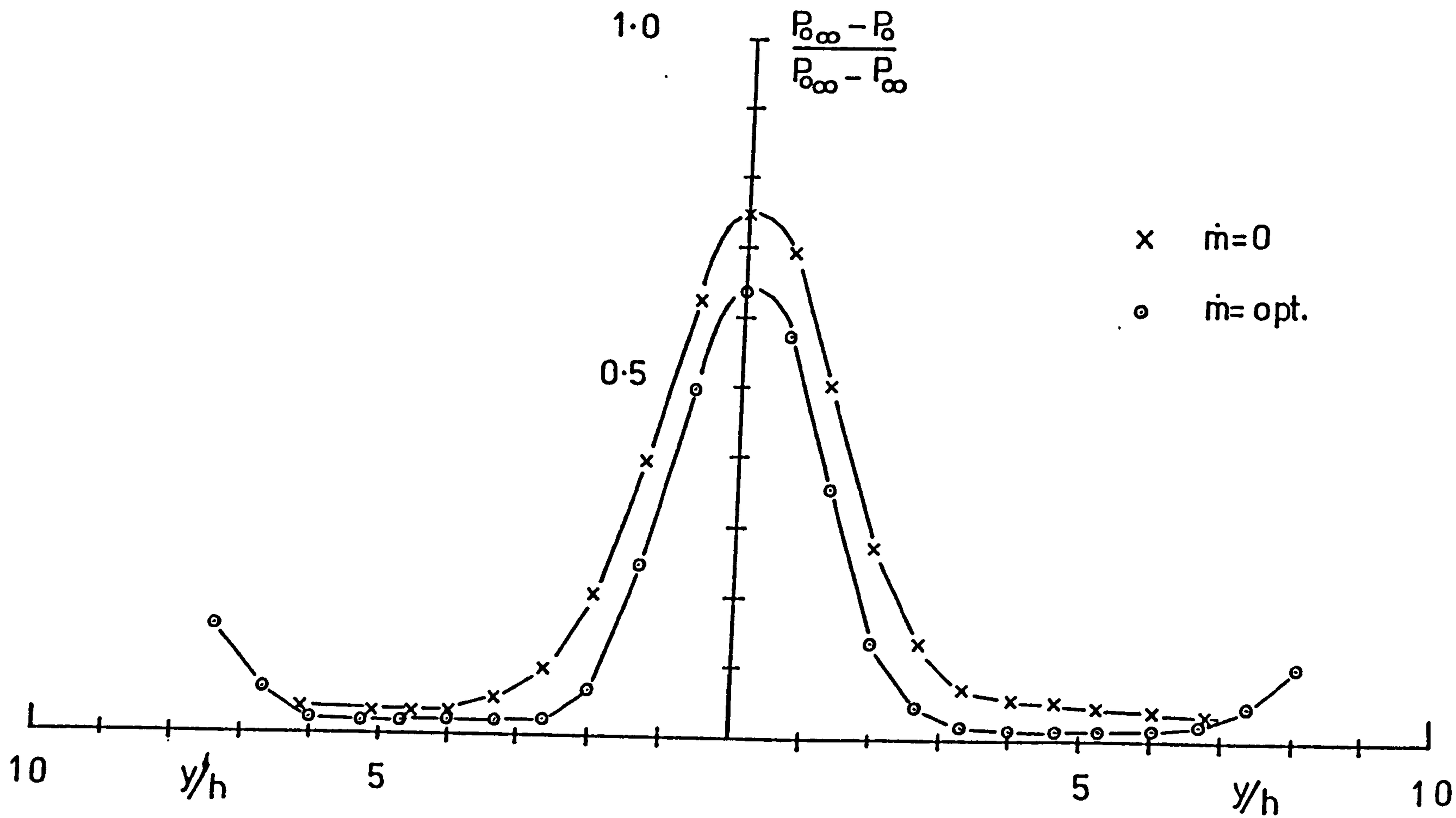

FIG. 29c. WAKE PROFILE

$M_\infty = 1.135$, $\alpha = 0°$ FLARED HOLES

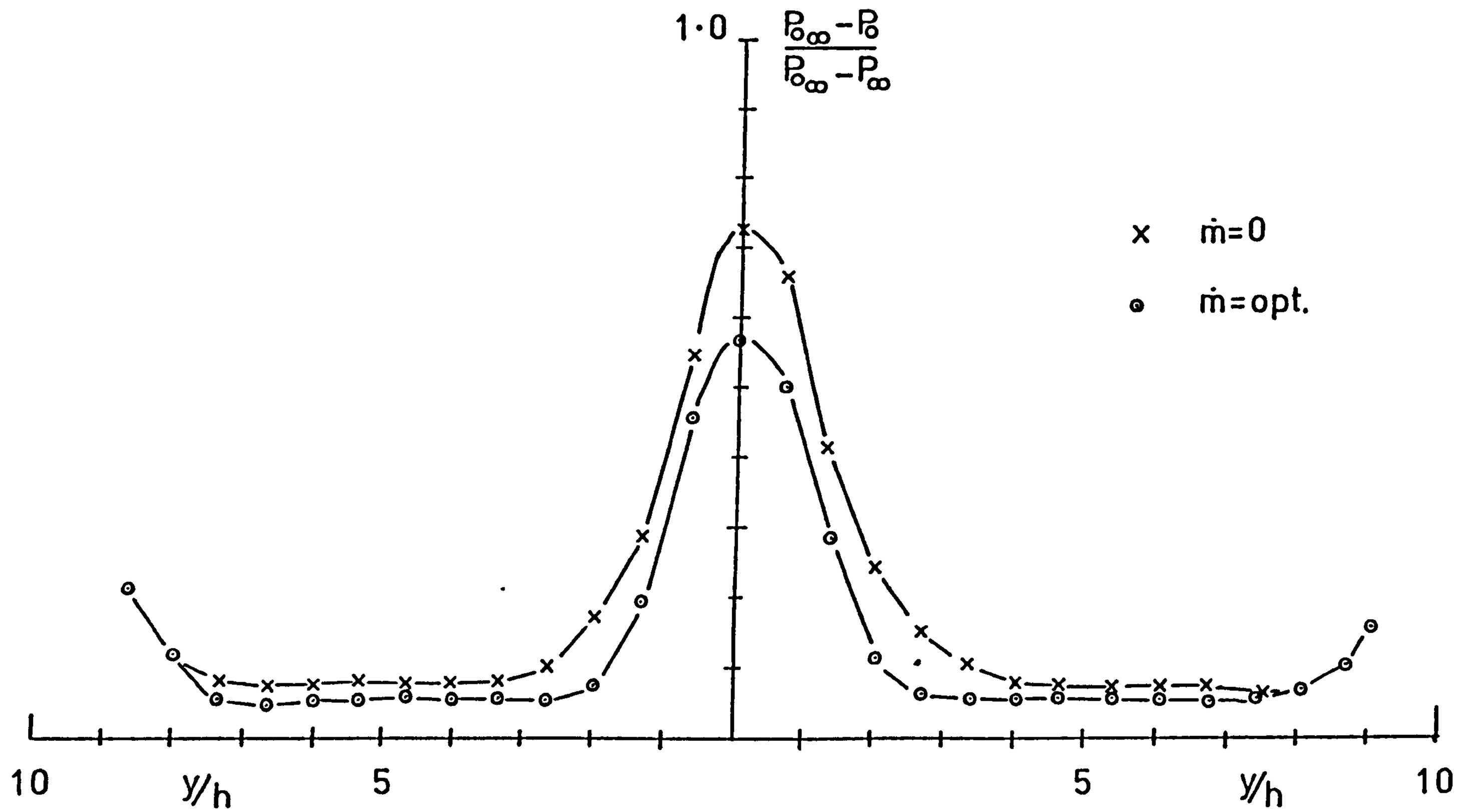

FIG.29d. WAKE PROFILE

$M_\infty = 1{\cdot}3$, $\alpha = 0^\circ$, FLARED HOLES

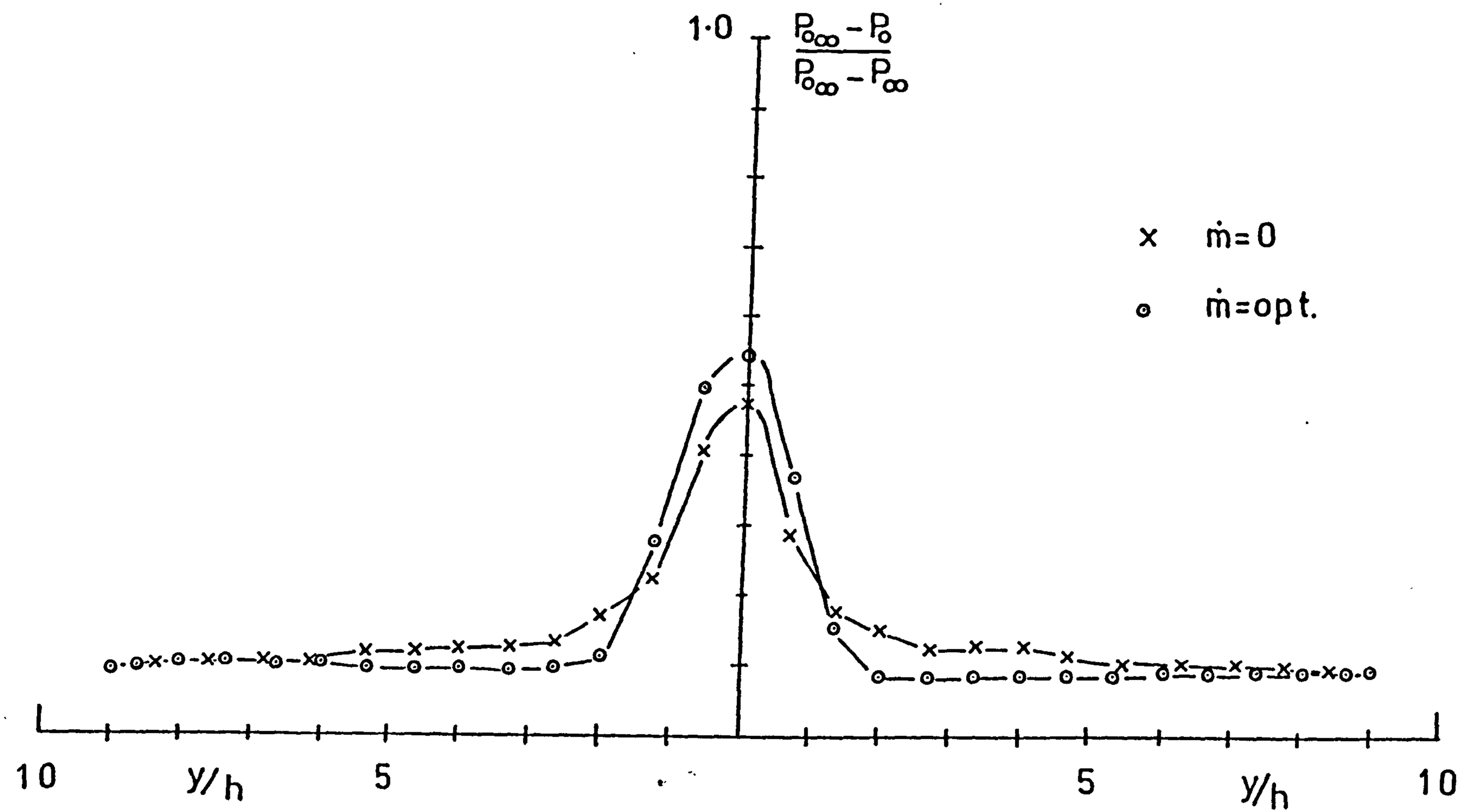

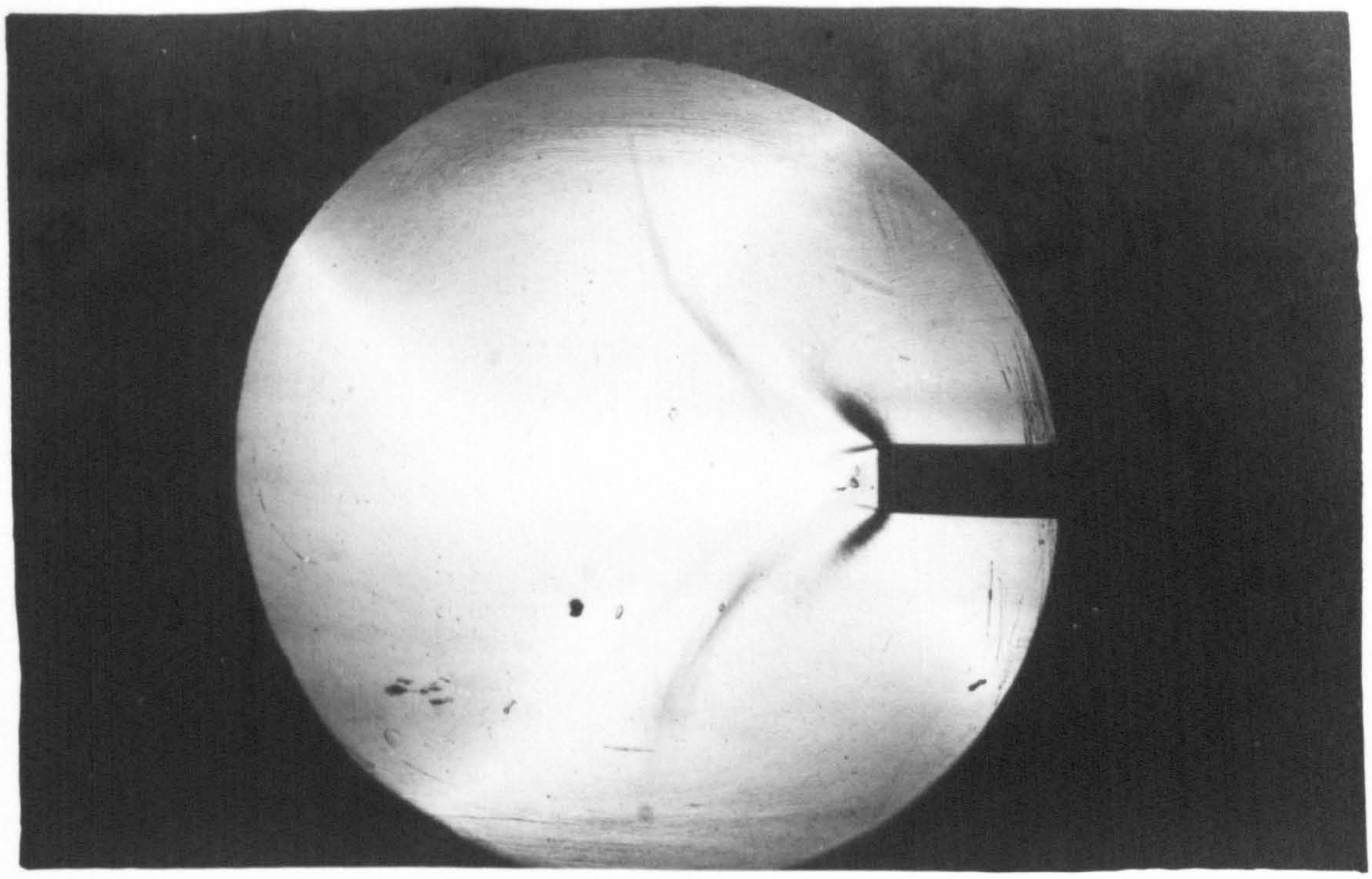

Plate 1a

Circular hole base, $M_\infty = 1.0$, $\dot{m} = 0$.

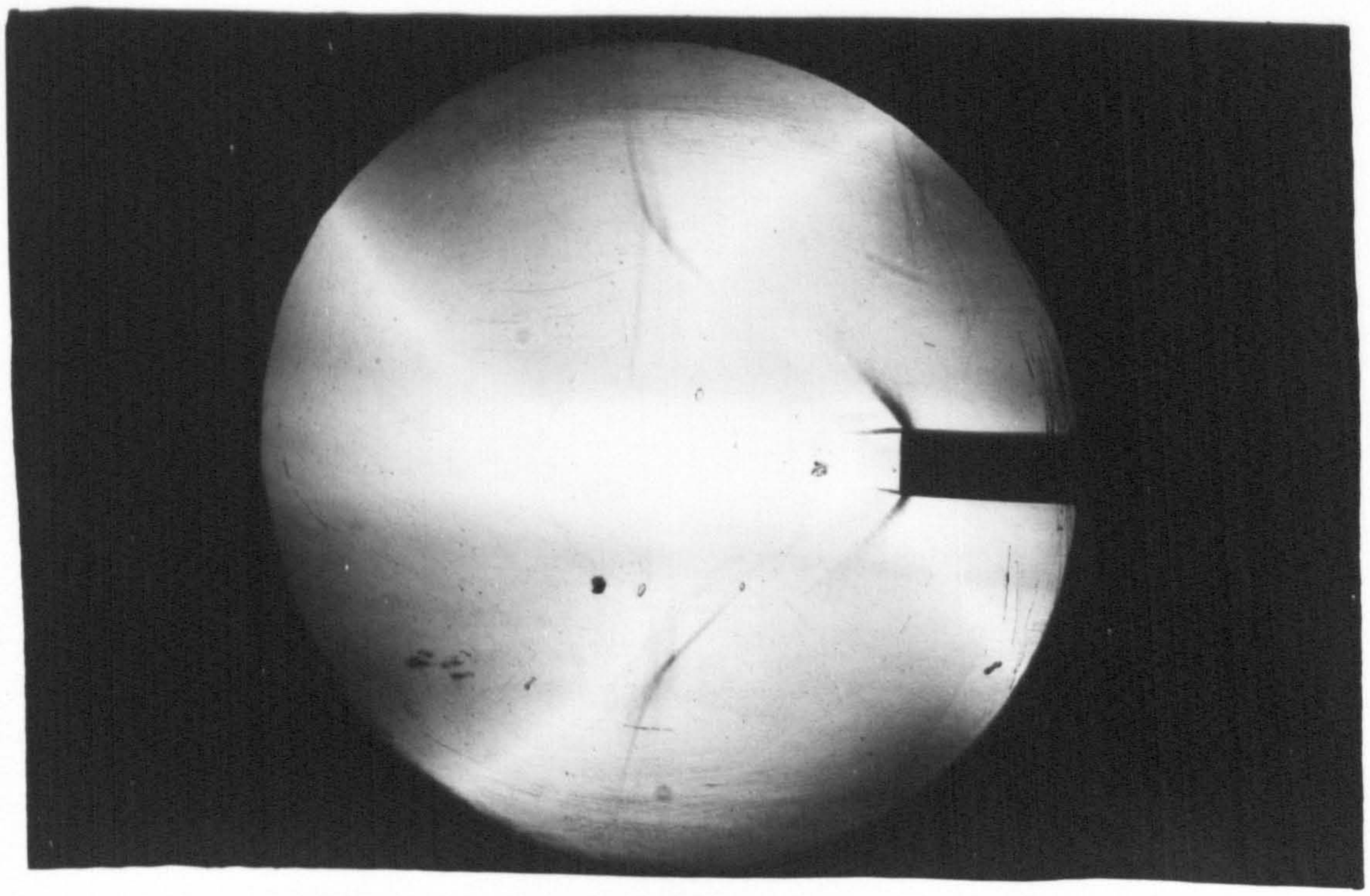

Plate 1b

Circular hole base, $M_\infty = 1.0$, $\dot{m} = \text{opt.}$

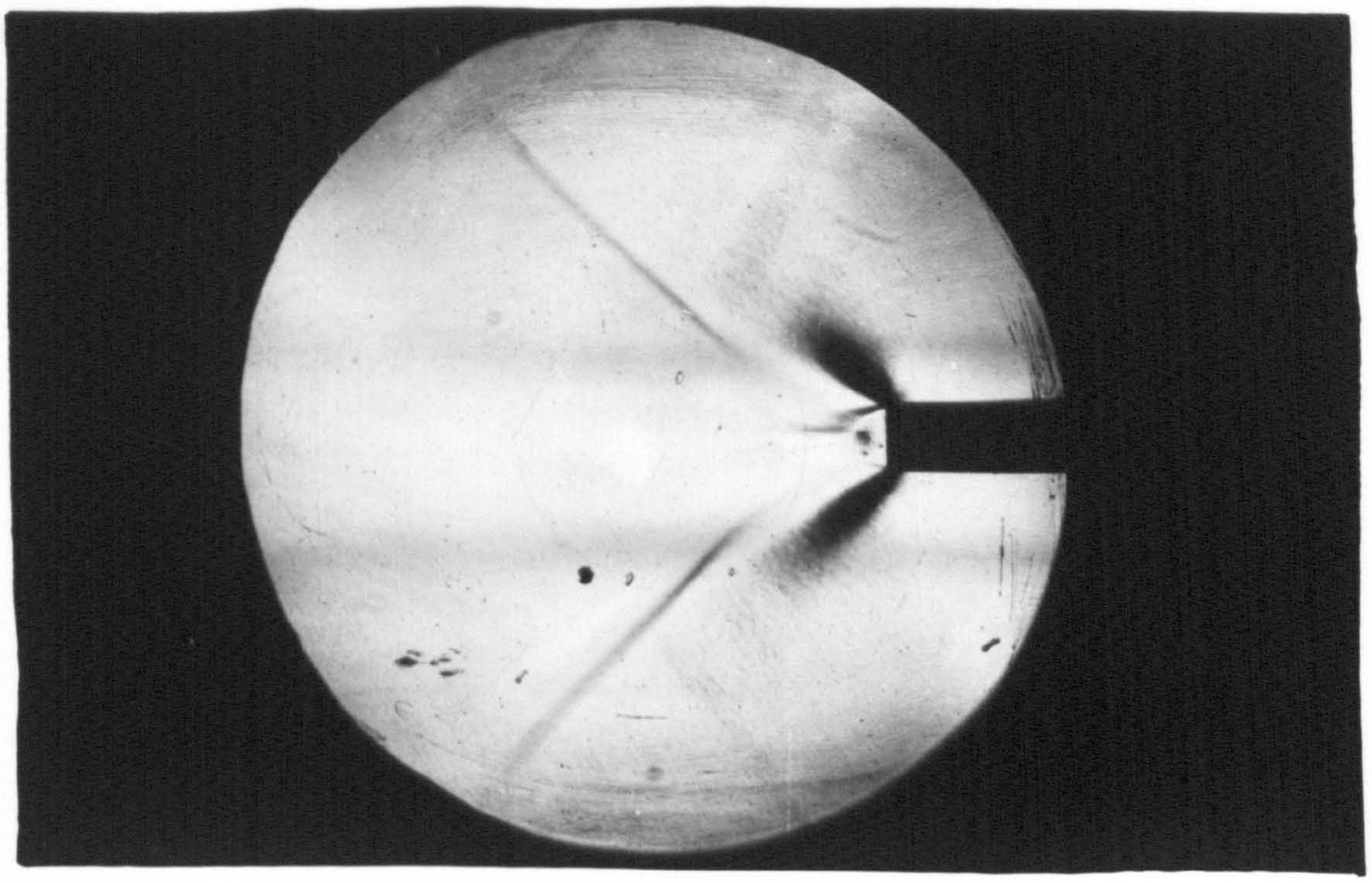

Plate 2a

Circular hole base, $M_\infty = 1.1$, $\dot{m} = 0$.

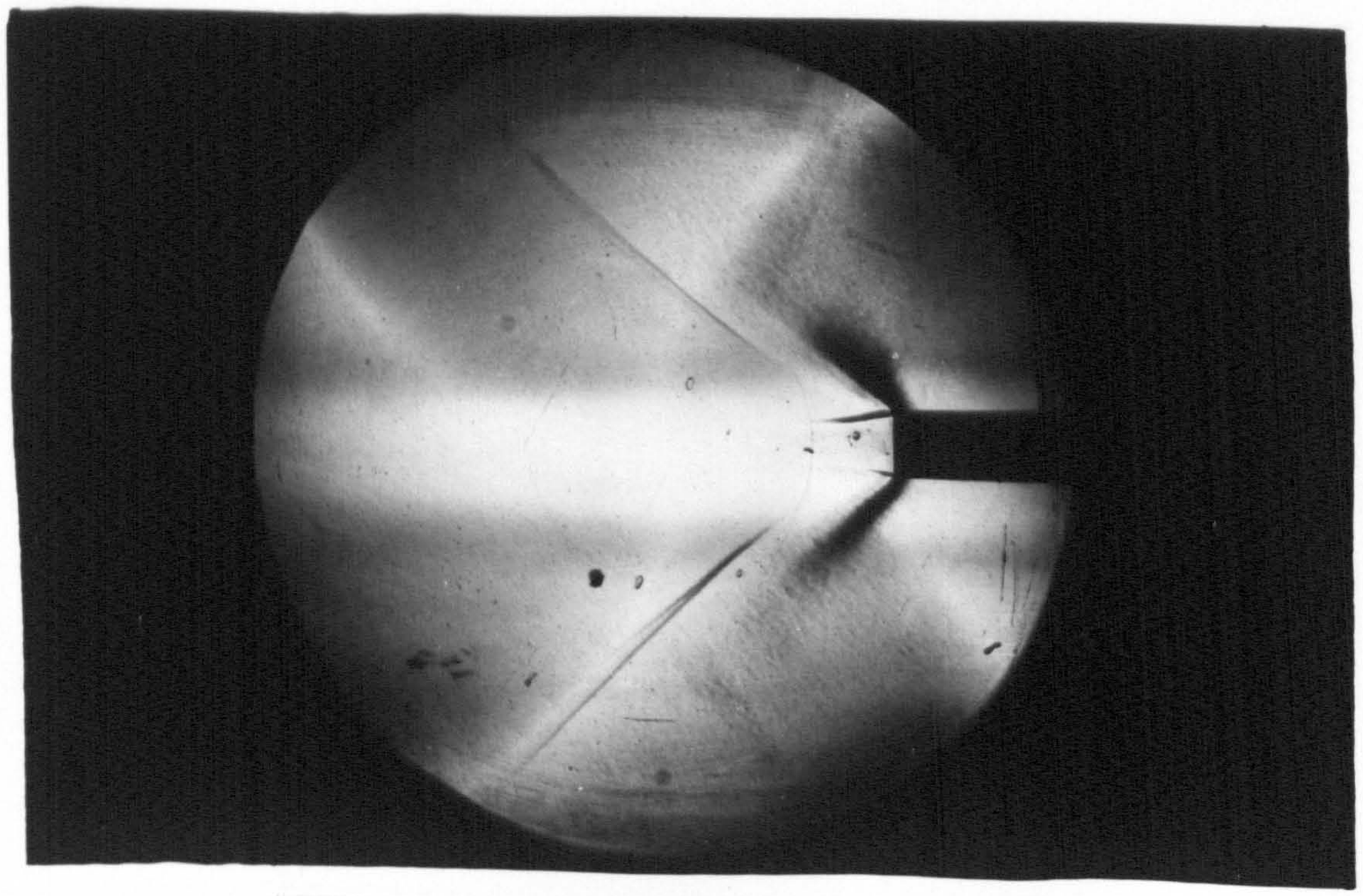

Plate 2b

Circular hole base, $M_\infty = 1.1$, $\dot{m} = \text{opt.}$

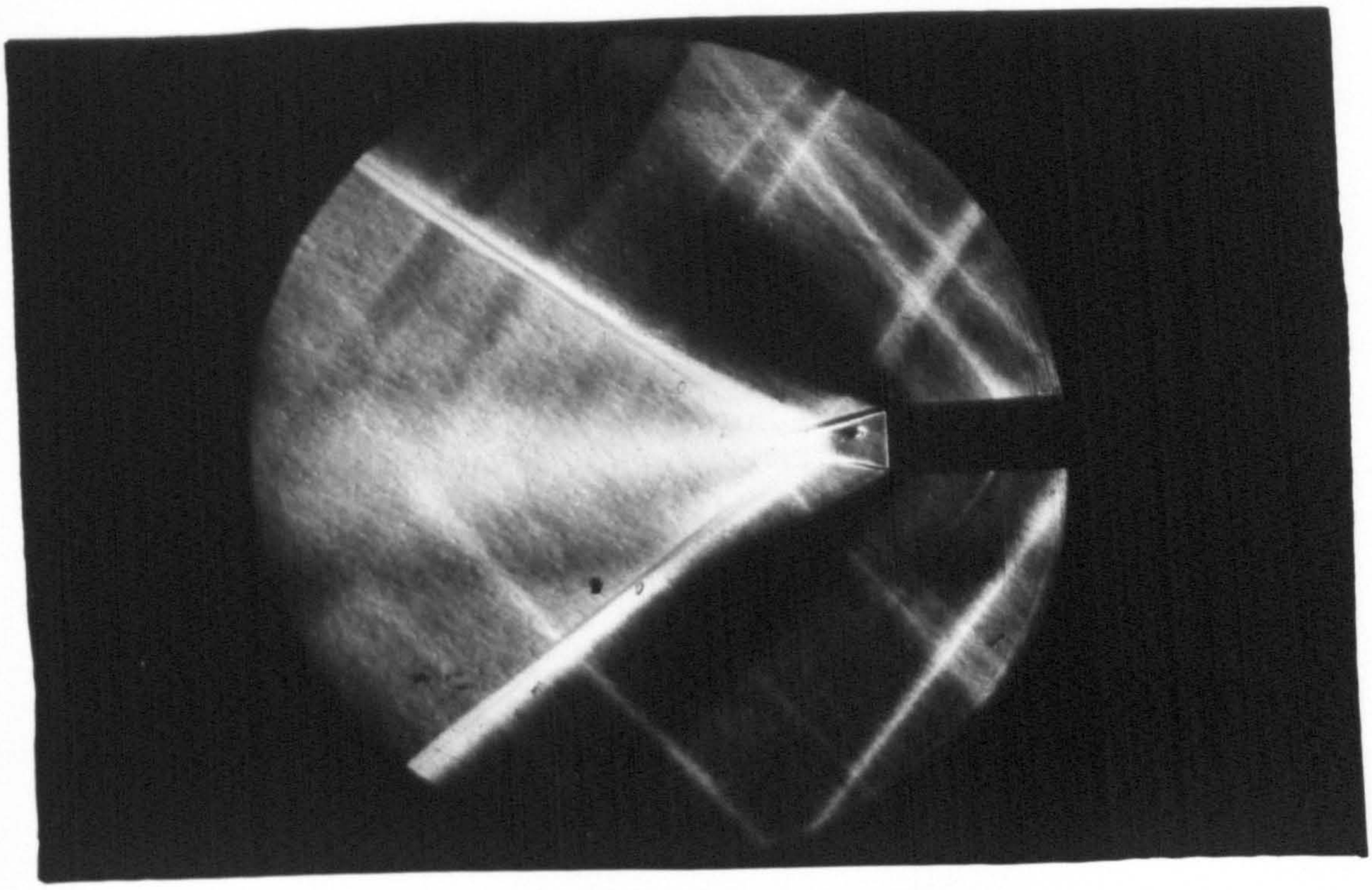

Plate 3a

Circular hole base, $M_\infty = 1.3$, $\dot{m} = 0$.

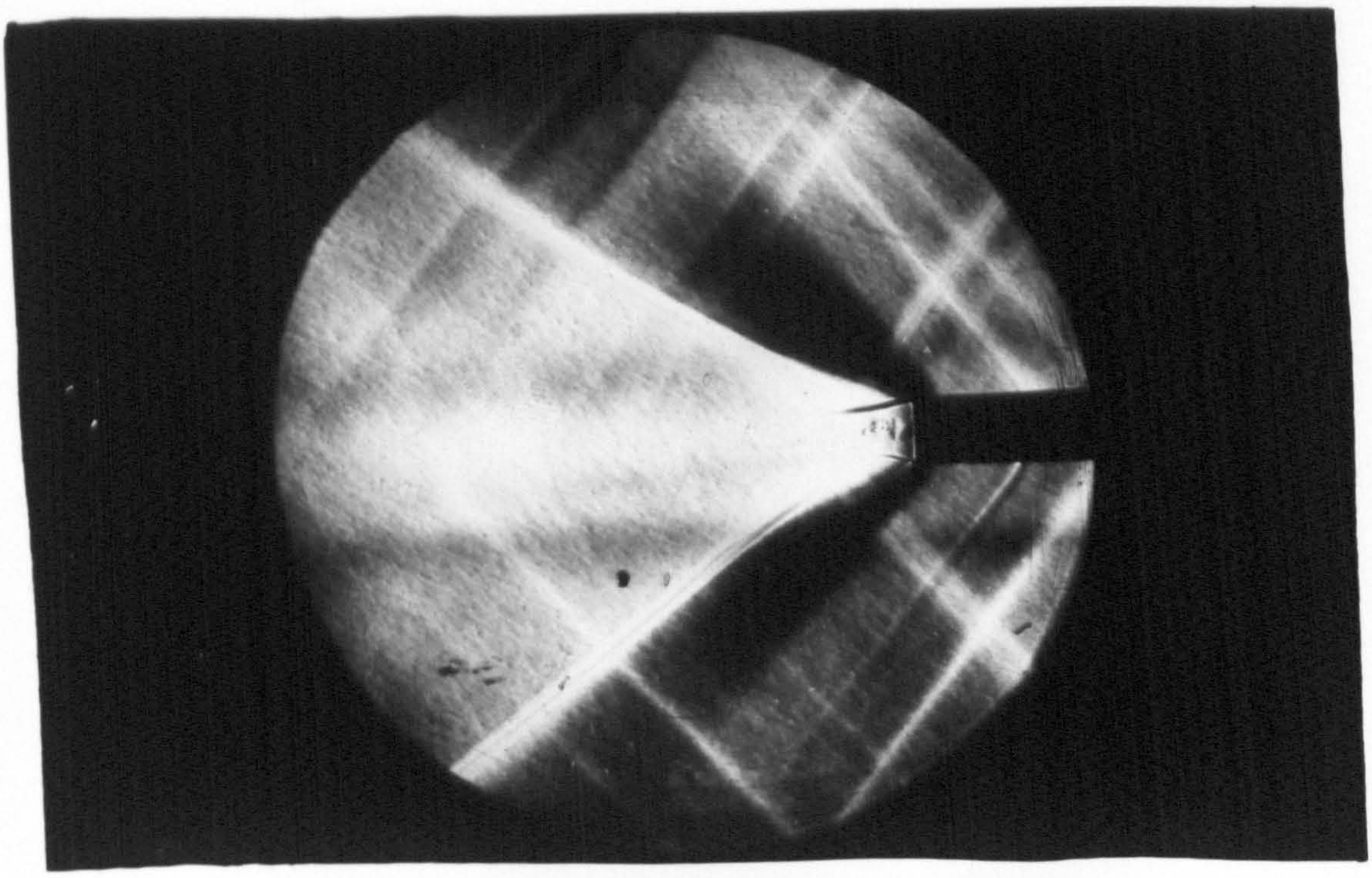

Plate 3b

Circular hole base, $M_\infty = 1.3$, $\dot{m}$=opt.

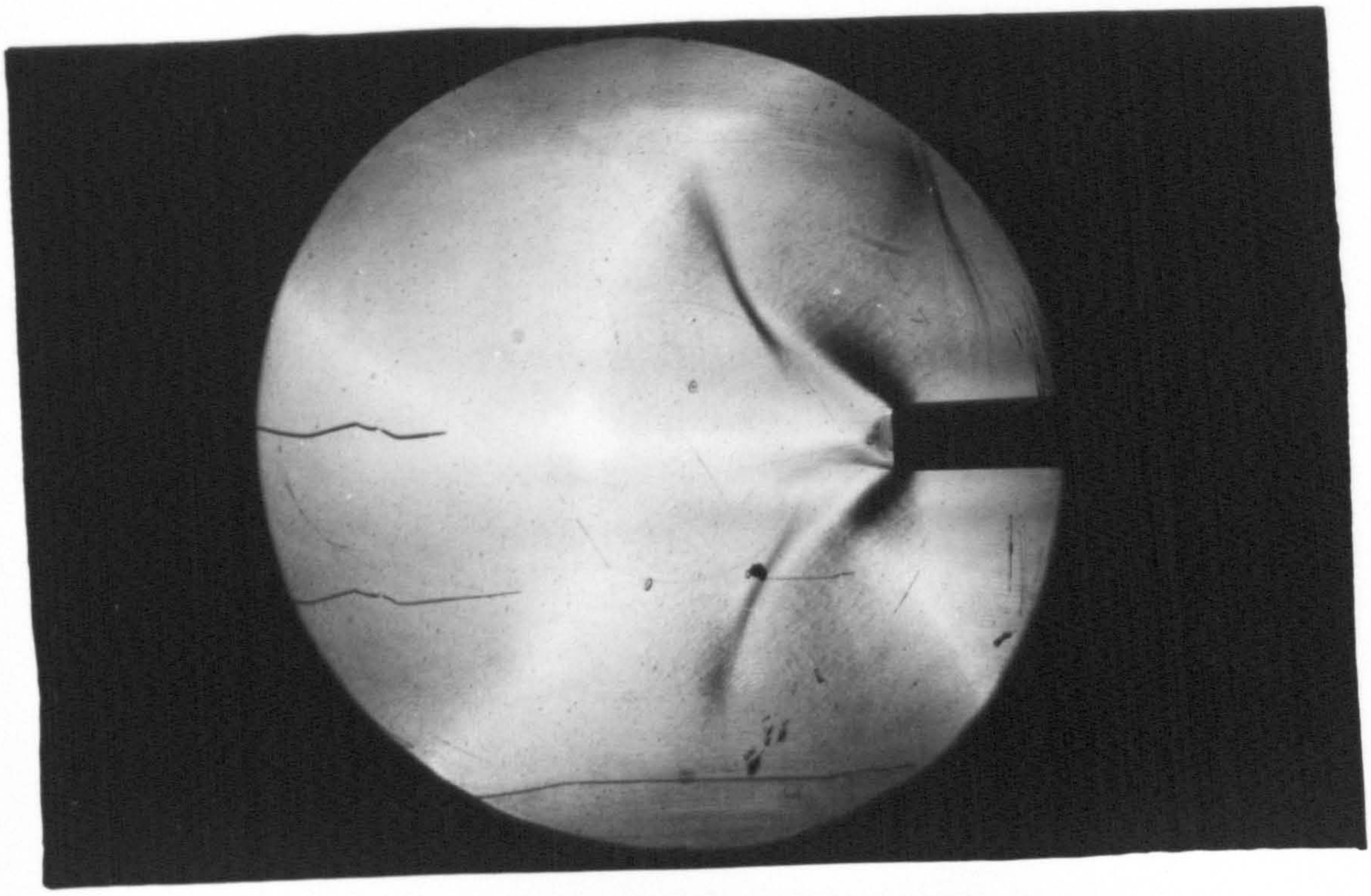

Plate 4a

Flared hole base, $M_\infty = 1.0$, $\dot{m} = 0$.

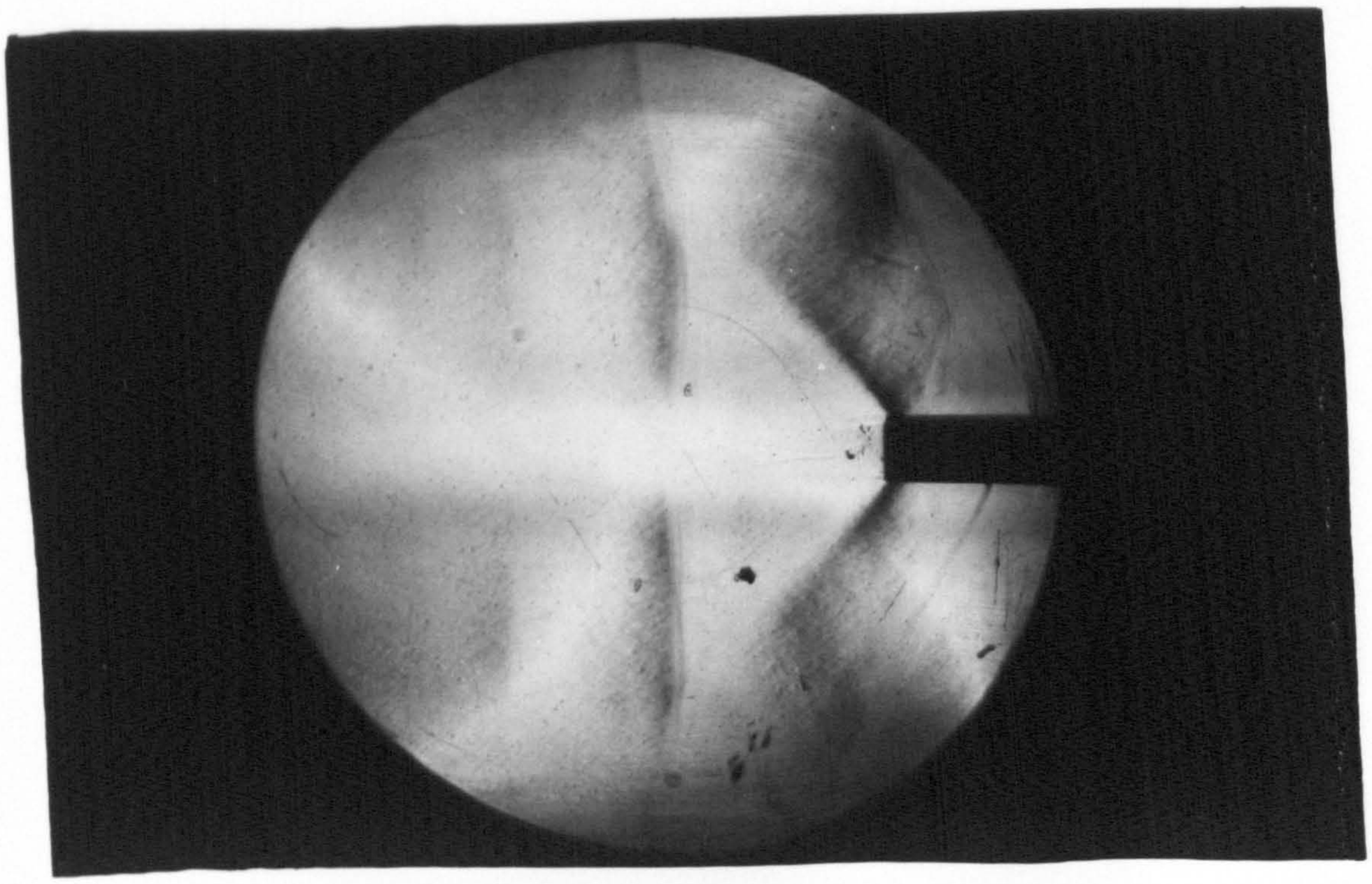

Plate 4b

Flared hole base, $M_\infty = 1.0$, $\dot{m} = \text{opt.}$

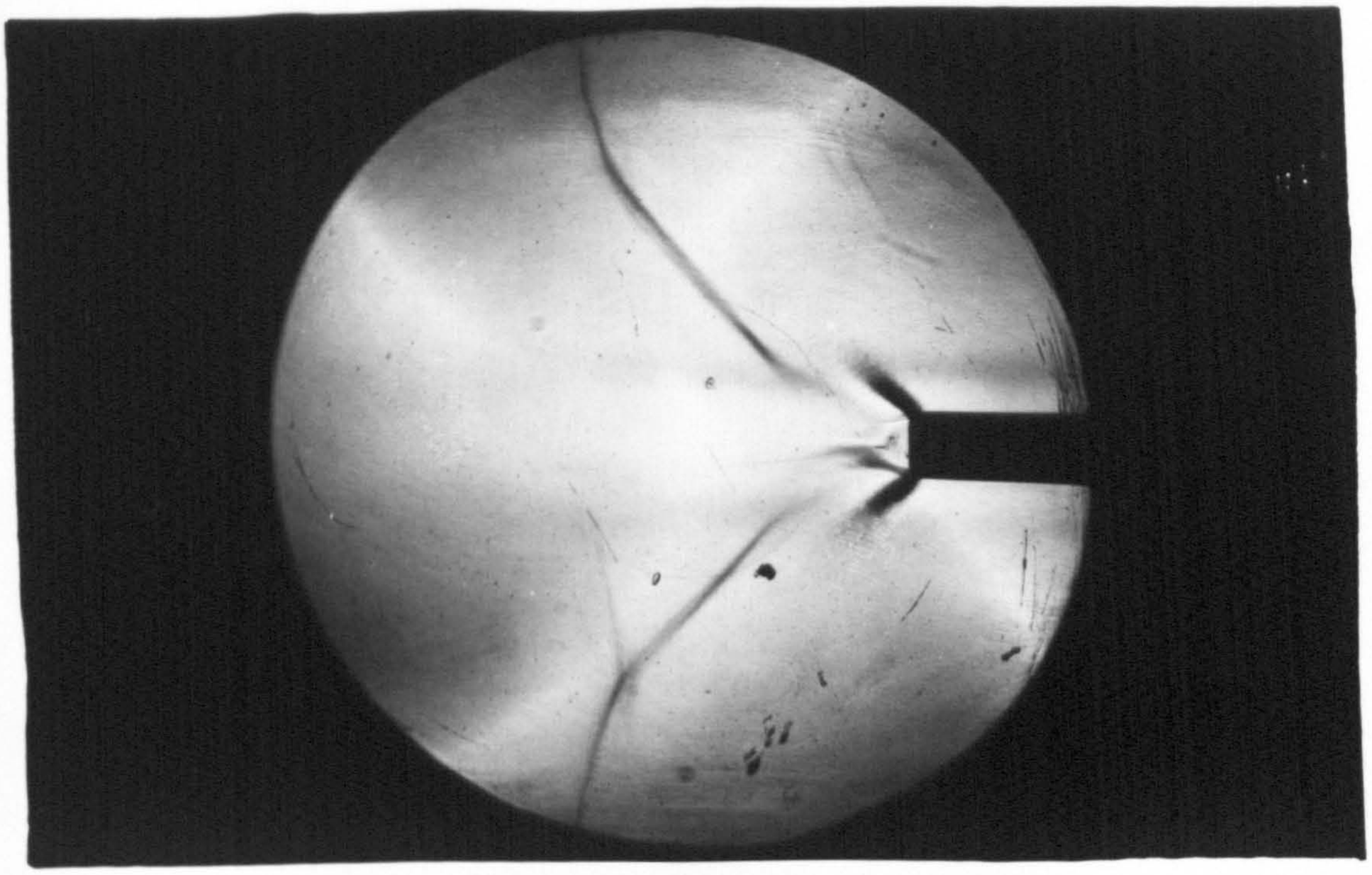

Plate 5a

Flared hole base, $M_\infty = 1.1$, $\dot{m} = o$.

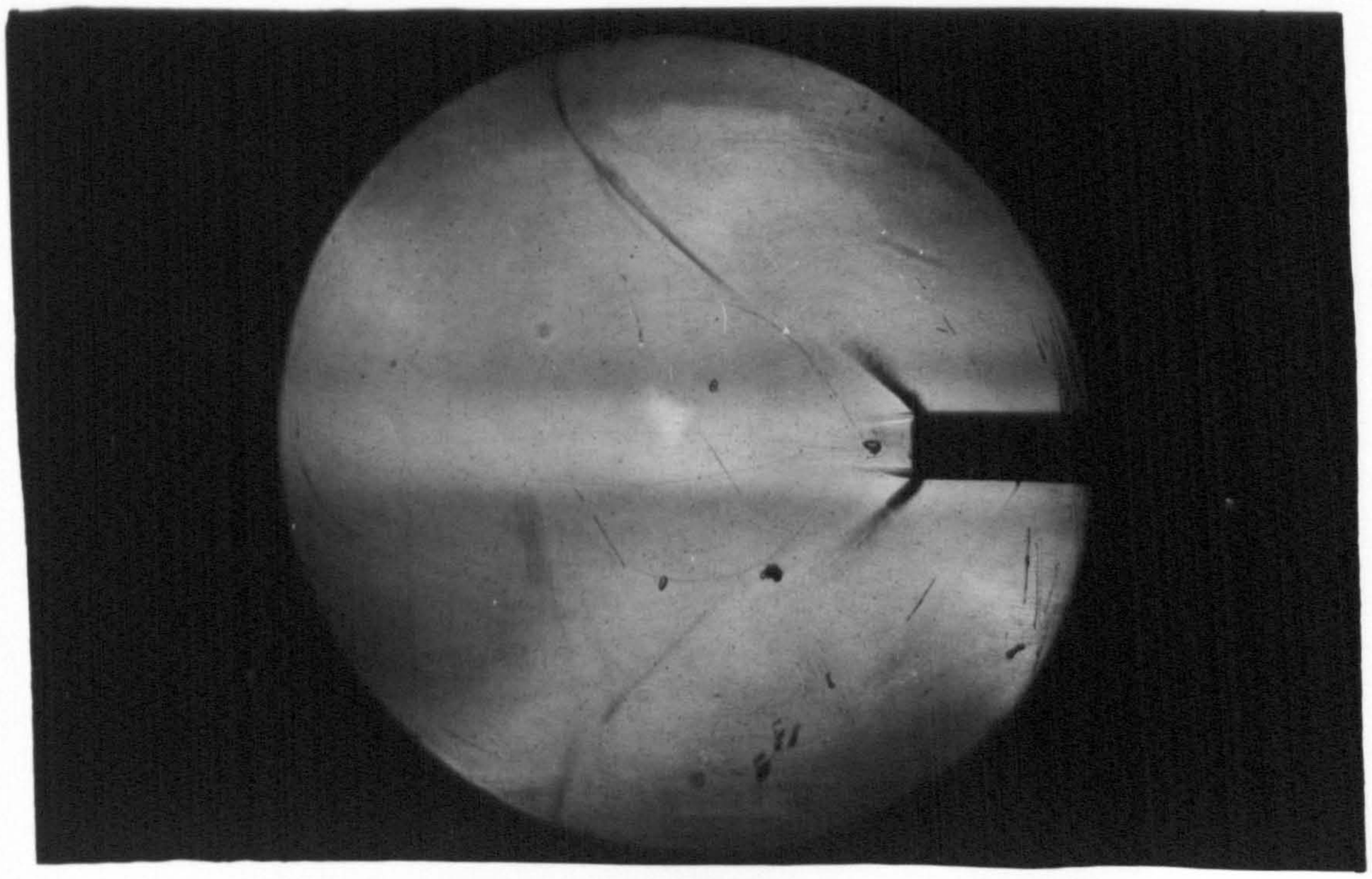

Plate 5b

Flared hole base, $M_\infty = 1.1$, $\dot{m}$ = opt.

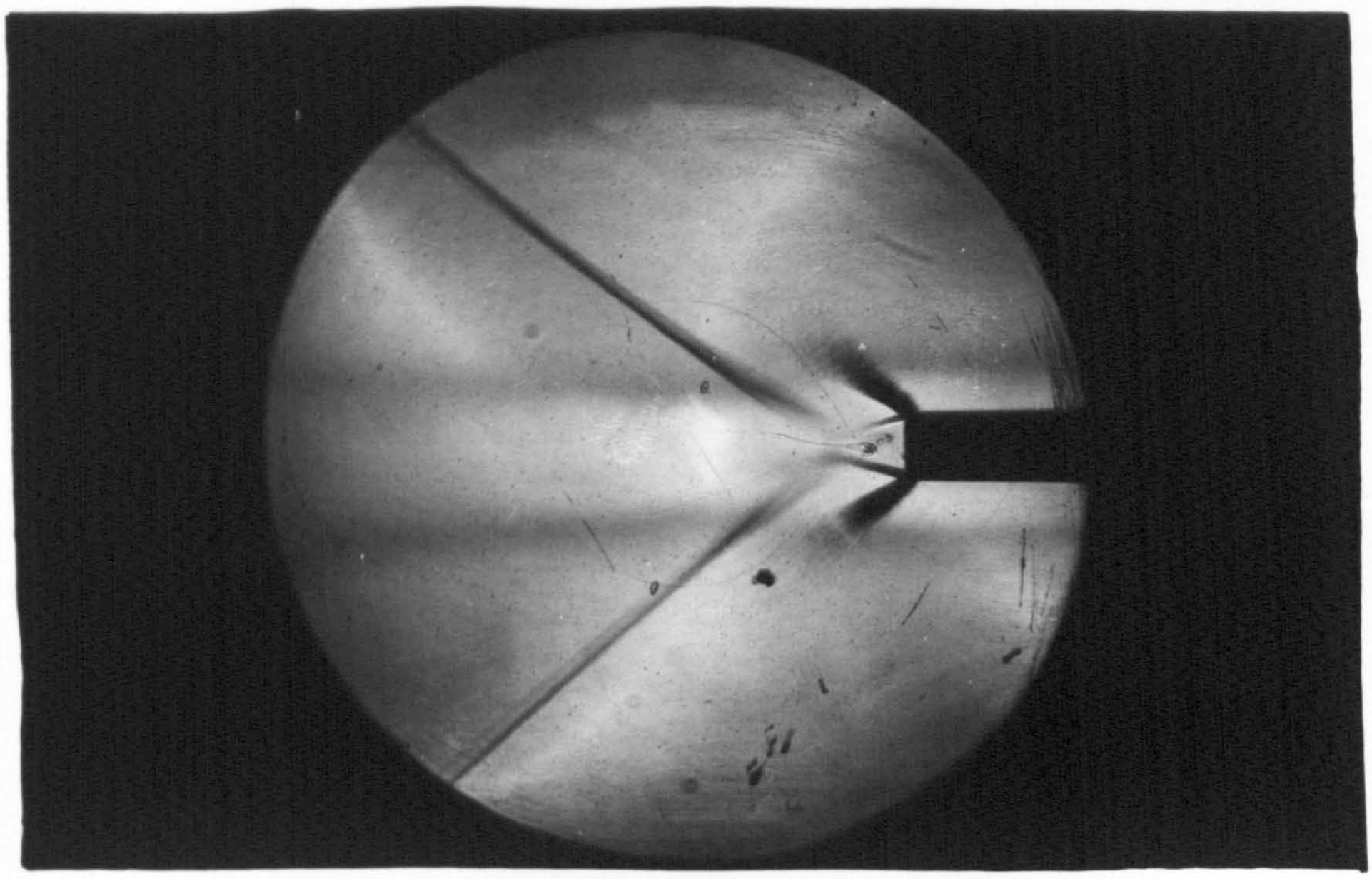

Plate 6a

Flared hole base, $M_\infty = 1.3$, $\dot{m} = 0$.

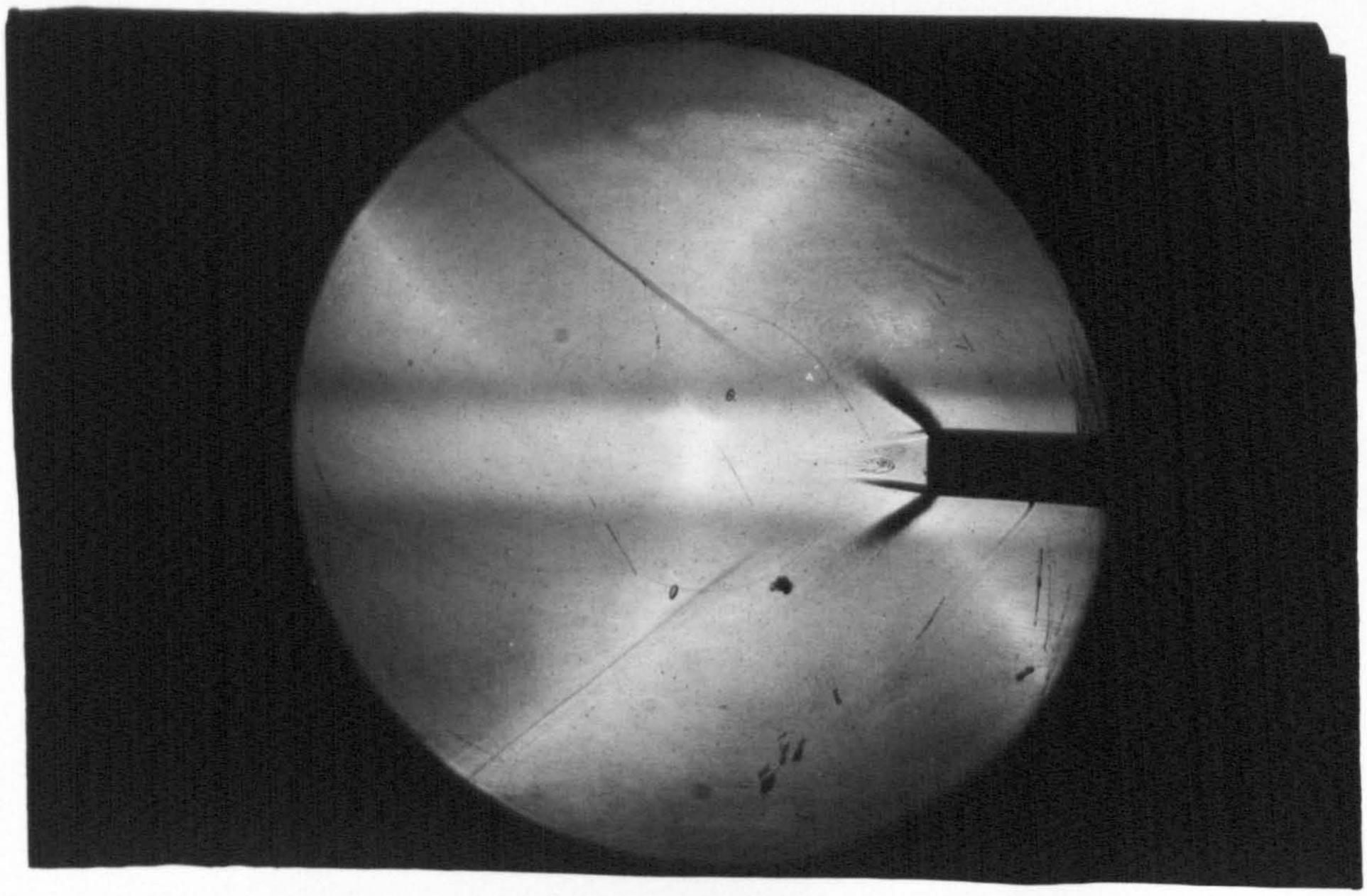

Plate 6b

Flared hole base, $M_\infty = 1.3$, $\dot{m} = \text{opt.}$